Design Optimization and Evaluation of Variable Profile Propellers using Panel Method

Auteur : Baqir Ali,
Promoteur(s) : Rigo, Philippe
Faculté : Faculté des Sciences appliquées
Diplôme : Master : ingénieur civil mécanicien, à finalité spécialisée en "Advanced Ship Design"
Année académique : 2023-2024
URI/URL : http://hdl.handle.net/2268.2/22242

With the support of the
Erasmus+ Programme
of the European Union

Design Optimization and Evaluation of Variable Profile Propellers using Panel Method

Master Thesis

Submitted on August 2, 2024

by Baqir Ali
baqir.ali@uni-rostock.de
Student ID No.: 223202140

First Reviewer

Dr.-Eng./Hiroshima Uni. Patrick Kaeding
patrick.kaeding@uni-rostock.de
University of Rostock
Albert-Einstein-Strasse 2
18059 Rostock. Germany

Second Reviewer

M.Sc. Adhil M Asif
a.asif@mmg-propeller.de
Mecklenburger Metallguss GmbH
Teterower Str. 1
17192 Waren (Müritz), Germany

Master Thesis

University of Rostock

Design Optimization and Evaluation of Variable Profile Propellers using Panel Method

The work in this thesis was carried out in:

Mecklenburger Metallguss GmbH
Teterower Str. 1
17192 Waren (Müritz)
Germany

Faculty Supervisor:	Dr.-Eng./Hiroshima Uni. Patrick Kaeding (University of Rostock, Germany)
	Dipl.-Ing. Gunnar Kistner (University of Rostock, Germany)
Direct Supervisor:	M.Sc. Adhil M Asif (MMG, Germany)

This document was set with LaTeXon August 2, 2024

Declaration of Authorship

I declare that this thesis and the work presented in it are my own and have been generated by me as the result of my own original research. Where I have consulted the published work of others, this is always clearly attributed. Where I have quoted from the work of others, the source is always given. With the exception of such quotations, this thesis is entirely my own work. I have acknowledged all main sources of help. Where the thesis is based on work done by myself jointly with others, I have made clear exactly what was done by others and what I have contributed myself. This thesis contains no material that has been submitted previously, in whole or in part, for the award of any other academic degree or diploma. I cede the copyright of the thesis in favour of the University of Rostock.

Rostock, August 2, 2024

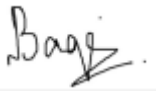

Baqir Ali

This page intentionally left blank.

Acknowledgement

I would like to extend his sincerest appreciation to Mr. Adhil M. Asif and Gunnar Kistner for their unwavering support, adept guidance, and reassuring mentorship throughout the thesis. They have been instrumental in the completion of this thesis. Moreover, I would like to thank Benjamin Klemmstein for his insightful inputs in running panMARE in open water configuration and cavitation and Lutz Kleinsorge for his valuable input for running optimizations. Furthermore, I would like to express his gratitude to the whole Research and Innovation team at MMG for providing insightful guidelines, and an excellent working atmosphere throughout the course of the thesis.

I am thankful to university professor Dr.-Ing. Patrick Kaeding and Dr.-Ing. Thomas Lindemann for their administrative support throughout the second year of EMSHIP at the University of Rostock.

A special thank goes to Prof. Philippe Rigo for providing an opportunity to be a part of EMSHIP.

This page intentionally left blank.

Abstract

Evaluation and Optimization of open water performance of variable profile propellers is conducted in this thesis. Variable profiles are generated by changing the radial distribution of camber of single NACA profile and by combining two different NACA profiles. CAESES is used for propeller modelling, parametrization and optimization. It is coupled with the panel code based solver panMARE for optimization of the design point evaluated using thrust identity method. Optimized solutions are validated using RANSE based CFD solver and top performing candidates are checked for cavitation using panMARE. It is observed that the variation of camber at normalized radial location of 0.6 has a significant impact on power. Performance improvement is observed for single profile blades but discrepancies between optimization results and CFD validation are observed, attributed to modelling defects and panel code method's limitations. Moreover, exploration of propeller blade with combination of two profiles indicated that the minimum power configuration is achieved when profile switching occurs at normalized radial location of 0.9, although actual performance improvement is not observed due to limitations in the correction factors used.

This page intentionally left blank.

Table of Content

This page intentionally left blank.

List of Figures

This page intentionally left blank.

List of Tables

This page intentionally left blank.

List of Abbreviations

Abbreviation	Meaning
MMG	Mecklenburger Metallguss
NACA	National Advisory Committee for Aeronautics
NACA4D	NACA 4-digit series
NACA16	NACA 16 series
NACA66mod	NACA 66 modified series
CFD	Computational Fluid Dynamics
RANS	Reynold's Averaged Navier Stokes
NSGA	Non-dominated Sorted Genetic Algorithm
NURBS	Non-Uniform Rational B-Spline
VLM	Vortex Lattice Method
BEM	Boundary Element Method
SST	Shear Stress Tranport
LRM	Light Running Margin
OWT	Open Water Test
PS	Pressure Side
SS	Suction Side
LE	Leading Edge
TE	Trailing Edge
ID	Inner Domain
OD	Outer Domain
RMS	Root Mean Square Values
LHS	Latin Hypercube Sampling
VP	Variable Profile
DSE	Design Space Exploration

1

Introduction

Propellers are critical component in marine propulsion systems, responsible for converting rotational energy into thrust. Propeller performance is evaluated on several key parameters including thrust, torque, and efficiency. Thrust is the force generated by the propeller to propel a ship forward, while torque refers to the rotational force required to spin the propeller. Efficiency measures how effectively the propeller converts input power into useful thrust. The performance of a propeller impacts several operational aspects such as fuel efficiency, speed, and manoeuverability. A well-performing propeller enhances fuel efficiency by maximizing thrust with minimal energy loss. The thrust and torque are generally represented in terms of dimensionless coefficients.

In the early stages of propeller design, engineers relied heavily on empirical methods and trial-and-error approaches. Screw propellers were developed using these techniques which was a breakthrough in propulsion technology. As the understanding of fluid dynamics improved, so did the methods for designing propellers, leading to the creation of more efficient designs that could produce greater thrust with less power.

With the advent of advanced parametrization tools and software, such as CAESES, the field of propeller design has entered a new era. Parametric modelling tools enable engineers to create highly detailed and accurate models of propellers, which can be used to simulate and analyse their performance. One of the key advantages of using parametric modelling tools is their ability to parametrize propeller designs, allowing for the systematic variation of key parameters such as blade shape, pitch, and diameter.

CAD tools such as CAESES provide an optimization toolkit and allow the user to optimize the designs by evaluating their performance by coupling simulation software. This parametrization, coupled with the Panel Code or Computational Fluid Dynamics (CFD) Software , has revolutionized the optimization process in propeller design. By integrating CAESES with a simulation software, designers can optimize the propeller's geometry to achieve the best possible balance between efficiency and cavitation resistance.

Typically, propellers are constructed using a single profile that is manipulated along the radial direction to form the propeller blade. While such designs have been historically effective, they have limitations in terms of efficiency and cavitation resistance, especially under varying operating conditions. This thesis explores the concept of using multiple profiles within a single propeller blade, to optimize open water performance through a variable profile approach. Cavitation is a phenomenon that results in formation of bubbles when the local pressure in the fluid drops below the vapor pressure. When these bubbles collapse, they significantly damage the propeller blades and reduce performance. The collapse of the cavitation bubbles leads

to blade erosion and material loss which shortens the service life of propeller and increases the maintenance costs. It also disrupts the smooth flow of water over the propeller blades, reducing thrust and increasing drag, which reduces overall efficiency. The sheet cavitation on the propellers can be seen in the Figure 1.1.

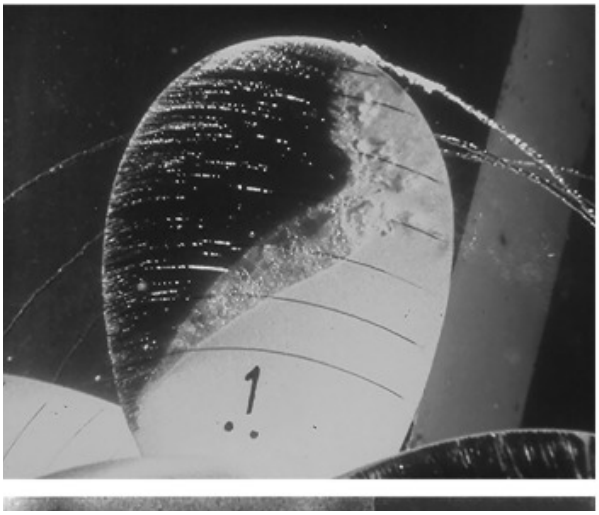

Figure 1.1: Sheet Cavitation (Carlton, 2018)

The motivation for this research stems from the need to improve the performance of propellers in several critical aspects. The current state of propeller design often results in a trade-off between efficiency and cavitation. In a marine environment where fuel efficiency and environmental regulations are becoming increasingly stringent, improving propeller design is not only beneficial but essential. The potential to optimize propeller performance by varying the profile along the blade radius is a promising avenue of research to address these challenges. Such a design approach could lead to a significant improvement in fuel efficiency and reduction in cavitation, thus contributing to more sustainable and economically viable marine operations.

The problem with current propeller designs lies in its inherent limitations. Single profile along the blade radius do not account for the varying flow conditions along the blade span, leading to suboptimal performance. This can lead to a higher power requirement, as well as a higher susceptibility to cavitation that not only reduces the efficiency but also causes noise and potential damage to the propeller.

The parameters of the blade such as pitch, rake and skew can be tuned to the flow conditions to get an optimal performance. The parameters that define a profile section such as camber and thickness distribution also have a strong influence on the performance. Guan et al. (2022) optimized the radial distribution of the skew, chord length, pitch, and camber ensuring the thrust coefficient and structural strength of the propeller. However, the thickness of the profile section is not optimized since it is limited by the required structural strength of the propeller.

This thesis explores the design optimization and evaluation of variable profile propellers using the Panel Method, leveraging the capabilities of CAESES. The study aims to develop a

robust framework for optimizing propeller parameters to enhance performance and ultimately contribute to more efficient and sustainable maritime operations.

1.1 Literature Review

Advancements in the design, evaluation, and optimization of marine propellers have focused on improving performance, efficiency and cavitation behaviour especially under varying operational conditions. A crucial aspect of this research is the development of sophisticated computational techniques and the integration of optimization algorithms, significantly improving the design process.

The performance of NACA sections is well documented in the literature. The NACA profiles have been developed for aerospace industry but have been used for marine applications with certain considerations. Brockett et al. (1780) modified the conventitional NACA66 profile for marine use and developed the minimum pressure envelopes for modified NACA66 profile and NACA16. The results showed a wider cavitation bucket for NACA66mod giving better performance. The same profiles have been chosen for the analysis in this thesis.

Significant new blade sections have been developed by optimizing the blade sections shape with the primary objectives of minimizing cavitation and reducing drag. Tamhane (2017) created a comprehensive framework for the design and optimization of marine propellers. A significant part of the research focuses on designing blade section with good cavitation performance and low drag. However, the blade section is optimized for a certain angle of attack that varies based on the radial location of the blade section. Similarly, Yamaguchi et al. (1999) designed new blade sections using the Eppler code with delayed cavitation inception while maintaining a high lift-to-drag ratio. The study investigates foil sections at three different thickness-to-chord ratios that depends on the radial location of the propeller.

Dang (2004) investigated new blade section designs aimed at widening of cavitation buckets. It was accomplished by unloading of the leading edge that provided a wide range of cavitation free performance. It is accomplished by using an S shaped camber and maximum thickness towards the leading edge of the blade. Similarly, Olivucci and Gaggero (2016) presented a multi-objective optimization framework for profile design under cavitating conditions. The framework utilized the Non-Dominated Sorted Genetic Algorithm (NSGA-II), boundary element methods, and RANS equation solvers (OpenFOAM). The primary objectives were to enhance cavitation inception speeds and reduce cavity volume while maintaining lift performance.

Karim et al. (2004) used micro genetic algorithm to optimize profile. They used Boundary element method based on potential theory optimize the profile. Lift to drag ratio is minimized with constraint on minimum pressure coefficient. The research discussed here focuses on the optimization of the blade section that performs better in cavitation and gives minimum drag. The performance of the profile depends on the flow conditions and angle of attack which depends on the radial location of the blade section. That is why study on the optimal use of the profile at the desired radial location is necessary.

Significant advancements in the parametric modelling techniques of the propellers have been

made in the recent years. Non-Uniform Rational B-Splines (NURBS) and other spline-based techniques are utilized for the accurate representation of complex geometries and facilitate the integration of optimization algorithms and computational fluid dynamics (CFD) simulations. Arapakopoulos et al. (2019) compared two models, which include a NURBS-based parametric model and a T-spline parametric model. They are evaluated for their efficiency in producing geometric representations that can be directly used in computational tools.

Wang et al. (2022) used Non-Uniform Rational B-Spline to develop a parametric model of a propeller. Optimization of spanwise parameters as well as the profile was carried out to obtain efficient performance. The study used Gene Expression Programming to combine advantages from genetic algorithms and genetic programming, allowing for efficient and flexible optimization. The non-dominated sorting genetic algorithm was employed to solve the optimization problem. The study demonstrates significant improvements in propeller design, validated through comparisons of open water efficiency between the optimized and baseline propellers.

Historically, different methods have been used to analyse the propeller blade performance. Their evaluation methods mainly consist of two categories; Potential Theory based methods and CFD. Early methods included lifting line methods and lifting surface methods that are based on the circulation theory (Carlton, 2018). The panel methods are used at early design stages to evaluate and optimize the performance as less computational effort involved.

Vortex Lattice Method (VLM) is also used for the evaluation of propeller performance that is based on potential theory. In VLM, the lifting surface is discretised into a grid (lattice) with discrete vortices at control points. Mishima (1996) used the Vortex Lattice Method in optimization study to maximize propeller efficiency while controlling sheet cavitation, incorporating constraints on cavity characteristics. Results showed that the optimized designs offered improved performance metrics compared to existing approaches, demonstrating the effectiveness of the proposed methodology in enhancing propeller efficiency and mitigating cavitation-related issues.

The panel methods are used at early design stages to evaluate and optimize the performance as less computational effort involved. Lee (1987) developed a potential theory-based panel method for the open water performance evaluation of the propeller in steady flow. Propeller hub effect was also included in the analysis by modelling the hub using the surface panels.

Coupling of the different methods have also been used to achieve good results with less computation effort. Wang et al. (2013) developed an algorithm that couples the Vortex Lattice Method and Lifting Line Method to perform full wake alignment. Both cavitation and open water performance were evaluated and similar results to the Boundary Element Method (BEM) were produced while significantly reducing computational time.

Coney (1989) did the parametric studies of the propellers using the vortex lattice lifting surface method. An algorithm was developed to evaluate optimum rpm and diameter of the propeller and minimum values of chord length and thicknesses were also determined. By evaluating these values, optimum camber and pitch were determined for desired circulation in radial direction.

Vesting et al. (2016) compared various optimization algorithms, such as (NSGA-II) and Particle Swarm Algorithm. The study highlighted a two-stage optimization process: the first stage of gathering knowledge through parametrized geometry curves, while the second stage of refining the design locally to meet specific performance targets. The application of these methodologies resulted in propeller designs that are comparable to or better than manually optimized designs.

Machine Learning algorithms are also being investigated recently to reduce the dependence on time consuming CFD simulations. Vesting and Bensow (2014) studied the feasibility of using surrogate methods to replace complex computations in advanced propeller optimization tasks. The study compared three different surrogate methods: Kriging, Feed Forward Neural Network, and Cascade Correlation Neural Network, utilizing an analytical test function to evaluate their capabilities. The research demonstrated that all surrogate methods effectively modified the parameter distributions in similar ways to optimize propeller geometry, enhancing efficiency and reducing cavitation.

1.2 Research Objective

The primary objective of this thesis is to evaluate a propeller blade design that incorporates different NACA profile sections along the radial direction. Such a propeller design can be achieved using two different methods.

1. By changing the camber and thickness distribution along the blade span.
2. By combining two different NACA series profiles.

Both approaches are investigated in this thesis. In the first case, the change in thickness distribution is not studied because the blade thickness is a critical parameter for the structural strength of the propeller and the existing thickness distribution already satisfies the structural requirements. The profile generated from the second method will be referred as Variable Profile henceforth.

The key goals of this research are:

- Development of a parametric model of propeller that allows for the variation in camber and interchangeable definition of NACA profiles at different radii.
- Evaluation of the performance against a selected baseline propeller using the Panel Method, focusing on power consumption and cavitation resistance.
- Implementation of an optimization algorithm that integrates the parametric blade model with the Panel Code for open water performance evaluation.
- Validation of the Optimal solution using Computational Fluid Dynamics Simulations.
- Evaluation of the Optimized Models for cavitation resistance using the Panel Code.

This page intentionally left blank.

2
Background

2.1 Propeller Geometry

At a basic level, a propeller works by accelerating water backward, generating a reaction force that moves the vessel forward. The flow at a radial section of a propeller blade can be analysed to understand how different parts of the blade contribute to thrust and efficiency.

A conventional propeller blade geometry consists of profile sections divided into radial directions and mapped on to a cylindrical surface at each radial location. Generally, the forces generated at a section are analysed and it typically involves examining the inflow velocity, the angle of attack, and the resulting lift and drag forces. The Figure 2.1 illustrates the geometric definition and flow characteristics of a marine propeller, depicted as a cross-sectional view of a propeller blade (Techet, 2005).

The propeller's blade profile is considered at a radial location (r). V_S is the component the velocity component of the water flowing through the propeller disc in the axial direction (along the shaft axis). This vector points from the hub in the direction of the blade motion. V_R is the resultant velocity, which is the vector sum of the rotational velocity ($2\pi rn$) and the forward velocity. The angle α is the angle of attack the profile at the radial location experiences and it affects the lift and drag forces on the blade. β is the pitch angle, defined between the chord line of the blade section and a line parallel to the propeller axis. The pitch angle varies along the radius of the blade and is a key factor in propeller performance, influencing thrust and efficiency.

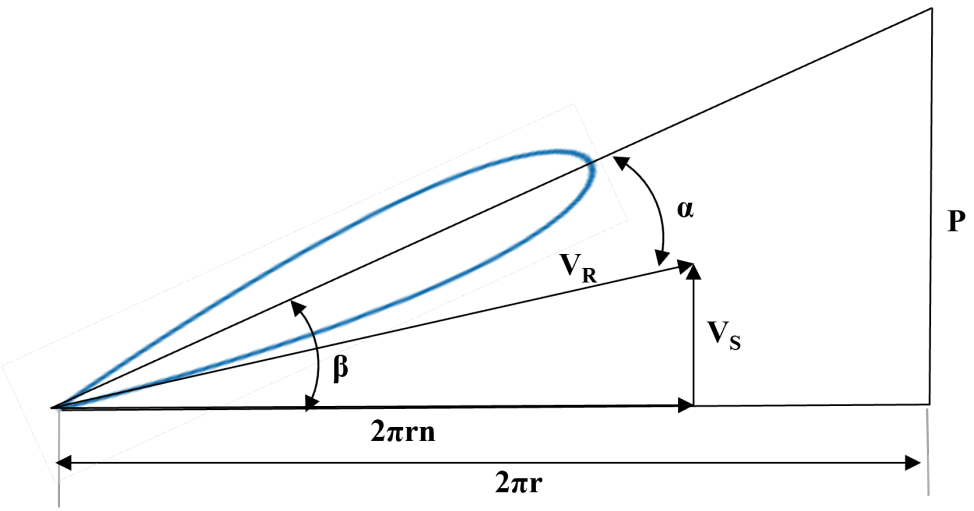

Figure 2.1: Propeller definition

The distribution of various geometric and performance-related parameters along the radial direction is important for the analysis and design of propeller blades. The key parameters are pitch, rake, skew, chord, thickness, and camber and their distribution along the radial direction.

Pitch: It is the distance the propeller would theoretically move forward in one complete rotation if there were no slip (i.e., the blade acts like a screw). It is basically the propeller blade's twist along its length (Ghose, 2004). It is crucial for determining the propeller's efficiency and thrust characteristics. The pitch typically varies from the root to the tip, adapting to the changing flow conditions along the radius.

Skew: It is the angular displacement of the blade sections relative to the radial axis, which helps to reduce pressure pulsations and noise (Carlton, 2018). Skewed blades are designed to smooth out the flow and reduce the impact of non-uniform inflow.

Rake: It is the axial displacement of the blade from the propeller's hub (Carlton, 2018). It affects the flow characteristics and can influence the cavitation behaviour. Positive rake angles can help reduce cavitation and improve hydrodynamic performance.

Chord: The chord length is the distance between the leading edge (L.E) and trailing edge (T.E) of the blade section. It varies along the radial direction and its distribution affects the lift and drag characteristics of the blade, influencing overall efficiency (Abbott and Von Doenhoff, 2012). The chord length is shown in the Figure 2.2.

Thickness: The thickness (t) of the profile is the maximum distance between upper and lower profile. The thickness distribution is critical for structural integrity and hydrodynamic performance. It ensures that the blade can withstand the operational stresses while maintaining efficiency. The thickness is shown in the Figure 2.2.

Camber: Camber is the curvature of the blade section, which has a direct effect on the lift generated by the blade (Abbott and Von Doenhoff, 2012). The camber distribution along the radial span is designed to increase the thrust. The camber can be of the profile is shown in the Figure 2.2.

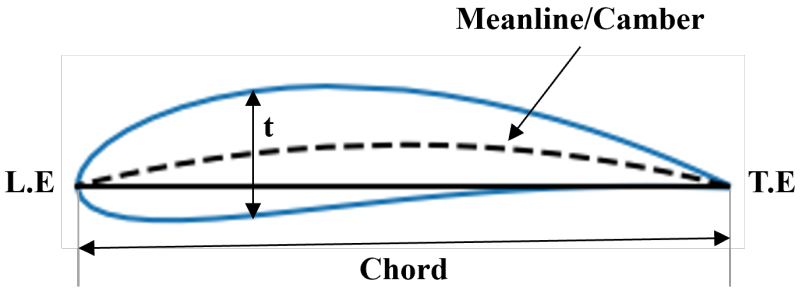

Figure 2.2: Profile Definitions

2.2 Propeller Theory

The results from simulations give the thrust and torque of the propeller blade. But these forces are converted into non-dimensional values to reduce the number of variables. These are described in the following section.

Advance ratio (J) is the dimensionless number that gives relation between the velocity of advance or ship speed (V_s) and propeller rotational speed (n) and propeller diameter (D).

$$J = \frac{V_s}{nD} \tag{2.1}$$

This advance ratio assumes uniform flow towards propeller but that is not the case when propeller is operating behind a ship hull. Taylor wake fraction (w) is the number that defines how much reduction in velocity is expected at the propeller inflow. It is given by,

$$w = 1 - \frac{V_P}{V_s} \tag{2.2}$$

V_P is the velocity at propeller inlet. The advance coefficient depending on the wake fraction is given by,

$$J = \frac{V_s(1-w)}{nD} \tag{2.3}$$

Thrust coefficient (K_T) is a dimensionless number that gives a relation between thrust (T), propeller speed, propeller diameter and density of the fluid (ρ) it is operating in.

$$K_T = \frac{T}{\rho n^2 D^4} \tag{2.4}$$

An alternate form of thrust coefficient that depends on the ship advance velocity rather than propeller speed (Carlton, 2018). It is given by,

$$C_{th} = \frac{T}{\frac{1}{2}\rho A_o V_s^2} \tag{2.5}$$

It can also be written in terms of advance ratio and thrust coefficient.

$$C_{th} = \frac{8}{\pi} \cdot \frac{K_T}{J^2} \tag{2.6}$$

Torque coefficient (K_Q) is a dimensionless number that gives a relation between torque (Q) and propeller speed and diameter and density of the fluid it is operating in.

$$K_Q = \frac{Q}{\rho n^2 D^5} \tag{2.7}$$

The efficiency of a propeller (η_o) is evaluated using the following expression,

$$\eta_o = \frac{J}{2\pi}\frac{K_T}{K_Q} \tag{2.8}$$

The delivered power of the propeller is given by,

$$P_{Delivered} = K_Q \rho n^2 D^5 \cdot 2\pi n \tag{2.9}$$

The power delivered by the propeller depends on the rotational speed of propeller, the propeller diameter and the torque coefficient of the propeller.

Propeller open water performance characteristics curves are graphical representations of a propeller operating in open water, free from the influence of a vessel's hull or other appendages. They are typically generated through experimental testing in controlled environments, such as towing tanks, or through computational simulations. A typical Open water performance curve is shown in the Figure 2.3.

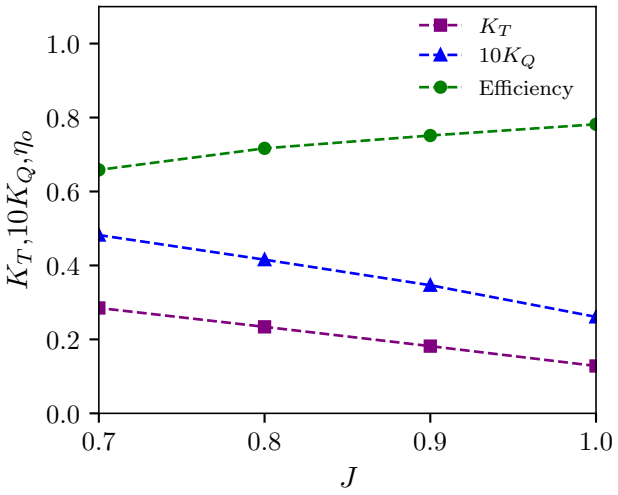

Figure 2.3: Typical Propeller Open Water Performance Curves

The propellers are designed on a particular vessel speed and then analysed for performance in detail. The evaluation of design point is also necessary to feed the optimizer. The goal of the optimization is to reduce the energy consumption of the propeller, since the thrust to be generated by the propeller is always the same, as it depends on ship hull and hull-propeller interaction. Therefore, the design point is evaluated at a constant thrust loading coefficient for different variants. This method is called thrust identity method (ITTC, 2014). The value of thrust loading coefficient only depends on ship parameters and propeller diameter. The thrust produced by the propeller must overcome the ship resistance (R_t) and thrust deduction due to hull-propeller interaction. It is given by,

$$T = \frac{R_T}{1-t} \tag{2.10}$$

Here t is the thrust deduction factor. Using equation 2.10 and equation 2.3 in the equation 2.6,

$$C_{th} = \frac{8}{\pi} \cdot \frac{R_T}{(1-t)(1-w)^2 \rho D^2 V_s^2} \tag{2.11}$$

The actual velocity of the water flowing to the propeller behind the hull is neither constant nor perpendicular to the propeller plane; instead, it has varying axial, tangential and radial velocities. Consequently, compared to operation in open water, the propeller's efficiency is influenced by its relative rotative efficiency.

Another parameter which is important for ship owners is the Light Running Margin (LRM). It is a buffer to account for variations in operating conditions, such as changes in ship loading and sea state. By maintaining a margin between the no-load and loaded conditions, operators make sure that the propeller operates within safe and efficient limits (Solutions, 2018). It is contractually obligated by the propeller manufacturers to meet the desired LRM. It is given by,

$$LRM = \frac{n_{inter} - n_{nominal}}{n_{nominal}} \times 100 \tag{2.12}$$

The LRM is evaluated by comparing the propeller speed at the design point with the nominal propeller curve. The Design Point and LRM can be visualized in Figure 2.4.

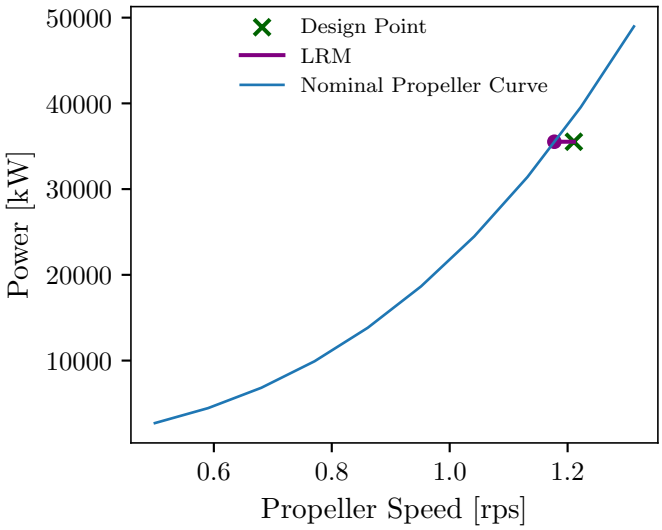

Figure 2.4: Propeller Nominal Curve, Design Point and LRM

Cavitation number (σ_o) is defined as the ratio of static pressure head to the dynamic pressure head. The cavitation number based on the propeller speed is used to evaluate the cavitation performance. The cavitation number is given by ,

$$\sigma_o = \frac{P_{atm} + \rho g h - p_v}{\frac{1}{2}\rho n^2 D^2} \tag{2.13}$$

Here, P_{atm} is the atmospheric pressure, p_v is the vapor pressure of the liquid and h is the depth at the shaft line (Ghose, 2004). The design cavitation number is evaluated at the shaftline depth. The cavitation number at the design point depends on the propeller interpolated speed, and it will change for each variant.

The important parameters in the case of cavitation that are considered for this study are the cavitating area and cavitation bucket width. The width of the cavitation bucket is defined

as the range of incidence angles or advance ratio within which cavitation does not occur, given a specific cavitation number (Carlton, 2018). This range is crucial because it defines the operational limits within which the blade can operate without experiencing cavitation. A wide cavitation bucket means a larger range of conditions can be tolerated without cavitation, indicating better cavitation resistance.

In evaluation of both parameters a 2% margin is taken in the cavitating area because of the panel code limitation (the panels at the leading edge always cavitate due to pressure jump). It is desired that the blade should not cavitate at the design point and has maximum bucket width which gives a wide window of cavitation free operation. Generally, cavitation bucket diagram is used to depict the behaviour of cavitation for propellers (Ghose, 2004). However, for the ease of calculation the plot of advance ratio versus blade cavitating area at the design cavitation number is used to evaluate the bucket width. Figure 2.5 shows the bucket width and the design point used for our evaluations. The python script for evaluating bucket width is given in the Appendix D.2.

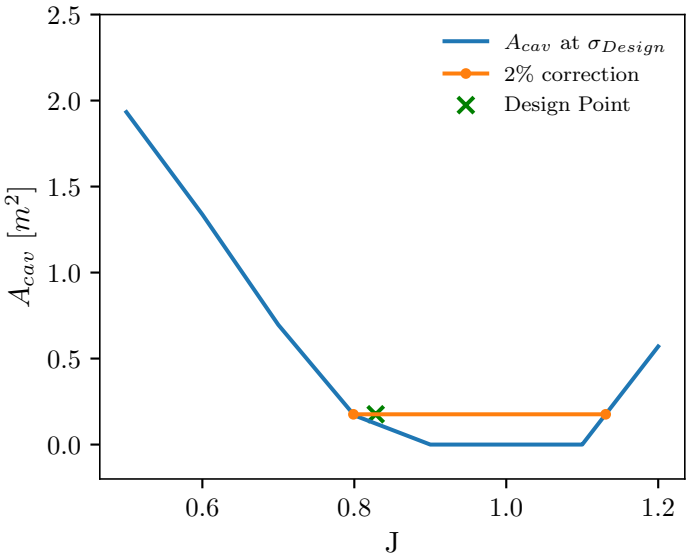

Figure 2.5: Cavitating Area vs Advance Ratio

3
Methodology

3.1 Propeller Modelling and Parametrization

Different methods are used to model propellers. The first one being cylindrical method which is a modelling technique used where the propeller blades are considered as sections cut from a cylindrical surface. This method simplifies the geometric representation and analysis of propeller blades by assuming that each blade section, when projected onto a cylindrical surface, maintains a constant radius from the propeller's axis. The primary advantage of the cylindrical method is its simplicity, which makes it easier to analyse the flow characteristics and performance of the propeller.

Key Features of this method are:

- The propeller blades are defined by a series of cross-sections that are aligned along the radial lines from the hub. Each section can be analysed individually, making it straightforward to compute local flow properties, such as velocity and pressure distribution.
- The propeller blade is divided into several radial sections, each described by a profile shape that can vary along the radius. These sections are often based on standard airfoil shapes or other predefined profiles. The local pitch and camber can also vary along the blade's span, allowing for a detailed design.

The helical method is another approach of modelling propellers, which considers the actual helical or twisted shape of the propeller blades as they rotate through the water. Unlike the cylindrical method, the helical method accounts for the fact that propeller blades are not flat but follow a helical path due to the rotational motion of the propeller.

Key Features of this method are:

- The blade sections are not mapped on a cylindrical surface. Instead, they follow a helical path, which accurately represents the three-dimensional nature of the propeller blades. This method captures the twist and varying pitch of the blades more accurately.
- This method is quite flexible when the propeller's radial distributions deviates significantly from conventional distributions. For example, a heavily raked propeller tip design. The chord length can be given the required pitch, skew and rake at radial locations to generate general blade geometry. This adaptability extends to the later stages of design, where specific profiles can be added and easily modified based on their definitions. This method is advantageous when the parametrization of the blade is required.

3.1.1 Blade Geometry Parametrization

Propeller radial distributions are normalized by dividing them by radius of the propeller for ease of parametrization. The distributions include blade pitch, rake, skew and chord. The geometry of the blade is created by the helical method using these parametrized distributions. A part of the helix is created at each radial section depending on the local chord, skew, rake and pitch. These partial helical curves are created at radial stations of the blade and are used as pathways to generate a surface called Centersurface. The Centersurface generated from the distributions is shown in the Figure 3.1.

Figure 3.1: Centersurface

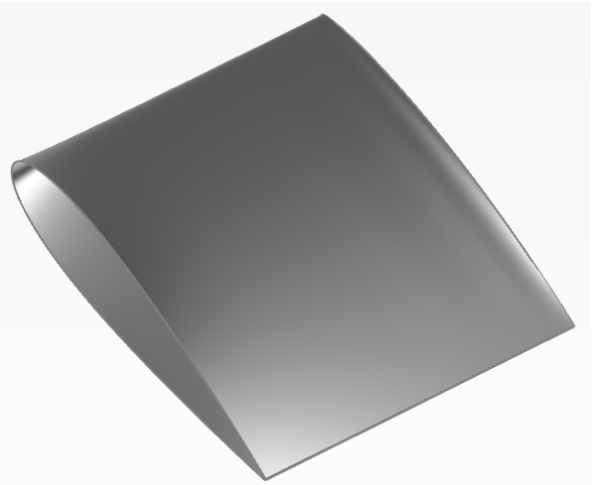

Figure 3.2: NACA4D Lofted Surface

The parametrized profiles are combined using the thickness and camber distributions and moved to a desired radial location to get a smooth lofted surface. This lofted surface is shown in the Figure 3.2. The center of lofted surface at each station is superimposed to the center of the Centersurface to get a smooth parametric blade of the propeller. The blade geometry is shown in the Figure 3.3.

Figure 3.3: Parametrized Blade

The separation of Centersurface from NACA lofted surface enables a decoupling of profiles from underlying blade definition.Thus allowing an interchangeability of profiles at any given radial sections. The lofted surface created can be a combination of two or more profiles and can easily be transformed into a blade.

3.1.2 Profile Parametrization

A 2d profile is obtained by combining a thickness curve and a mean line to obtain a cambered profile. The thickness curve defines the basic shape of the profile while the meanline is used to define camber. The details on how to combine these curves to obtain a cambered profile are given by Abbott and Von Doenhoff (2012). Different profiles used in this study are discussed here. The main parameters that define a profile are

- Chord
- Maximum Thickness
- Maximum Camber
- Maximum Camber Position

However, these parameters vary among the profiles chosen. For example, for NACA16 and NACA66mod, the location of maximum camber is determined by the type of meanline and it is treated as a separate parameter.

3.1.2.1 NACA 4-Digit Profile

Although NACA 4-digit series airfoils are not used in the marine industry for propellers, they are used here for analyses because they are easy to parametrize. The basic thickness form of the NACA 4-digit series is given by the following equation (Abbott and Von Doenhoff, 2012).

$$\pm y_t = \frac{t}{0.2}\left(0.2969\sqrt{x} - 0.1260x - 0.3516x^2 + 0.2843x^3 - 0.1015x^4\right) \tag{3.1}$$

where:

- y_t = ordinate in fraction of the chord
- x = abscissa in fraction of the chord
- t = maximum thickness in fraction of the chord

A profile of any thickness can be created by increasing the parameter t. The camber for NACA 4-digit series is given by the following equation.

$$y_c = \begin{cases} \frac{m}{p^2}\left(2px - x^2\right) & \text{for } 0 \leq x \leq p \\ \frac{m}{(1-p)^2}\left((1-2p) + 2px - x^2\right) & \text{for } p < x \leq c \end{cases} \tag{3.2}$$

where:

- y_c = ordinate of meanline in fraction of the chord
- m = maximum ordinate of mean line expressed as fraction of the chord.
- p = chordwise position of maximum ordinate.

The camber is defined by the two parameters here. Changing m will increase the camber resulting in a curved profile. Change in p results in the shifting of the location of maximum camber point and it can be moved near the L.E or T.E. The NACA4D profiles (NACA0006) with camber and without camber (NACA2506) are shown in the Figure 3.4 A parameterised model of NACA 4D series is available in CAESES and is hence directly incorporated for the study.

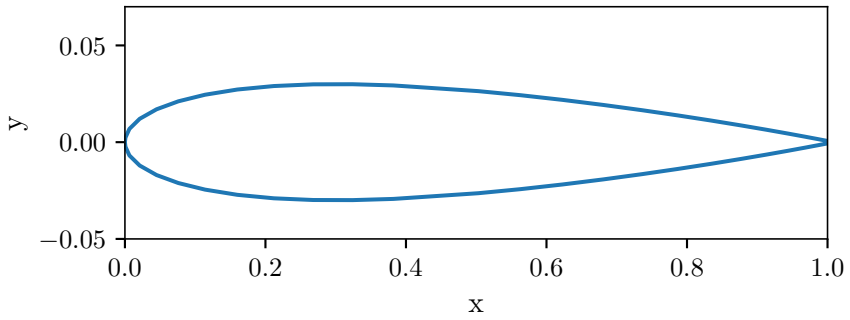

(a) NACA0006 Profile

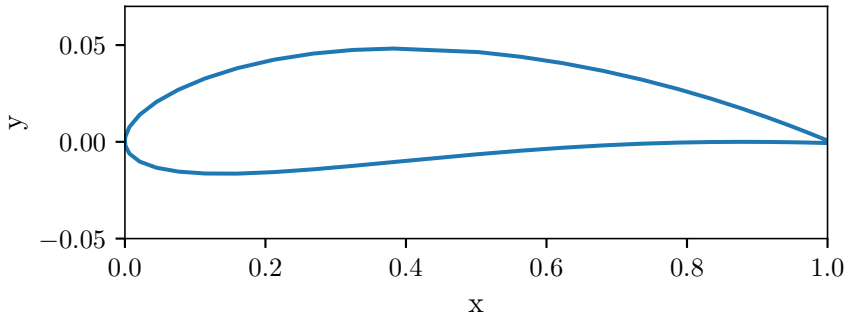

(b) NACA2506 Profile

Figure 3.4: NACA 4-digit series profiles

3.1.2.2 NACA 16 Profile

The basic thickness form of NACA16 series is given by the following equations (Lindsey et al., 1948).

Leading edge to maximum thickness location:

$$\pm y_1 = 0.01t\left(0.989665x_1^{1/2} - 0.23925x_1 - 0.0410x_1^2 - 0.5594x_1^3\right) \tag{3.3}$$

Maximum Thickness location to trailing edge:

$$\pm y_2 = 0.01t\left[0.010 + 2.325(1-x_2) - 3.420(1-x_2)^2 + 1.460(1-x_2)^3\right] \tag{3.4}$$

The leading edge radius was also incorporated to get a smooth profile. It is given by the following equation:

$$\text{L.E. radius} = 0.0048972\,(t)^2 \tag{3.5}$$

The maximum thickness location is kept constant at x/c = 0.5 for all variants. The meanlines that give uniform pressure distribution are used to define camber in the NACA16 and NACA66mod section. The pressure distribution remains constant till point **a** and drops linearly to zero at the trailing edge. They are given by the following equation (Abbott and Von Doenhoff, 2012):

$$\begin{aligned} y_c = \frac{c_l}{2\pi(a+1)}\Bigg\{\frac{1}{1-a}\Bigg[\frac{1}{2}(a-x)^2\ln|a-x| - \frac{1}{2}(1-x)^2\ln(1-x) \\ + \frac{1}{4}(1-x)^2 - \frac{1}{4}(a-x)^2\Bigg] - x\ln x + g - hx\Bigg\} \end{aligned} \tag{3.6}$$

where

$$g = \frac{-1}{1-a}\left[\frac{a^2}{2}\ln a - \frac{1}{4}a^2 + \frac{1}{4}\right] \tag{3.7}$$

$$h = \frac{1}{1-a}\left[\frac{1}{2}(1-a)^2\ln(1-a) - \frac{1}{4}(1-a)^2\right] + g \tag{3.8}$$

- c_l = Coefficient of lift
- a = fraction of the chord till where the load distribution is uniform

The type of meanlines is chosen within the range of a = 0 - 1 with the interval of 0.1. The most used meanlines are $a = 0.8$ and $a = 1$. Increasing the coefficient of lift increases the camber of the profile resulting in a curved profile. Changing the value of a change the location of the maximum camber and modifies the overall shape of the camber. The desired parameter is maximum camber which depends on the lift coefficient for each meanline. The maximum camber for each meanline is evaluated and the lift coefficient is substituted by maximum camber. This approach ensures consistency across different profiles and is aligned with the reference camber distribution, which is the function of maximum camber.

The NACA16 profile with camber (NACA16-006) and with camber (NACA16-306 $a = 0.8$) is shown in the Figure 3.5.

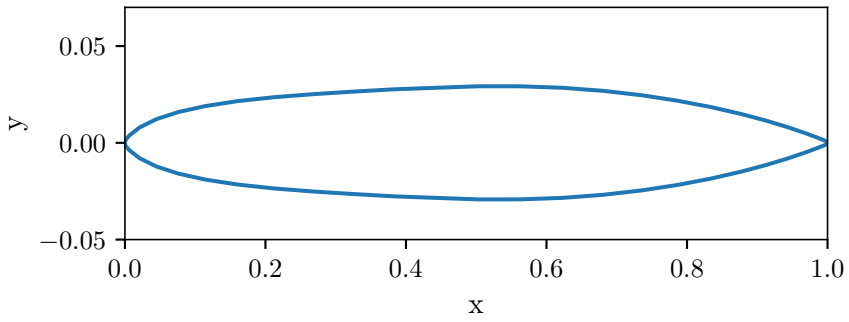

(a) NACA16-006 Profile

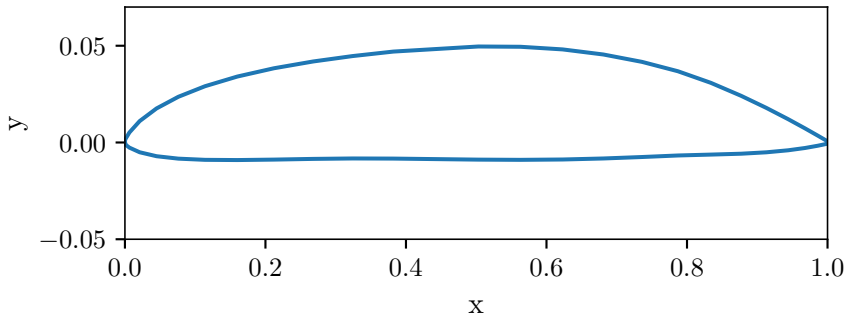

(b) NACA16-306 $a = 0.8$ Profile

Figure 3.5: NACA 16 series profiles

3.1.2.3 Modified NACA 66 Profile

NACA66 modified is the conventional NACA66 series thickened at the trailing edge for the ease of manufacturing. These profiles are used from CAESES directory, and a parabola is fitted after the maximum thickness location to get the required trailing edge thickness (Brockett et al., 1780). The parabola is given by the following equation,

$$y = -1.5427x^2 + 1.3884x + 0.1876 \tag{3.9}$$

The camber is defined by the meanlines described in Section 3.1.2.2. The NACA66mod without camber (NACA66-006 (mod)) and with camber (NACA66-306 (mod) a=0.8) is depicted in the Figure 3.6.

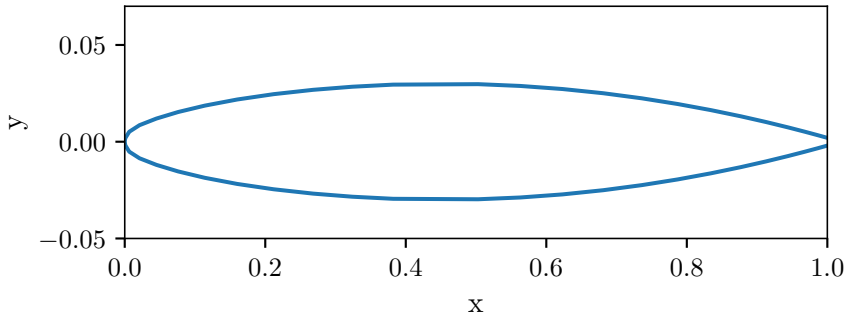

(a) NACA66-006 (mod) Profile

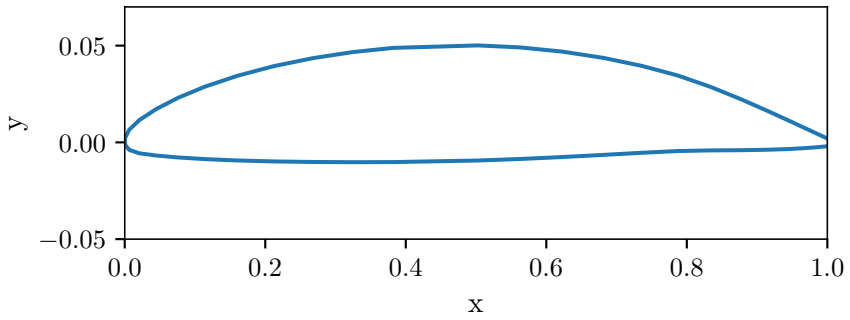

(b) NACA66-306 (mod) $a = 0.8$ Profile

Figure 3.6: Modified NACA 66 series profiles

3.1.3 Variable Profile Blade

The Variable Profile blade was developed by numbering the above-mentioned profiles and combining them to achieve a smooth blade. As described in the Section 3.1.1, a lofted surface was created by combining different profile sections. The profiles are numbered as integers and the combination of these numbers define the type of Variable Profile. The profile numbering is given in the Table 3.1.

Table 3.1: Numbering scheme of profiles

Profiles	Numbering System
NACA4D	1
NACA16	2
NACA66mod	3

The base profile is defined as the initial profile located at the root of the blade, which remains consistent until the switch station. A switch station is the radial location after which a different profile section is added to get a smooth blade. Beyond the switch station, the profile transitions to the designated switch profile. If the number of base profile and switch profile is identical, the blade will exhibit a single profile throughout. It is important to note that the NACA4D is not utilized in combination with other profiles, as it fails to produce

a smoothly lofted transition between the profiles. When the Base profile is NACA66mod and NACA16 is the switch profile, the propeller blade is referred to as Variable Profile 32 (VP32). When the Base profile is NACA16 and switch profile is NACA66mod, it is referred to as Variable Profile 23 (VP23). The parameters of the Variable Profile are listed in the Table 3.2. The lofted surface for VP32 and VP23 are shown in the Figure 3.7 and 3.8.

Table 3.2: Variable Profile Parameters

Parameters	Values
Base Profile	[1, 3]
Switch Profile	[1, 3]
Switch Station	[0.4, 0.9]

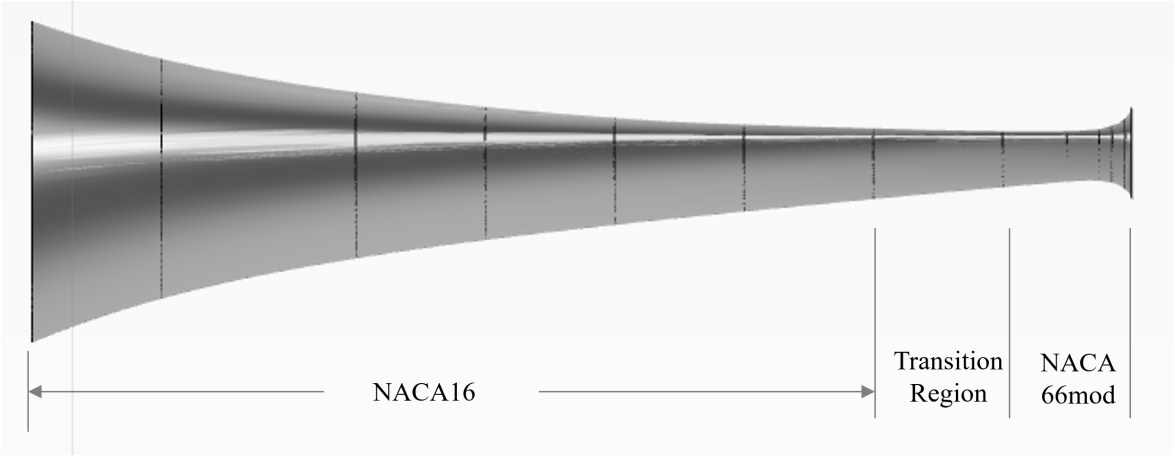

Figure 3.7: VP23 Profile Lofted Surface

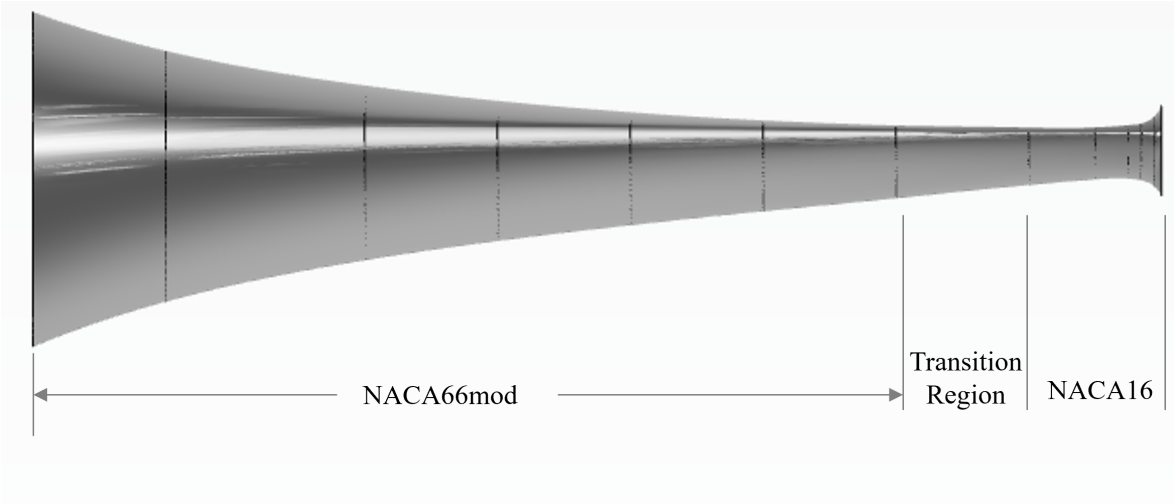

Figure 3.8: VP32 Profile Lofted Surface

3.2 Evaluation Methods

The simulation tools used for the evaluation of open water performance are described in this section. These open water tests are conducted on full-scale propeller blade.

3.2.1 Panel Method

The panel code panMARE is a command-driven program developed by TUHH that uses a three-dimensional low-order panel method to simulate arbitrary potential flows in marine applications. In this approach, the geometry of the body is discretised into flat quadrilateral elements. Appropriate boundary conditions are then applied, and a linear system of equations is solved to determine local velocities and pressure distribution. (TUHH). The fundamental equations are provided here but details can be found by Berger et al. (2016).

The panel method panMARE employs potential theory to analyse flow dynamics to compute the flow around various bodies submerged in a fluid. The configuration of the system is shown schematically in Figure 3.9. It shows the bodies involved, the surrounding fluid area and the corresponding nomenclature. These bodies, which may be solitary or multiple in number, are enclosed by a domain boundary that includes potential additional boundaries such as walls, a free surface, and the seabed. These elements constitute the external boundaries of the fluid domain. (TUHH).

The outward-facing normal of the surface points in the direction of fluid domain. As these bodies navigate through the domain, they are subjected to translations, rotations, and deformations in various combinations. The velocities associated with these movements are precisely known at every point on the surface. In cases where lift-generating bodies are involved, an additional wake surface is implemented to impede the flow around the around the trailing edge of the profile to fulfil the Kutta condition. This configuration ensures a comprehensive analysis of the fluid dynamics influenced by the structural movements within the domain.

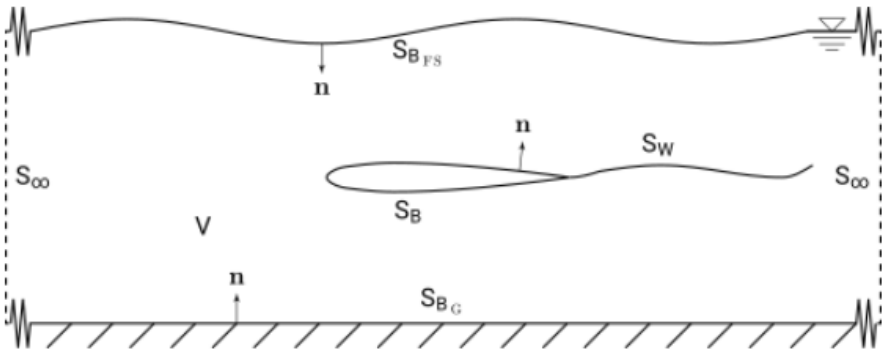

Figure 3.9: panMARE Boundaries. (TUHH).

In potential theory, the flow is presumed to be inviscid, irrotational, and incompressible, which allows for a simplification of the conservation equations. Consequently, this leads to the formulation of the incompressible and irrotational equation of continuity, commonly

known as the Laplace equation, for the velocity potential, which is given by,

$$\Delta\Phi = \nabla^2\Phi = 0 \tag{3.10}$$

The pressures are then evaluated using the Bernoulli equations given by,

$$\frac{p}{\rho} + gz + \frac{1}{2}v^2 + \frac{\partial\Phi}{\partial t} = \text{const.} \tag{3.11}$$

The velocity potential at a point in the fluid can be described by the following equation:

$$\Phi = \frac{1}{4\pi}\int_{S_B}\left[\mu\frac{\partial}{\partial n}\left(-\frac{1}{r}\right) - \sigma\left(-\frac{1}{r}\right)\right]dS + \frac{1}{4\pi}\int_{S_W}\left[\mu\frac{\partial}{\partial n}\left(-\frac{1}{r}\right)\right]dS + \Phi_{\text{ext}}$$

The body surface of the propeller is discretised using panels characterized by constant doublet and source strengths. For the wake sheet, only doublet strengths are utilized. As illustrated in Figure 3.10, the profile of the propeller is modelled using these panels. The wake sheet is attached to the trailing edge of the propeller profile and is constructed using wake panels that are aligned according to the flow direction. Each body panel, representing a segment of the propeller surface, moves through the fluid domain with a specific velocity, reflecting the interaction between the propeller and the surrounding fluid.

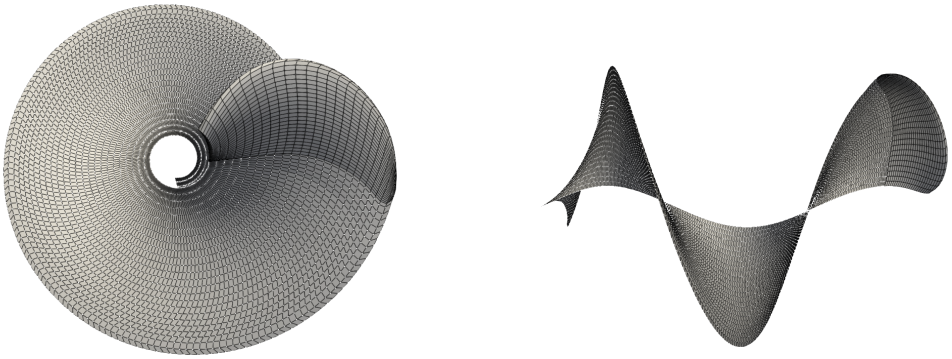

(a) Front View **(b)** Side View

Figure 3.10: panMARE Discretised Blade Panels

panMARE uses a low-order potential-based boundary element method to address the unsteady cavitating flow around propellers. The method involves solving for the steady-state oscillatory solution by incremental time-stepping. An iterative scheme is employed to evaluate the cavity shape and the dynamic boundary conditions. The solution is particularly characterized by its rapid convergence and consistency with fully nonlinear results. Two boundary conditions are introduced, which influence both the potential solution as well as the thickness of the cavitation sheet (Fine, 1992).

3.2.1.1 Blade Meshing and Mesh Independence

The blade is divided into pressure side surface and suction side surface. Both surfaces are divided into equal number of panels in spanwise and chordwise directions. This is called a Uniform Mesh. A higher number of panels are typically allocated towards LE and TE to better capture the high curvature areas. The resulting panel mesh is called Biased Mesh. However, in this study, only a uniform mesh without bias towards the leading edge is utilized. This approach showed satisfactory results for both cavitation analysis and open water tests (OWT). The meshed blade is shown in the Figure 3.11

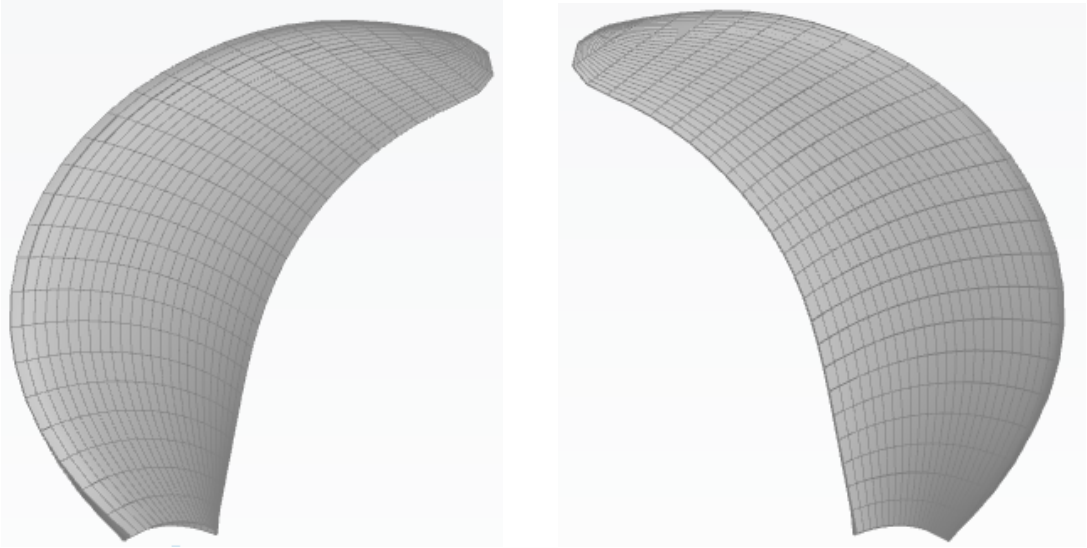

(a) Suction Side **(b)** Pressure Side

Figure 3.11: Blade Surface with Panel mesh

A mesh independence study is conducted to evaluate the appropriate number of panels for accurate results. Figure 3.12a and 3.12b shows the results for the K_T and $10K_Q$ for different number of panels in chord and span direction.

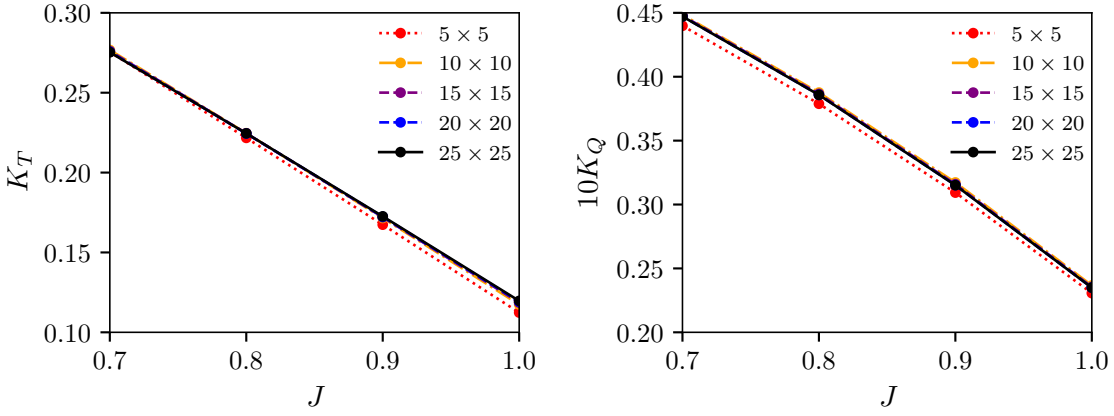

(a) Thrust Coefficient Convergence **(b)** Torque Coefficient Convergence

Figure 3.12: Open Water Performance Curves for number of panels

The percentage difference is plotted against the number of panels per blade giving a good understanding of the results (Figure 3.13). For both K_T and K_Q, the difference is less than 0.1% for 25x25 panels and higher. Therefore, 25 panels in each chordwise and spanwise direction are used for the analysis.

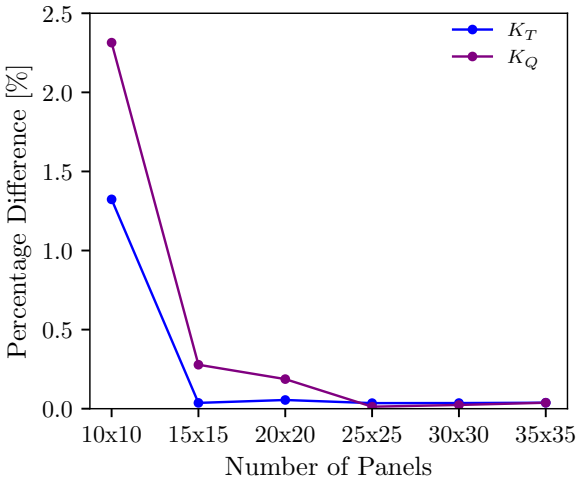

Figure 3.13: Grid Independence for panMARE

3.2.2 Computational Fluid Dynamics

For validation of the results from panMARE, RANS equations based simulations are conducted. ANSYS CFX is used to evaluate the performance of a single blade. The necessary steps involved in the modelling of the CFD simulation are detailed in this section.

3.2.2.1 Computational Domain

Only a single blade is modelled with a part of hub and cap to evaluate the accurate value of thrust and torque generated. The computational domain consists of an outer domain which contains an inlet and outlet for fluid. It also contains interfaces with the inner domain. The inner domain is the rotating domain that gives the rotational velocity to the fluid. It also contains the blade and the part of hub and cap. The sizes of domains are based on the industry experience. Figure 3.14 and Figure 3.15 show the major interfaces and sizes of the inner and outer domain.

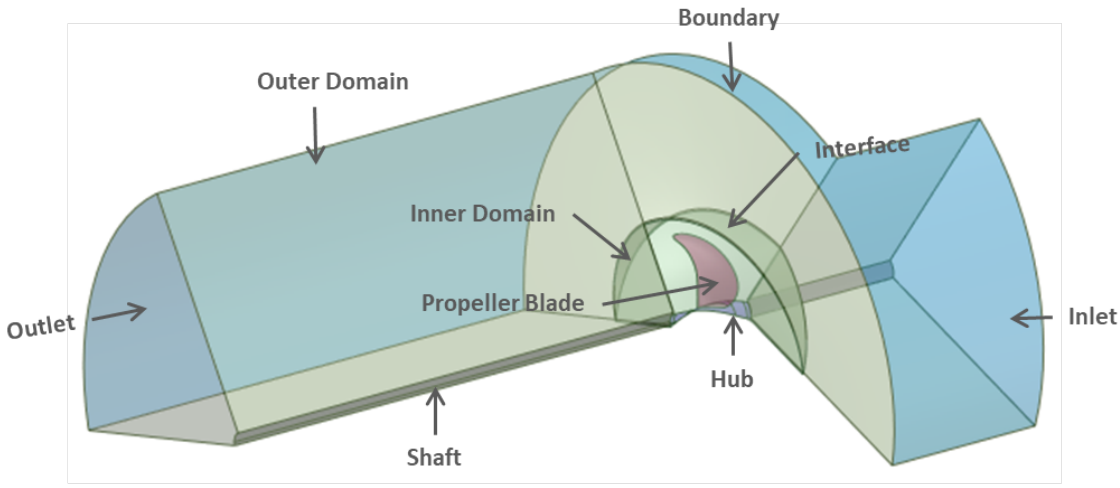

Figure 3.14: Computational Domains

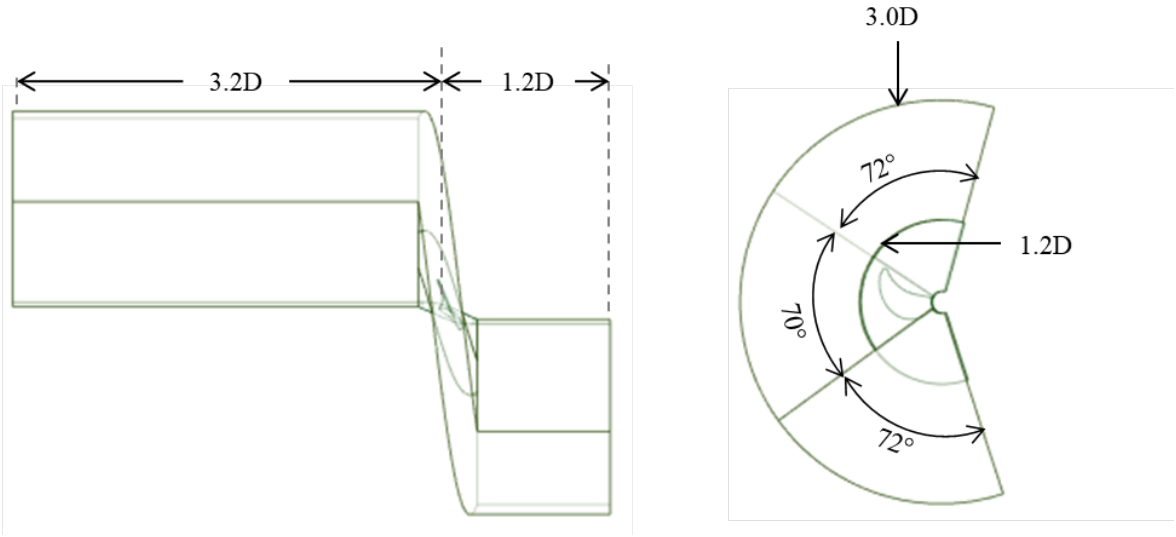

Figure 3.15: Computational Domain Major Dimensions

3.2.2.2 Governing Equations

This section details the governing equations used in the Reynolds-Averaged Navier-Stokes (RANS) simulation to analyse fluid flow around the propeller. The RANS equations are used in combination with the $k-\omega$ Shear Stress Transport (SST) turbulence model to accurately capture the complex turbulent flow characteristics.

The RANS equations are derived by decomposing the instantaneous velocity and pressure fields into their mean and fluctuating components (Wilcox et al., 1998). This decomposition leads to the following set of equations for incompressible flow:

$$\frac{\partial \overline{u_i}}{\partial t} + \overline{u_j}\frac{\partial \overline{u_i}}{\partial x_j} = -\frac{1}{\rho}\frac{\partial \overline{p}}{\partial x_i} + \nu\frac{\partial^2 \overline{u_i}}{\partial x_j^2} - \frac{\partial \overline{u_i' u_j'}}{\partial x_j} \tag{3.12}$$

$$\frac{\partial \overline{u_i}}{\partial x_i} = 0 \tag{3.13}$$

where:

- $\overline{u_i}$ = mean velocity components
- t = time
- ρ = fluid density
- $\overline{p}$ = mean pressure
- ν = kinematic viscosity
- $\overline{u_i' u_j'}$ = Reynolds stress tensor

The $k-\omega$ SST (Shear Stress Transport) model is used to model the turbulence effects. This model combines the advantages of the $k-\omega$ model in the near-wall region and the $k-\epsilon$ model in the free-stream region, providing more accurate predictions of flow separation and other turbulence phenomena.

The transport equations for the turbulent kinetic energy (k) and the specific dissipation rate (ω) are given by:

$$\frac{\partial k}{\partial t} + \overline{u_j}\frac{\partial k}{\partial x_j} = P_k - \beta^* k\omega + \frac{\partial}{\partial x_j}\left[(\nu + \sigma_k \nu_t)\frac{\partial k}{\partial x_j}\right] \tag{3.14}$$

$$\frac{\partial \omega}{\partial t} + \overline{u_j}\frac{\partial \omega}{\partial x_j} = \alpha\frac{\omega}{k}P_k - \beta\omega^2 + \frac{\partial}{\partial x_j}\left[(\nu + \sigma_\omega \nu_t)\frac{\partial \omega}{\partial x_j}\right] + 2(1-F_1)\frac{\sigma_{\omega 2}}{\omega}\frac{\partial k}{\partial x_j}\frac{\partial \omega}{\partial x_j} \tag{3.15}$$

where:

- P_k = production of turbulent kinetic energy
- ν_t = turbulent viscosity
- β^*, β, α, σ_k, σ_ω, $\sigma_{\omega 2}$ = model coefficients
- F_1 = blending function

The Reynolds stress tensor $\overline{u_i' u_j'}$ is modelled using the Boussinesq hypothesis, which relates the Reynolds stresses to the mean velocity gradients:

$$\overline{u_i' u_j'} = \nu_t\left(\frac{\partial \overline{u_i}}{\partial x_j} + \frac{\partial \overline{u_j}}{\partial x_i}\right) - \frac{2}{3}k\delta_{ij} \tag{3.16}$$

where:

- δ_{ij} = Kronecker delta

The turbulent viscosity ν_t is computed as:

$$\nu_t = \frac{k}{\omega} \tag{3.17}$$

The combination of the RANS equations with the $k-\omega$ SST turbulence model provides a

robust framework for simulating turbulent flows around the propeller. This approach captures the complex interactions between the fluid and the propeller, including flow separation and turbulence effects, ensuring accurate predictions of the flow characteristics and propeller performance.

3.2.2.3 Y+ Evaluation

While performing CFD simulations, especially using the RANS equations with turbulence model of $k-\omega$ SST model, the dimensionless wall distance Y^+ is an important parameter. It ensures that the boundary layer effects, and turbulence characteristics are captured effectively in the near-wall region (Wilcox et al., 1998).

The Y^+ value is a dimensionless distance used to describe the location of the first cell center off the wall in a CFD grid. It is defined as:

$$Y^+ = \frac{yu_\tau}{\nu} \tag{3.18}$$

The friction velocity u_τ is given by:

$$u_\tau = \sqrt{\frac{\tau_w}{\rho}} \tag{3.19}$$

Inflation layers are employed to capture this effect. The first cell height and the number of layers in the inflation are specified. The first cell height depends on the Reynolds number and at a specific region. The recommended ranges for Y^+ values are:

- $Y^+ \approx 1$: For resolving the viscous sublayer directly, which is often required for high-fidelity simulations.
- $Y^+ \approx 30$: For using wall functions, which approximate the near-wall region without directly resolving it.

The Y^+ value targeted for all the validation cases is taken as 30 evaluated at the root of the propeller blade. The inflation layers around the blade are shown in the Figure 3.16. The Y^+ contour of the MMG reference propeller blade is shown in the Figure 3.17a & 3.17b.

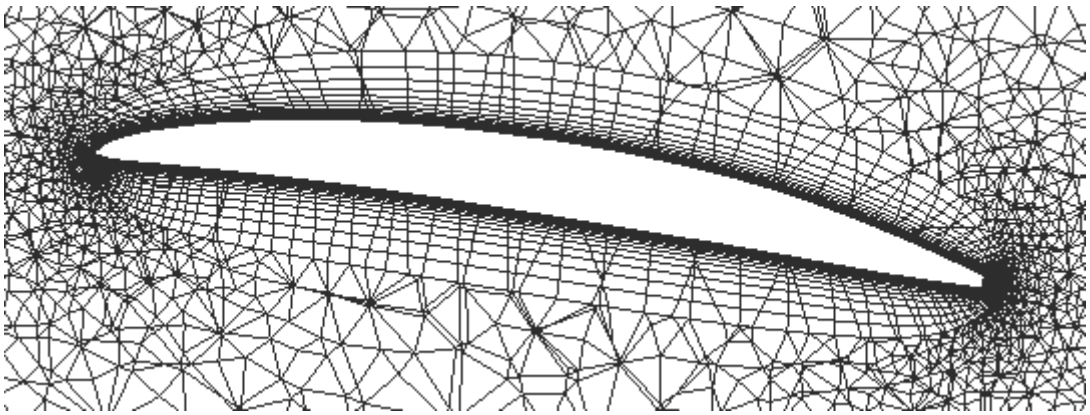

Figure 3.16: Chordwise Inflation Layers at r/R = 0.7

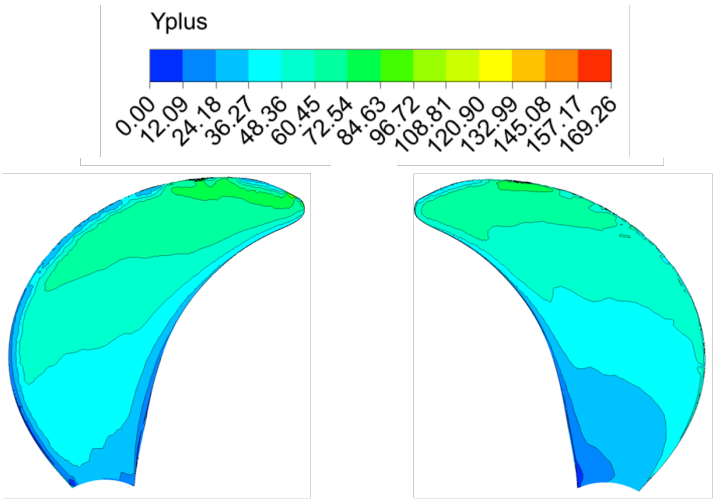

(a) Suction Side **(b)** Pressure Side

Figure 3.17: Y^+ Contours for MMG Baseline Propeller Blade

3.2.2.4 Meshing Strategy

ANSYS Meshing Tool is used for the meshing of Inner Domain (ID) and Outer Domain (OD). Tetrahedron mesh is used for the entire analysis. The inflation layers are defined using the first cell height. Patch names are created to assign mesh size to the faces. The sizes given to ID and OD are given in the Table 3.3 and 3.4. Pressure surface, suction surface, blade tip and trailing edge surface are refined. Moreover, refinement is also given to the leading edge to capture its effect on flow. Interfaces are meshed with similar refinement to achieve mesh conformity. The meshed blade is shown in the Figure 3.18. The meshed domains are also shown in the Figure 3.19b and 3.19a.

Table 3.3: Outer Domain Mesh Sizes

Patch Name	**Mesh Size [m]**
Inlet	0.8
Outlet	0.8
Side	0.8
Shaft	0.075
cyclic 1_1	0.8
cyclic 1_2	0.8
Prop Inlet	0.2
Prop Side	0.2
Prop Outlet	0.2

Table 3.4: Inner Domain Mesh Sizes

Patch Name	**Mesh Size [m]**
Prop Inlet	0.2
Prop Side	0.2
Prop Outlet	0.2
Hub_cap	0.1
Cyclic 2_1	0.22
Cyclic 2_2	0.22
PS & SS Surface	0.1
Tip & TE Surface	0.004
Leading Edge	0.004

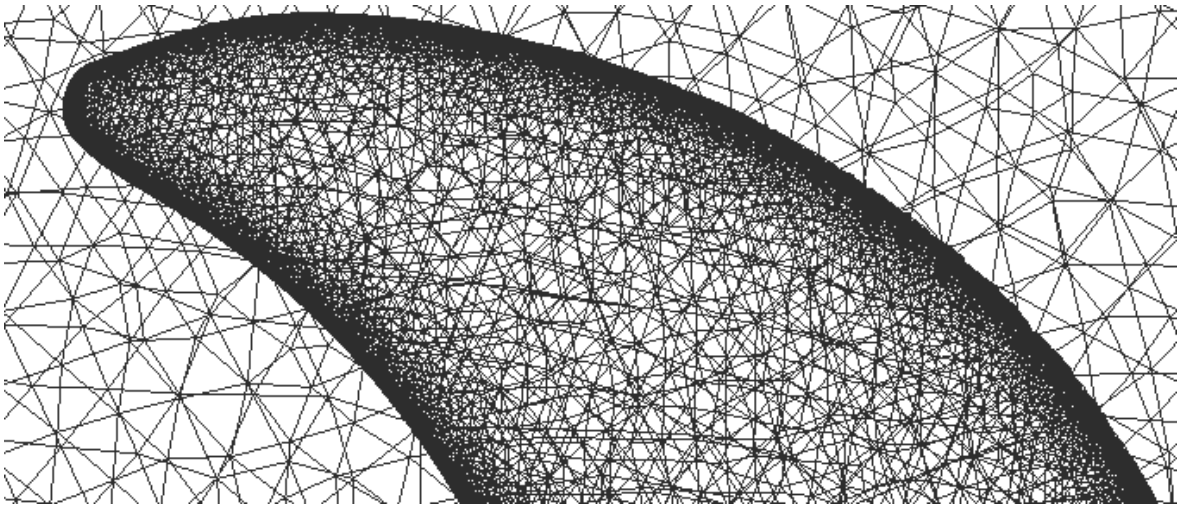

Figure 3.18: Meshed blade surface in ID

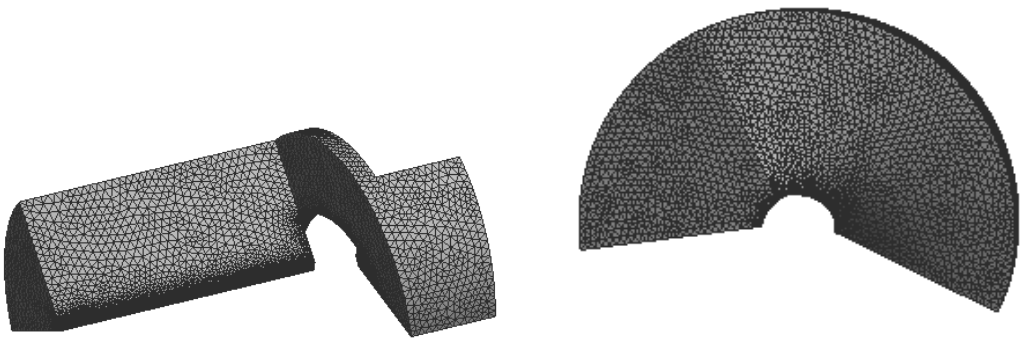

(a) Meshed Outer Domain **(b)** Meshed Inner Domain

Figure 3.19: Meshed Domains

3.2.2.5 Boundary Conditions

The physics of the setup is defined in the ANSYS CFX. The properties given to the patches made in previous sections are summarized in the Table 3.5

Table 3.5: Boundary Conditions

Name	Boundary Condition
OD	Stationary Domain
ID	Rotational Domain
Inlet	Velocity Inlet
Outlet	Pressure Outlet
Side	Free Slip Wall
Blade	No Slip Wall
Hub_cap	No Slip Wall
Interfaces	Domain Interface
Shaft	Free Slip Wall

The propeller rotational speed is defined as a boundary condition within the Inner Domain, and it is set to 1.2 rps. The inlet velocity is determined based on the advance ratio to be evaluated, as per equation 2.1.

3.2.2.6 Solution Convergence

The criterion for the solution convergence is the RMS values of the field variables. The tolerance that was set for these variables was 1×10^{-6}. A maximum number of iterations of 650 was found to be suitable for convergence and is used as stopping criteria. The convergence of the field variables and the desired output parameters (propeller blade thrust and torque) is shown in the Figure 3.20a and 3.20b. Notably, the residual convergence achieved is approximately 3.1×10^{-4}. The thrust and torque converge in 100 iterations.

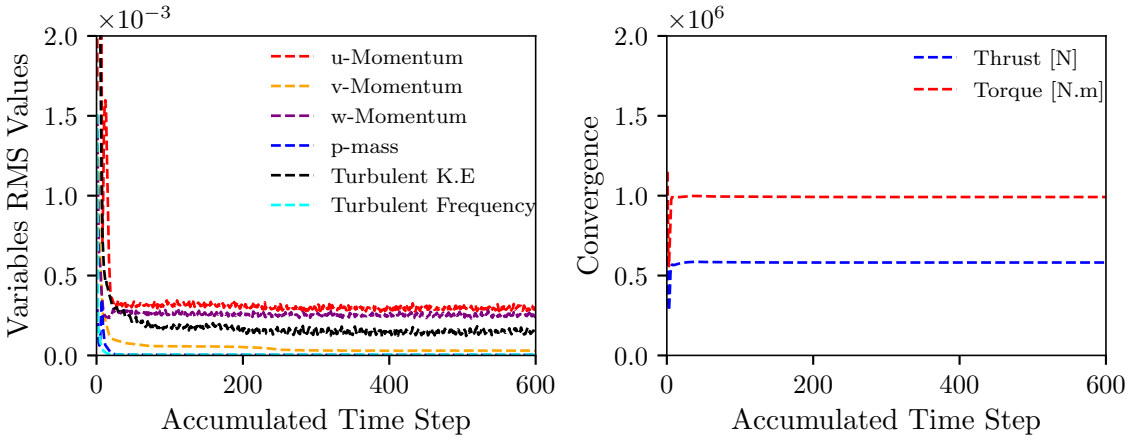

(a) Convergence of Residuals **(b)** Convergence of Thrust and Torque

Figure 3.20: RANS Convergence

3.2.2.7 Mesh Independence

A mesh independence study for the analysis is also conducted to ascertain the accuracy of solution. The mesh is generated with three different meshes (coarse, medium and fine). The sizes of the mesh given in the Table 3.3 and 3.4 are varied by the $\sqrt[3]{2}$. The fine mesh is generated by decreasing the size of the mesh by $\sqrt[3]{2}$ while the coarse mesh is generated by increasing the size by $\sqrt[3]{2}$. The variation in the K_T and K_Q is shown in the Figure 3.21.

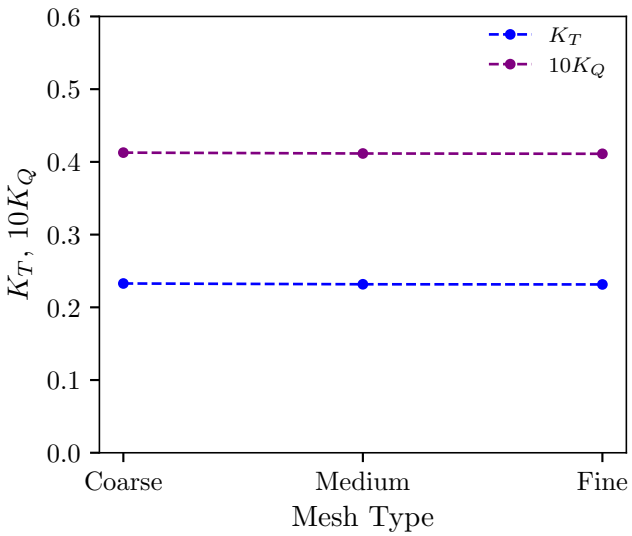

Figure 3.21: Thrust and Torque Coefficient Convergence

The percentage difference is evaluated for the different mesh sizes at J = 0.8 are given in the Table 3.6. For fine mesh, the difference is less around 0.1%. To save computational effort, the medium mesh size is used for the validation.

Table 3.6: Mesh Independence at J = 0.8

Mesh	Number of Elements	K_T	Percentage Difference	$10K_Q$	Percentage Difference
Coarse	2468341	0.23278	-	0.41274	-
Medium	2925925	0.23171	0.46	0.41154	0.29
Fine	3811998	0.23147	0.10	0.41112	0.11

3.2.3 Correction Factors

Klasson (2011) compares the accuracy of different computational methods with the Model Tests for predicting the open water performance of propellers. It highlights that the CFD provides the most accurate predictions but requires significant computational resources. The boundary element method offers a quicker alternative with sufficient accuracy for practical use. In model tests conducted at towing tank facilities, results are typically scaled up to account for scale effects due to Reynolds number. These corrections are necessary to accurately reflect full-scale conditions. But different methods used for scaling give different results introducing a deviation in the results (Bulten et al., 2014). Therefore, CFD simulations are used as a benchmark for the studies, providing a more consistent basis for comparison and validation across different variants.

The difference between the dimensionless propeller coefficients obtained from panMARE and ANSYS CFX is attributed to the Kutta Condition is imposed on the trailing edge in panMARE which prevents it from capturing the boundary layer and flow separation effects. Therefore, validation using a RANS eqauations based solver is carried out to compare the results. To make the results of panel code reliable, correction factors are applied to minimize errors. This step is crucial as the optimal solution depends on the choice of evaluation method and the optimal solution is expected to be with 1-2% gain in performance. Therefore, a high deviation between panMARE results and CFX results could give no net gain in performance. The correction factors evaluated using the ANSYS CFX for different profiles are given in the Table 3.7. Correction factors of NACA16 a = 0.8 Baseline are used for variable profile blade.

Table 3.7: Percentage Correction Factors for different profiles

Parameter	NACA16a0.8			NACA66moda0.8			NACA4D		
J	K_T	K_Q	η_o	K_T	K_Q	η_o	K_T	K_Q	η_o
0.7	-3.35	-2.02	-1.36	0.10	2.21	-2.07	-1.72	2.10	-3.75
0.8	-2.56	-0.55	-2.02	1.43	4.07	-2.53	-0.10	3.67	-3.64
0.9	-1.89	0.64	-2.52	2.85	5.86	-2.84	1.60	5.07	-3.30
1	-1.77	1.128	-2.86	4.33	7.40	-2.86	3.34	6.26	-2.75

The Open Water Performance curve for these profiles are given in the Figures below.

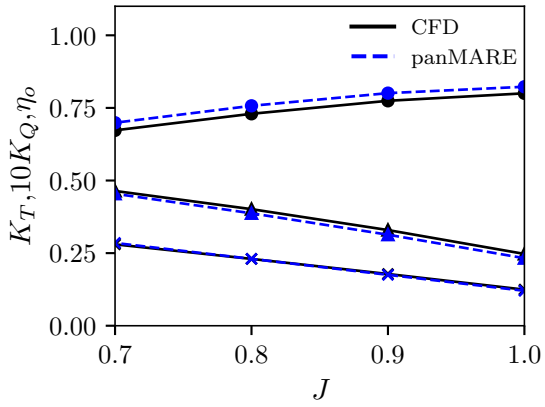

Figure 3.22: NACA4D Open Water Performance Curve (CFD vs panMARE)

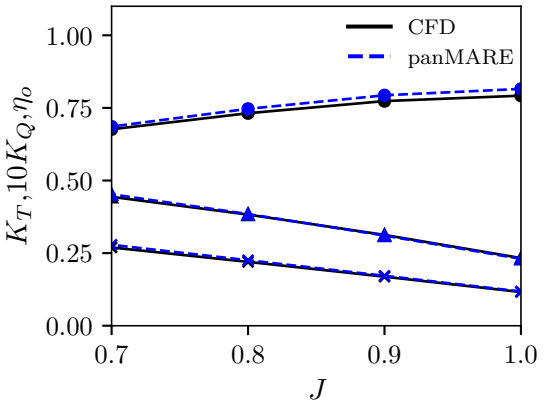

Figure 3.23: NACA16 a=0.8 Open Water Performance Curve (CFD vs panMARE)

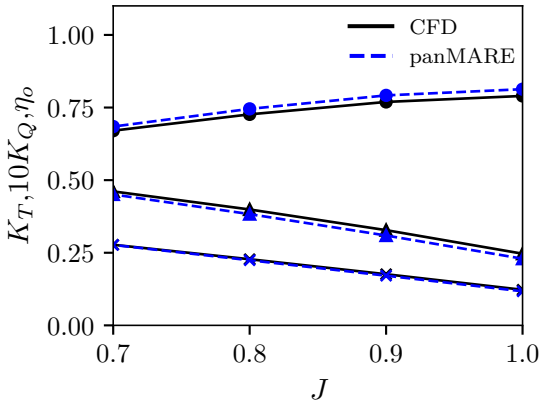

Figure 3.24: NACA66mod a=0.8 Open Water Performance Curve (CFD vs panMARE)

3.3 Optimization

Optimization is performed within the CAESES framework, complying with the recommended practice described by CAESES. First, the design space is explored to evaluate the influence of the design variables on the objective function. To evaluate this influence, a sensitivity analysis is performed using the Latin Hypercube Sampling (LHS). It is also referred as the Design Space Exploration (DSE). Subsequently, a local optimization with Dakota Local optimization is performed on the best variant of DSE to refine the design. However, the local optimization is also performed on baseline models with meanlines a=0.8 and a=1 (Section 3.1.2.2), because of their extensive use in the Propeller design.

Latin Hypercube Sampling is a statistical method used to generate a distribution of plausible collections of parameter values from a multidimensional distribution, which makes it particularly useful for sensitivity analysis. A key feature of LHS is stratified sampling, where each input distribution is divided into equal probability intervals with samples taken from each interval to ensure comprehensive exploration of the possible values (McKay et al., 2000). It is more efficient than random sampling, achieving better statistical properties with fewer samples. Additionally, LHS ensures that each input parameter is sampled independently, which prevents clustering of sample points (Dalbey et al., 2021; Adams et al., 2020).

Local Optimization in CAESES uses a gradient free local optimization strategy to find the best solution. It is a recommended method by CAESES to optimize an existing good design (CAESES, 2024).

3.3.1 Objective Function, Constraints and Design Variables

The main objective of the analysis is to reduce power delivered by the propeller and also keeping LRM in a specified range.

Objective function:

$$\text{minimize: } \mathbf{Power}$$

Constraint:

$$\mathbf{LRM}_{baseline} \leq \mathbf{LRM} \leq \mathbf{LRM}_{max}$$

The minimum LRM is set to be equal to the MMG Baseline value that is set as a benchmark for the study. The camber distribution is varied by using a cubic curve with weights that are connected to the camber distribution at three different points. These locations are at blade root, 0.6r/R and Blade tip. The variation in camber distribution is shown in the Figure 3.25. The change in the position of these points pulls the original camber distribution to modify them. Net variation allowed for these points is 9.5% of chord. This limit is chosen because it is the maximum allowed camber for NACA 4-digit series. Camber position is varied between 0.2 to 0.8 for NACA4D while type of meanline is varied from 0 to 1 for NACA16 and NACA66mod. For variable profile, the ranges of the design variables are the ones referred in Table 3.2. The ranges of all the design variables are tabulated in the Table 3.8.

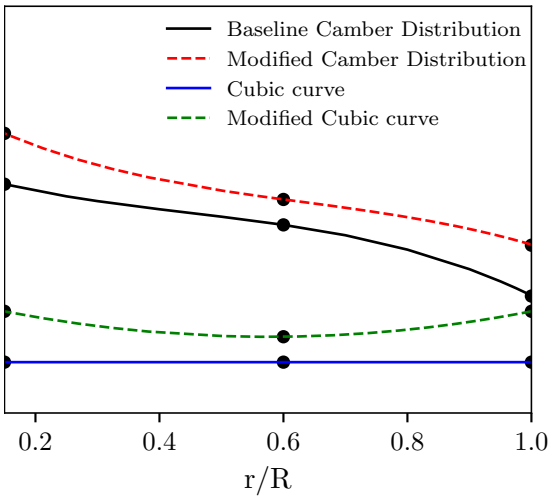

Figure 3.25: Variation of Camber Distribution

Table 3.8: Design Variables and their bounds

Design variables	**Lower Bound**	**Default**	**Upper Bound**
Camber point at Root (c_{root})	-0.035	0	0.060
Camber point at 0.6 r/R ($c_{0.6r/R}$)	-0.027	0	0.068
Camber point at Tip (c_{tip})	-0.013	0	0.082
Maximum Camber Position (p)	0.2	0.5	0.8
Type of meanline	0	0.8	1

This page intentionally left blank.

4

Case Studies

This chapter discusses the results of the propeller optimization analysis. First, a benchmark for open water performance and cavitation with the MMG baseline propeller is established. Following this, the performance optimization results are studied for the NACA profiles and Variable Profiles along with the sensitivity analysis. The validity of the results are then assessed by comparing the results with the CFD simulations.

4.1 Benchmark

4.1.1 Propeller Particulars

The propeller selected for analysis is conventional MMG propeller designed for 8000 TEU container vessel. The key features and parameters of the propeller are summarized in Table 4.1, providing an overview of the critical specifications used in the modelling process. The propeller geometry is shown in the Figure 4.1

Table 4.1: Propeller Particulars

Parameters	Values
Number of blades	5
Diameter [m]	9.6
Hub Diameter [m]	1.5
P/D	1.083
EAR	0.584

(a) Front View **(b)** Side View

Figure 4.1: Propeller Geometry

4.1.2 Distributions

The distribution of the MMG Baseline propellers used for benchmarking are given the following figures.

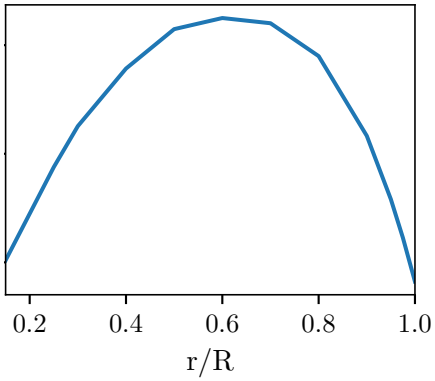

Figure 4.2: Pitch distribution

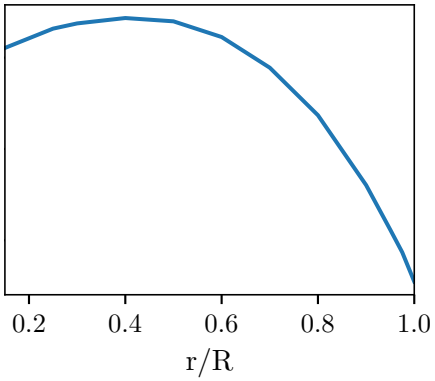

Figure 4.3: Skew distribution

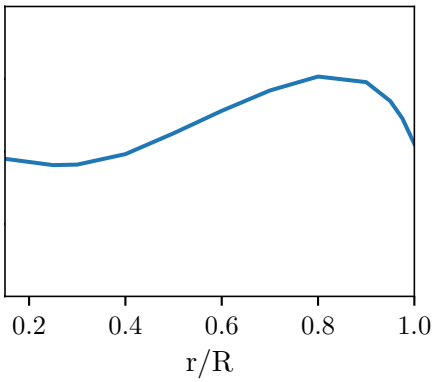

Figure 4.4: Rake distribution

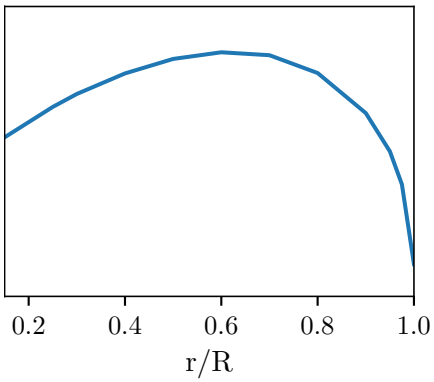

Figure 4.5: Chord distribution

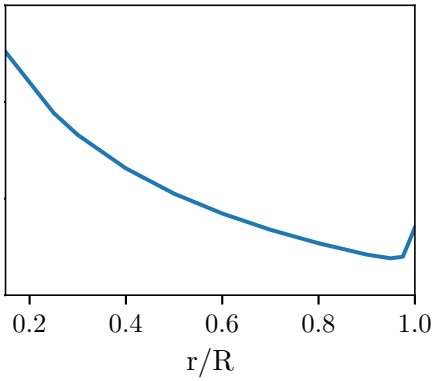

Figure 4.6: Thickness distribution

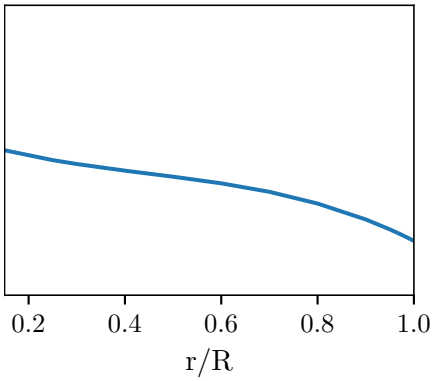

Figure 4.7: Camber distribution

4.1.3 Design Point

The propeller Design point is evaluated using the thrust identity method described in section 2.2. The parameters used for the design point evaluation are given in the Table 4.2. The script for evaluating power and LRM at design point is given in the Appendix D.1.

Table 4.2: Parameters for Design Point Evaluation

Parameters	Values
Vessel Speed [kn]	22.8
Wake Fraction	0.166
Rotative Efficiency	1.003
J_T	0.83958
K_T	0.21395

4.1.4 Results

A propeller with MMG Baseline profile and distributions is the benchmark for the comparison. The design point of a propeller generally lies between the advance ratio of 0.7 to

1.0. Therefore, Open Water test is conducted at these four advance ratios. The Pressure distribution on propeller blade evaluated using CFD is shown in the Figure 4.8a and 4.8b.

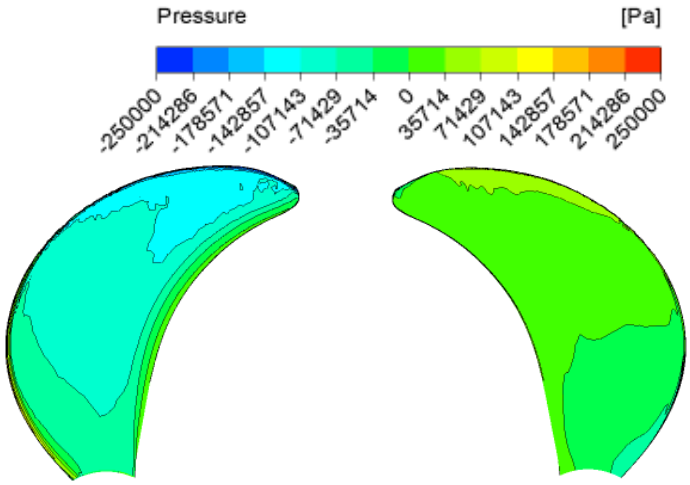

(a) Suction Side **(b)** Pressure Side

Figure 4.8: Pressure Contours of MMG Baseline Propeller Blade

The thrust and torque of the blade are evaluated from simulation and converted to the dimensionless coefficient. The performance curves are evaluated with CFD. The performance curves show typical behaviour where increases in advance ratio leads to a decrease in thrust and torque coefficient. This is due to the decrease in the angle of attack on the propeller blade as the ship speed increases. The performance curves of the propeller are shown in the Figure 4.9.

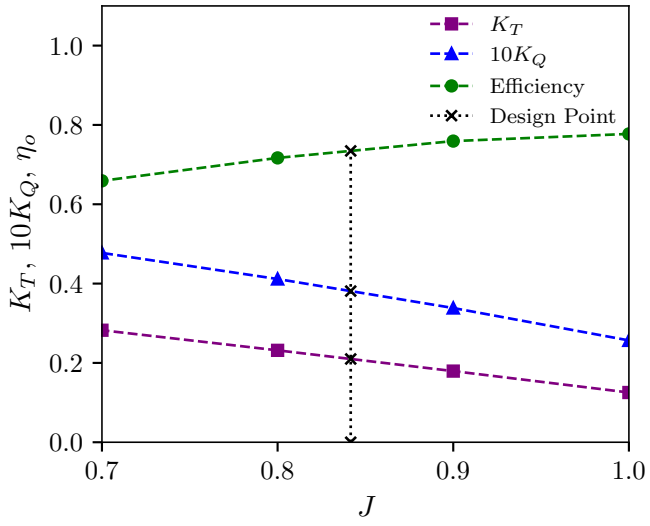

Figure 4.9: MMG Baseline Propeller Performance Curves

The design point evaluated using the thrust identity method is also shown in the Figure 4.9. The performance parameters of the MMG baseline are given in the Table 4.3. The design

point lies between the advance ratio of 0.8 and 0.9. The LRM evaluated using the method comes out to be 2.45%.

Table 4.3: MMG Baseline Performance Results

Parameters	Values
J	0.84163
K_T	0.20992
K_Q	0.03811
η_o	0.73822
Power $[kW]$	35525.95
$n_{nominal}[rps]$	1.17757
$n_{inter}[rps]$	1.20645
LRM [%]	2.45

4.2 Scenario-I

This section discusses the optimization carried out with single profile. The camber distribution and other parameters are varied to get an optimum power consumption. The LRM evaluated for all the cases must be greater than the LRM of benchmark which is 2.45%.

4.2.1 NACA4D

The optimization problem for NACA4D as following.

$$\begin{aligned} &\text{minimize:} && \mathbf{Power} \\ &\text{subject to:} && \mathbf{2.45\% \leq LRM \leq 6\%} \\ & && \mathbf{-0.035 \leq c_{root} \leq 0.060} \\ & && \mathbf{-0.027 \leq c_{0.6r/R} \leq 0.068} \\ & && \mathbf{-0.013 \leq c_{tip} \leq 0.082} \\ & && \mathbf{0.2 \leq p \leq 0.8} \end{aligned} \tag{4.1}$$

4.2.1.1 Sensitivity Analysis

The dependence of power on the design variables is discussed in this section. A design space exploration on propeller with baseline distributions and NACA4D profile is studied using the Dakota Sensitivity Analysis by Latin Hypercube Method (see section 3.3). The effect of variation in camber at root is small. The power decreases slightly by decreasing the camber along the radial direction. However, the change in camber at root changes the overall distribution of the camber in radial direction. The effect of variation of camber at root on the delivered power is depicted in the Figure 4.10.

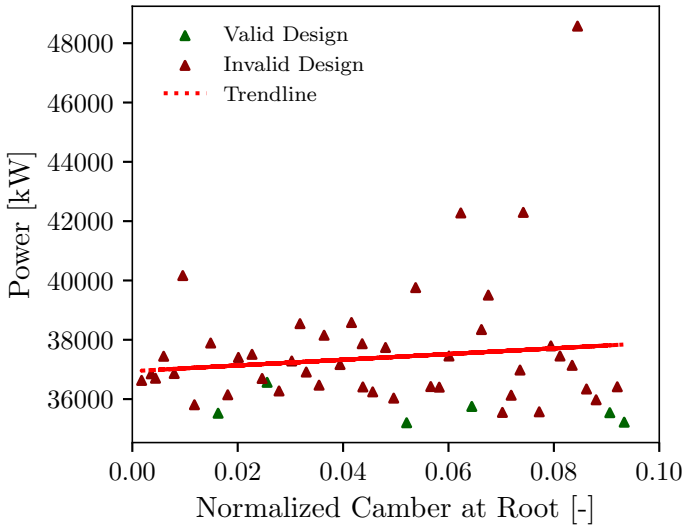

Figure 4.10: Variation of Power with Root Camber

Change in camber at the 0.6r/R has the highest influence on the power. The majority of thrust developed by a propeller is from 0.6r/R and upwards. The influence of the camber at r/R = 0.6 is depicted in the Figure 4.11. From the figure it can be seen that for high camber the power exceeds 40000 kW which is an anomaly. These outliers pop up because of the limitation of design point evaluation script. As camber increases, the design advance ratio increases. Since the simulations are only conducted for advance ratio between 0.7-1, any design point beyond $J = 1$ will result in incorrect output. It is the limitation of interpolation function used to evaluate the design point.

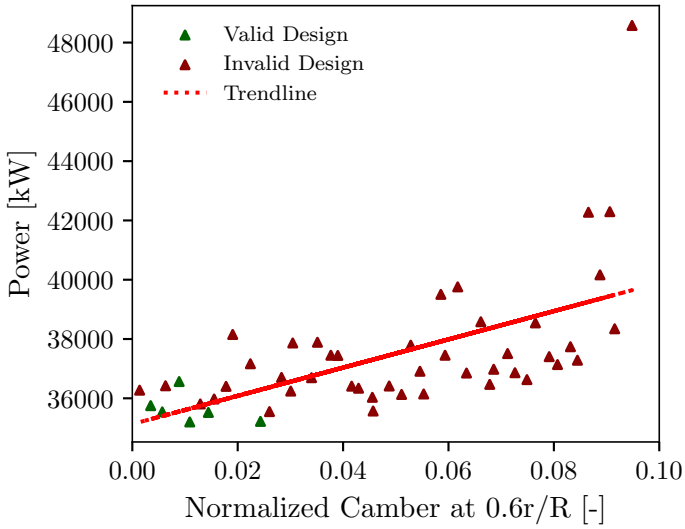

Figure 4.11: Variation of Power with Camber at 0.6r/R

The effect of variation in camber at the tip on the delivered power is less impactful as compared to the camber at 0.6r/R. Its influence is greater than the root camber variation as the slope of trendline is higher as compared to the root camber. The influence of the tip

camber is shown in the Figure 4.12.

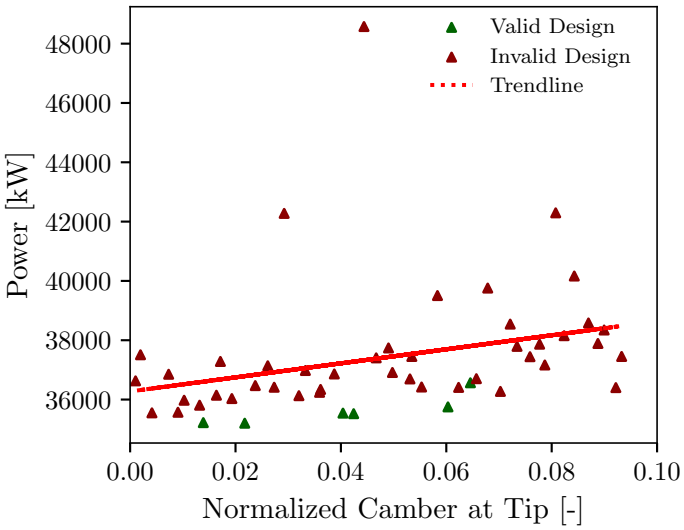

Figure 4.12: Variation of Power with Camber at Tip

The Maximum Camber Position for NACA4D has a small effect on the delivered power. The variation of Maximum Camber Position against the objective function is depicted in the Figure 4.13.

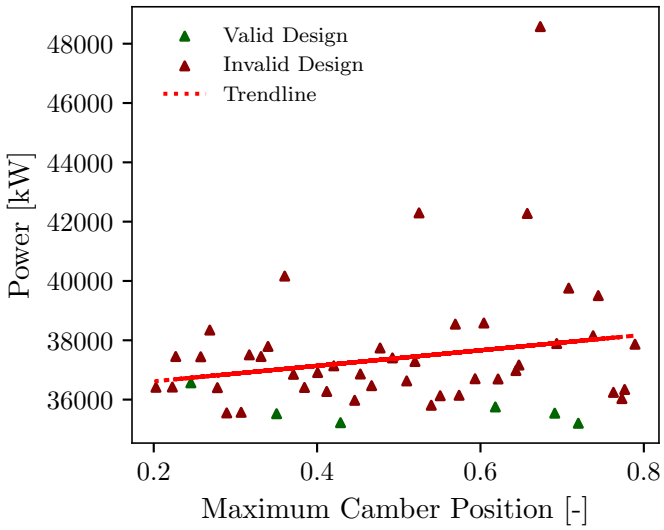

Figure 4.13: Variation of Power against Maximum Camber Position

4.2.1.2 Local Optimization

The local optimization on NACA4D is carried out near the baseline camber distribution. The optimizer converges below 50 iterations, and the same number of iterations were given to other profiles as well. The convergence of the results is given in the Figure 4.14.

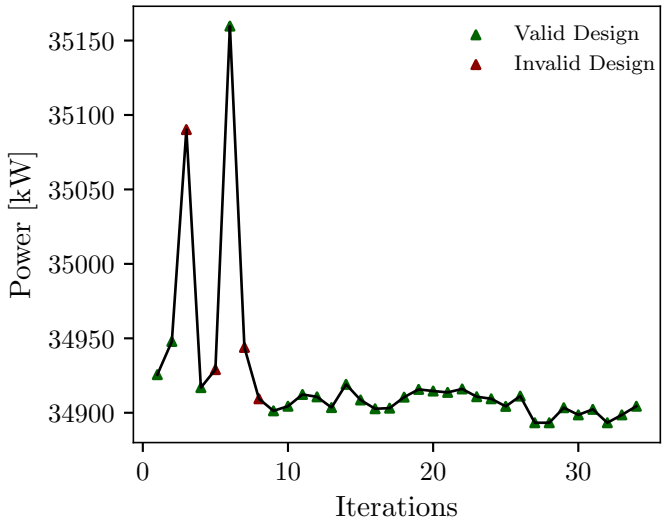

Figure 4.14: NACA4D Optimization

The minimum power at design point for the baseline and optimized NACA4D profile are compared with the Baseline MMG Design. The results of the performance of optimized NACA4D profiles are given in the Table 4.4. For NACA4D Baseline, 1.69% improvement was found and about 1.78% for the optimized version. The Open Water Performance curves are given in Appendix B.2 and the pressure distribution on the blade is given in the Appendix A.2.

Table 4.4: NACA4D Design Point Performance Results

Parameters	**NACA4D Baseline**	**NACA4D Optimized**
J	0.84003	0.84493
K_T	0.20921	0.21153
K_Q	0.03725	0.03787
η_o	0.75121	0.75143
Power $[kW]$	34925.59	34893.30
$n_{nominal}[rps]$	1.17091	1.17055
$n_{inter}[rps]$	1.21293	1.20590
LRM [%]	3.59	3.02
Power Reduction [%]	**1.69**	**1.78**

The comparison of the Camber Distribution is given in the Figure 4.15. The maximum camber position for NACA4D optimized version is 0.498 which is quite close to 0.5. The optimized blade is in the vicinity of the baseline version and is a local optimum. It is important to note that the NACA4D profiles are generally not used in Marine propellers design because of their thin trailing edge. They are incorporated in the study as a starting point because of their ease of parametrization. Furthermore, they do not perform well in cavitation as described in the section 5.

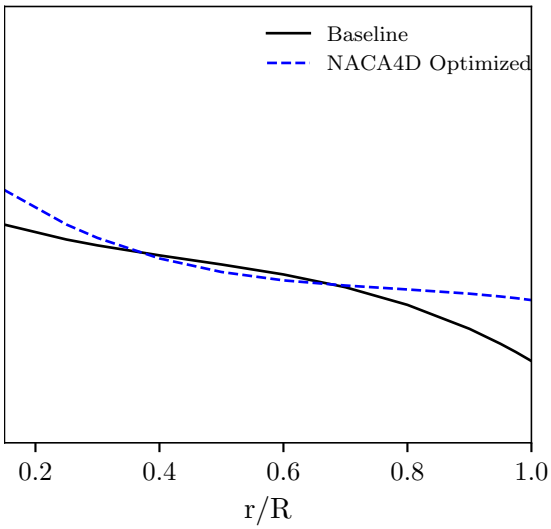

Figure 4.15: NACA4D Camber Distribution

4.2.1.3 Validation

For NACA4D, the results for validation are given in the Table 4.5. The results of CFD are quite close to panMARE results because of the inclusion of correction factors. The pressure distribution on the blade evaluated by CFD is given in the Appendix B.1 and comparison of Open Water performance curves is given in the Appendix B.2.

Table 4.5: NACA4D Design Point Performance CFD Results

Parameters	**NACA4D Baseline**	**NACA4D Optimized**
J	0.84010	0.84642
K_T	0.20924	0.21221
K_Q	0.03726	0.03805
η_o	0.75133	0.75169
Power $[kW]$	34919.51	34871.55
$n_{nominal}[rps]$	1.17084	1.17031
$n_{inter}[rps]$	1.21283	1.20377
LRM [%]	3.59	2.86
Power Reduction [%]	**1.71**	**1.84**

4.2.2 NACA16

The optimization problem defined for the NACA16 profile is given as follows

$$\begin{aligned} \text{minimize:} \quad & \mathbf{Power} \\ \text{subject to:} \quad & \mathbf{2.45\%} \leq \mathbf{LRM} \leq \mathbf{6\%} \\ & \mathbf{-0.035} \leq \mathbf{c}_{root} \leq \mathbf{0.060} \\ & \mathbf{-0.027} \leq \mathbf{c}_{0.6r/R} \leq \mathbf{0.068} \\ & \mathbf{-0.013} \leq \mathbf{c}_{tip} \leq \mathbf{0.082} \\ & \mathbf{0} \leq \mathbf{a} \leq \mathbf{1} \end{aligned} \tag{4.2}$$

4.2.2.1 Sensitivity Analysis

The sensitivity study for the camber weights for NACA16 is assumed to be same as the NACA4D as described in the Section 4.2.1. The trends are assumed to be similar because the increase in camber results in increased torque and hence the delivered power. But its influence depends on the radial location on the blade.

The Maximum Camber Position for NACA4D and the Type of Meanline has a similar effect on the geometry and performance of the propeller blade. In both cases, the location of maximum camber varies along the chord. Essentially changing the meanline alters the 2d distribution of camber along chord length and moves the location of the maximum camber along chord length. The maximum camber position for the meanline varies from 0.3 for a=0 to 0.5 for a=1. The variation of Maximum Camber Type of Meanline against the objective function is depicted in the Figure 4.16. The influence of Type of Meanline on power is also very small.

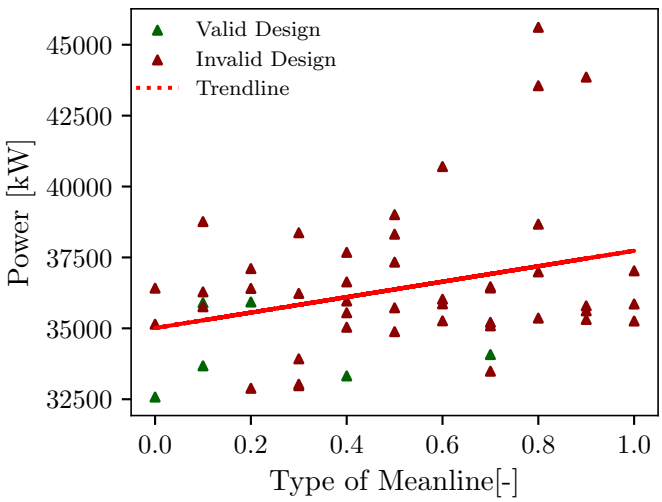

Figure 4.16: Variation of Power against Type of Meanline

4.2.2.2 Local Optimization

NACA16 profiles are most commonly used in the marine industry for propeller design. Three different optimized versions of the NACA16 profiles with different meanlines are obtained. Apart from the a=0.8 and a=1, the best variant from design space exploration is also optimized. The convergence plots of these optimized versions is given in Appendix A.1. The design point of these optimized versions is given in the Table 4.6.

Table 4.6: NACA16 Design Point Performance Results

Parameters	**NACA16 a=0.8 Baseline**	**NACA16 a=0.8 Optimized**	**NACA16 a=0 Optimized**	**NACA16 a=1 Optimized**
J	0.82948	0.85350	0.86385	0.84482
K_T	0.20469	0.21520	0.21846	0.21132
K_Q	0.03617	0.03826	0.03734	0.03768
η_o	0.74744	0.76443	0.80486	0.75441
Power $[kW]$	35222.44	34199.10	32186.90	34730.10
$n_{inter}[rps]$	1.17420	1.16284	1.14051	1.16874
$n_{inter}[rps]$	1.22835	1.19379	1.17949	1.20605
LRM [%]	4.61	2.66	3.42	3.19
Power Reduction [%]	**0.85**	**3.73**	**9.40**	**2.24**

The maximum reduction in delivered power is 9.4% achieved by the optimizer for the variant NACA16 a = 0 Optimized (Best design space exploration candidate). This is too good to be true as it was observed for the models with lower meanlines. The results are validated by CFD (discussed in subsequent section). This is because of the problems in geometry for lower meanlines (irregular leading edge). This can be seen in the Figure 4.17. Moreover, the correction factors are evaluated only for meanline a=0.8 which affects the design point and optimized solution evaluation. The camber distribution of the optimized profiles is given in the Figure 4.18.

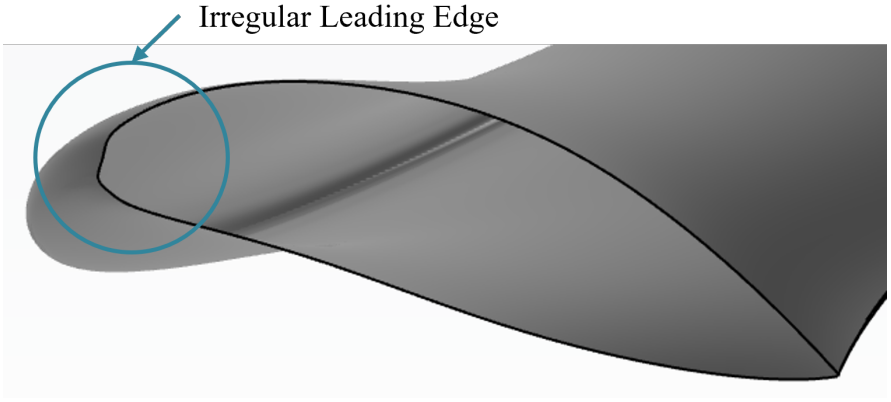

Figure 4.17: NACA16 a = 0 Optimized blade geometry (Faulty L.E at root)

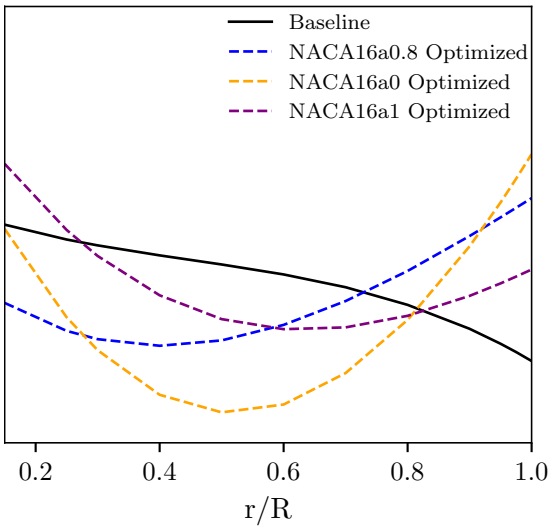

Figure 4.18: NACA16 Camber Distribution

The distribution suggests that the decrease in camber at 0.6r/R gives least power since the torque is less as the camber reduces. The camber on root and tip has a slight effect on power that is why the camber at tip varies significantly from the baseline. The optimization convergence plots for NACA16 are given in the Appendix A.1 and the pressure distribution at J = 0.8 on the blade is given in Appendix A.2.

4.2.2.3 Validation

The results for NACA16 are given in the Table 4.7. The results obtained are quite different from the optimization. Reduction in power is observed for all the variants except for NACA16 a=0 Optimized variant. This is because of the irregular leading edge and different meanline used for correction factors as discussed earlier. For the NACA16 a=0 Optimized, the LRM is 9.74% which is out of the range of the constraints.

The maximum power reduction achieved is for NACA16 a=1 Optimized of about 1.14%. However, the improvement is about half as compared to the results obtained from panMARE. The reason for difference in results is the change of geometry and the effect of viscous drag and flow separation.

Table 4.7: NACA16 Design Point Performance CFD Results

Parameters	NACA16 a=0.8 Baseline	NACA16 a=0.8 Optimized	NACA16 a=0 Optimized	NACA16 a=1 Optimized
J	0.82968	0.83312	0.78856	0.83620
K_T	0.20477	0.20616	0.18614	0.20753
K_Q	0.03619	0.03670	0.03134	0.03695
η_o	0.74752	0.74522	0.74587	0.74781
Power [kW]	35215.46	35270.42	35513.67	35121.59
$n_{nominal}[rps]$	1.17413	1.17474	1.17744	1.17308
$n_{inter}[rps]$	1.22807	1.22299	1.29209	1.21849
LRM [%]	4.59	4.11	9.74	3.87
Power Reduction [%]	**0.87**	**0.72**	**0.03**	**1.14**

4.2.3 NACA66mod

The optimization problem NACA66 mod profile is same as NACA16 (Equation 4.2).

4.2.3.1 Senstivity Analysis

The sensitivity study for the camber distribution for NACA66mod is assumed to be same as the NACA4D as described in the Section 4.2.1. Moreover, the effect of variation of type of meanline on power is also small and assumed to be similar to NACA16 (See Section 4.2.2).

4.2.3.2 Local Optimization

NACA66mod profiles are also optimized with three different meanlines similar to NACA16. The DSE best version is also with meanline a=0 and is also optimized using local optimization. The pressure distribution on the blade for advance ratio of 0.8 is given in the Appendix A.2. The convergence plots are given in the Appendix A.1. The results of design point evaluation are also given in the Table 4.8.

Table 4.8: NACA66mod Design Point Performance Results

Parameters	**NACA66mod a=0.8 Baseline**	**NACA66mod a=0.8 Optimized**	**NACA66mod a=0 Optimized**	**NACA66mod a=1 Optimized**
J	0.83754	0.85120	0.86911	0.84598
K_T	0.20811	0.21369	0.22178	0.21180
K_Q	0.03719	0.03775	0.03835	0.03781
η_o	0.74624	0.76725	0.80030	0.75457
Power $[kW]$	35181.40	34016.30	32466.40	34706.80
$n_{nominal}[rps]$	1.17375	1.16081	1.14361	1.16848
$n_{inter}[rps]$	1.21654	1.19702	1.17235	1.20439
LRM [%]	3.65	3.12	2.51	3.07
Power Reduction [%]	**0.97**	**4.25**	**8.61**	**2.31**

The maximum improvement in Power is 8.61% observed for the variant with a=0 meanline. A similar issue as observed earlier in the case of NACA16 can be observed here with unclean geometry of NACA66mod. The Open Water Performance curves of these variants show the difference between the panMARE and CFD results (Appendix B.2). The camber distribution for the optimized versions is shown in the Figure 4.19. A completely different camber distribution was observed for the optimized versions with meanline a=0.8 and a=0 with high camber at root and tip and low camber at 0.6r/R.

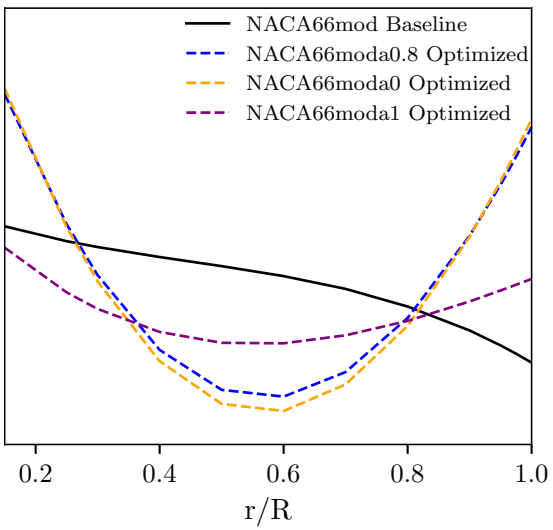

Figure 4.19: NACA66mod Camber Distribution

4.2.3.3 Validation

The results for NACA66mod are given in the Table 4.9. No improvement in power is observed for NACA66mod a=0.8 optimized and NACA66mod a=0 optimized. The camber distribution for both variants is shown in Figure 4.18, and it is observed that the high camber is attained on the root of blade. Such high thickness to higher camber ratios, result in an irregular leading edge whose effect is not completely captured by the potential solver. This is because of the Kutta condition as the flow in panMARE leaves at trailing edge. But in case of CFD, irregular surface results in flow separation increasing the drag. The irregular L.E at the root of NACA66mod a = 0 Optimized propeller blade is shown in the Figure 4.20.

Table 4.9: NACA66mod Design Point Performance CFD Results

Parameters	**NACA66mod a=0.8 Baseline**	**NACA66mod a=0.8 Optimized**	**NACA66mod a=0 Optimized**	**NACA66mod a=1 Optimized**
J	0.83775	0.82051	0.79373	0.83854
K_T	0.20820	0.20108	0.18968	0.20853
K_Q	0.03722	0.03549	0.03229	0.03730
η_o	0.74632	0.74022	0.74242	0.74650
Power [kW]	35175.57	35706.64	35885.38	35155.92
$n_{nominal}[rps]$	1.17368	1.17958	1.18156	1.17347
$n_{inter}[rps]$	1.21623	1.24179	1.28368	1.21509
LRM [%]	3.62	5.27	8.64	3.55
Power Reduction [%]	**0.99**	**-0.51**	**-1.01**	**1.04**

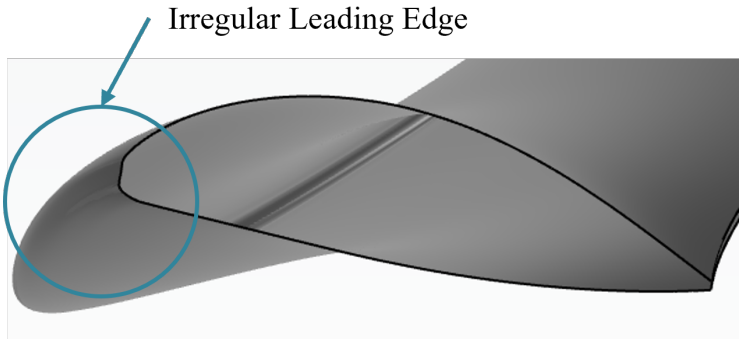

Figure 4.20: NACA66mod a = 0 Optimized blade geometry (Faulty L.E at root)

4.3 Scenario-II

This section comprises of analysis of Variable Profile where the combination of two different NACA sections are used to develop a blade.

4.3.1 Variable Profile

The optimization problem defined for the Variable profile is given as:

$$\begin{aligned} \text{minimize:} \quad & \mathbf{Power} \\ \text{subject to:} \quad & \mathbf{2.45\%} \leq \mathbf{LRM} \leq \mathbf{6\%} \\ & \mathbf{-0.035} \leq \mathbf{c}_{root} \leq \mathbf{0.060} \\ & \mathbf{-0.027} \leq \mathbf{c}_{0.6r/R} \leq \mathbf{0.068} \\ & \mathbf{-0.013} \leq \mathbf{c}_{tip} \leq \mathbf{0.082} \\ & \mathbf{0} \leq \mathbf{a} \leq \mathbf{1} \\ & \mathbf{0.4} \leq \mathbf{switchstation} \leq \mathbf{0.9} \end{aligned} \tag{4.3}$$

Switch station is added to constraints as the location of switch profile is important parameter to study.

4.3.1.1 Senstivity Analysis

The sensitivity study for the camber weights for Variable Profile is also assumed to be same as the NACA4D as described in the Section 4.2.1. Moreover, the effect of variation of type of meanline on power is also small and assumed to be similar to NACA16 (See Section 4.2.2). Switch station is an important design variable for Variable Profile Propeller and its effect on power is also evaluated. The effect of switch station on the power is not high as depicted in the Figure 4.21.

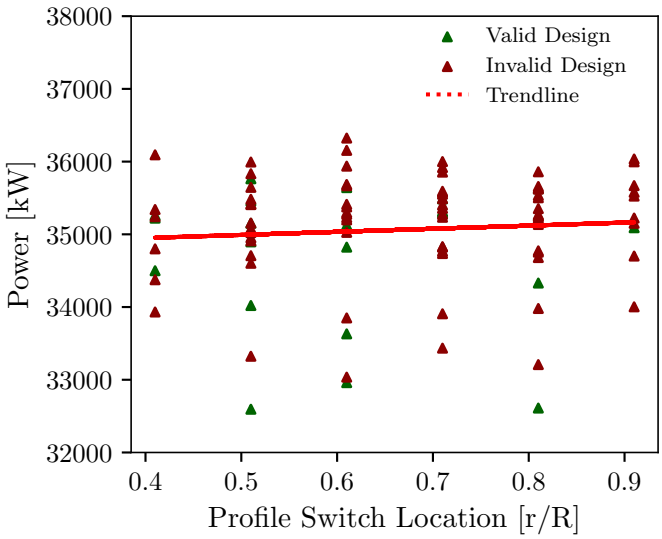

Figure 4.21: Variation of Power against Switch Station

4.3.1.2 Local Optimization

The Variable Profile blade is only examined with the meanline a=0.8. The design space exploration with all the variables suggested that the reduction in power is maximum when the switching of profile happens after r/R=0.8. This means that the profile is switched at 0.9 r/R to give an enough transition region to get a smooth profile. Therefore, the camber distribution is optimized at a=0.8 and switch station of 0.9. The results for the Variable Profile Blade listed in the Table 4.10.

Table 4.10: Variable Profile Design Point Performance Results

Parameters	**VP32 a=0.8 Optimized**	**VP23 a=0.8 Optimized**
J	0.84929	0.85619
K_T	0.21261	0.21628
K_Q	0.03727	0.03838
η_o	0.77142	0.76830
Power $[kW]$	33812.8	33982.5
$n_{nominal}[rps]$	1.15855	1.16044
$n_{inter}[rps]$	1.19970	1.19004
LRM [%]	3.55	2.55
Power Reduction [%]	**4.82**	**4.34**

Maximum power reduction is achieved by the Variable Profile 32 of about 4.82%. The Open Water Performance curves of the propeller is given in the Appendix B.2 and the Pressure Distribution on the Propeller blade a J=0.8 is given in the Appendix A.2. The camber distribution of the optimized versions is given in the Figure 4.22.

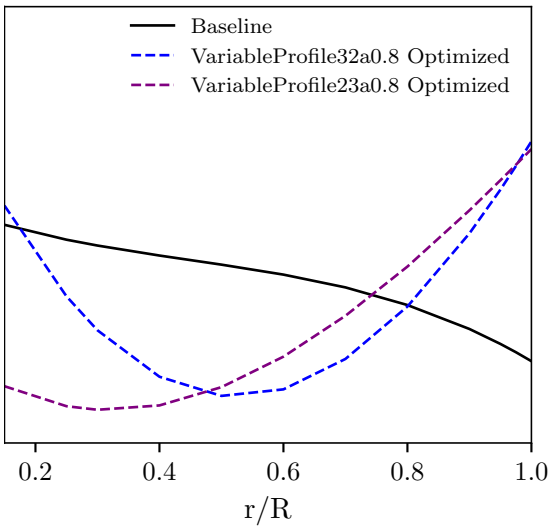

Figure 4.22: Variable Profiles Camber Distribution

4.3.1.3 Validation

The results for Variable Profile are given in the Table 4.11. The results obtained for the Variable Profile blades do not show any reduction in power. The correction factors used for the Variable Profile blade are same as the NACA16 a=0.8 correction factors. Due to this reason, the optimizer is not able to find an accurate optimum.

Table 4.11: Variable Profile Design Point Performance CFD Results

Parameters	**VP32 a=0.8 Optimized**	**VP23 a=0.8 Optimized**
J	0.81955	0.82815
KT	0.20072	0.20405
KQ	0.03532	0.03635
eta	0.74156	0.74022
Power [kW]	35662.41	35568.62
nnominal[rps]	1.17909	1.17805
ninter[rps]	1.24325	1.23033
LRM [%]	5.44	4.44
Power Reduction [%]	**-0.38**	**-0.12**

5 Cavitation

5.1 Benchmark

The MMG Baseline propeller is used as benchmark for cavitation analysis for comparison against the best performing candidates of the optimization.. The cavitation number evaluated for the vessel is based on the propeller speed. It is evaluated on the shaft line depth. The parameters used to evaluate the parameters are given in the Table 5.1.

Table 5.1: Parameters for Cavitation Number Evaluation

Parameters	Values
Ship Draft [m]	13
Shaft Height from keel [m]	4.9
Stern Wave Height [m]	1.564
Propeller Diameter [m]	9.6
Density $[kg/m^2]$	1026.02
Atmospheric Pressure [Pa]	101325
Vapor Pressure [Pa]	1670

As described in Section 2.2, cavitation area and the cavitation bucket width are evaluated. The results of the analysis are summarized in the Table 5.2. The python script used for cavitation bucket width evaluation is given in the Appendix D.2.

Table 5.2: MMG Baseline Cavitation Results

Parameters	Value
σ_{design}	2.841
A_{cav} [m^2]	0.07
PS/SS Surface Area [m^2]	8.80
2% margin [m^2]	0.18
Bucket Width	0.332

The cavitation bucket diagram for the MMG Baseline is shown in the Figure 5.1. It is important to note that the design cavitation number will be different for each variant as it depends on the design point and the propeller speed. The cavitation results of all other variants are compared with the MMG Baseline at the design point evaluated for each variant.

The width of the bucket is evaluated at the σ_{design}.

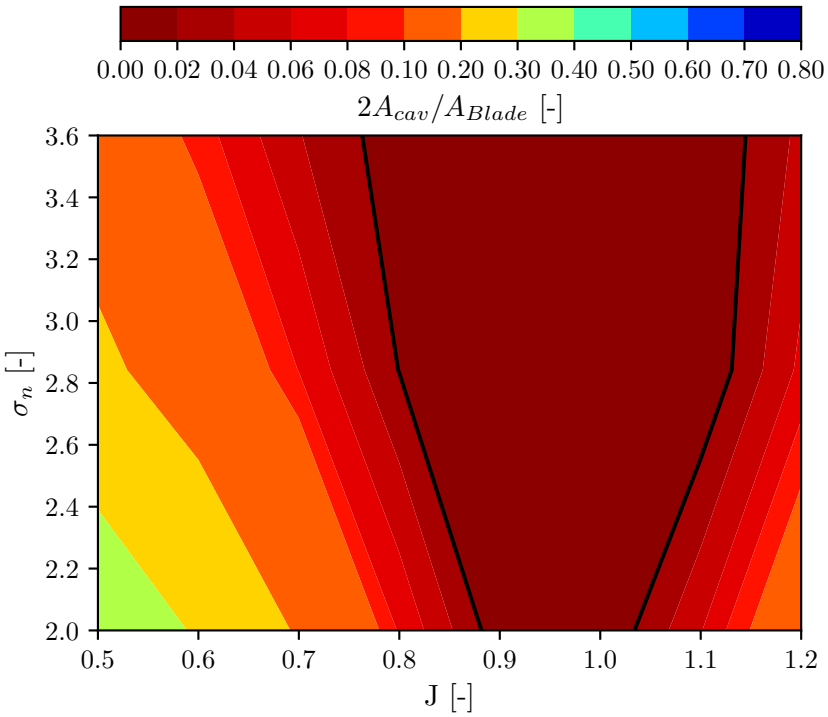

Figure 5.1: MMG Baseline Cavitation Bucket Diagram

5.2 Results

The optimized profiles that showed positive power reduction in validation and are within the constraints are studied for the cavitation behaviour. The Variable Profile Propellers are also studied for cavitation. As discussed earlier, the bucket width is evaluated for the variants and compared against the MMG Baseline bucket width.

NACA4D profile blades are the worst in case of cavitation. The NACA4D Baseline variant is cavitating at the design point so this design is not feasible. Although, NACA4D Optimized variant is not cavitating at the design point (2% margin), its bucket width is about 11.4% less than MMG Baseline. Poor cavitation performance and a thin trailing edge are the reasons why these profiles are not used for propeller design. The results of the cavitation of NACA4D are given in the Table 5.3. The Cavitation Bucket Diagram and the cavitation area versus advance ratio plots for the NACA4D profile blades is given in the Appendix C.1 and C.2.

Table 5.3: NACA4D Cavitation Results

Parameters	**NACA4D Baseline**	**NACA4D Optimized**
σ_{design}	2.83	2.87
$A_{cav}[m^2]$	0.201	0.054
PS/SS Surface Area [m^2]	8.740	8.750
2% margin [m^2]	0.175	0.175
Bucket Width	0.276	0.294
Increase in Bucket Width [%]	**-16.97**	**-11.37**

For NACA 16 blades, no variant is cavitating at the design point. The bucket width for the NACA16 Baseline and NACA16 a=0.8 Optimized is however less than the MMG Baseline. NACA16 a=1 Optimized showed good behaviour in cavitation with 2.48% increase in the bucket width. Results of the cavitation analysis of the NACA16 profiles are given in the Table 5.4. The detailed cavitation bucket diagrams of the NACA16 profiles are given in the Appendix C.

Table 5.4: NACA16 Cavitation Results

Parameters	**NACA16 a=0.8 Baseline**	**NACA16 a=0.8 Optimized**	**NACA16 a=1 Optimized**
σ_{design}	2.762	2.785	2.805
A_{cav} [m^2]	0.126	0.057	0.080
PS/SS Surface Area [m^2]	8.691	8.723	8.701
2% margin [m^2	0.174	0.174	0.174
Bucket Width	0.298	0.313	0.340
Increase in Bucket Width [%]	**-10.15**	**-5.74**	**2.48**

In the case of NACA66mod profile, the Baseline NACA66mod a=0.8 variant does not perform well in cavitation. Its bucket width is found to be 3% less than the MMG Baseline. However, for optimized version of the NACA66mod with a=0.8 meanline performed best in terms of cavitation with 7.2% increase in the cavitation bucket width. The detailed results of the NACA66mod profile are given in the Table 5.5.

Table 5.5: NACA66mod Cavitation Results

Parameters	**NACA66mod a=0.8 Baseline**	**NACA66mod a=1 Optimized**
σ_{design}	2.816	2.821
A_{cav} [m^2]	0.092	0.045
PS/SS Surface Area [m^2]	8.684	8.696
2% margin [m^2]	0.174	0.174
Bucket Width	0.322	0.356
Increase in Bucket Width [%]	**-3.07**	**7.15**

Although the Variable Profile blade does not yield good performance in terms of power, their cavitation performance is quite good. Increase in cavitation bucket width is observed in both profiles. 5% increase in cavitation bucket width is observed for the Variable Profile 32 a=0.8 profile blade.

Table 5.6: Variable Profile Cavitation Results

Parameters	**VP32 a=0.8 Optimized**	**VP23 a=0.8 Optimized**
σ_{design}	2.695	2.752
A_{cav} [m^2]	0.058	0.056
PS/SS Surface Area [m^2]	8.714	8.740
2% margin [m^2]	0.174	0.175
Bucket Width	0.349	0.338
Increase in Bucket Width [%]	**5.00**	**1.88**

6
Discussion

The key points of the results are discussed below.

- The correction factors are employed to improve the results of panMARE. The design point depends on the accuracy of the results. The correction factors are necessary since the panel code does not account for the flow separation and the viscous drag. That is why the CFD results for Torque coefficients for different profiles have the largest errors as compared to the Thrust coefficient (Table 3.7).
- The study of the design variables shows that the variation of camber at 0.6r/R has the maximum effect on the power. The trend shows that increasing the camber increases the power. For this reason, all the camber distributions have low camber at r/R=0.6 as compared to the MMG Baseline. The effect of all other design variables is less than camber at 0.6r/R on power.
- The study of optimization carried out on profiles yield 12 different variants among which three are with baseline distributions. The maximum power reduction achieved by the optimization was for NACA16 a=0 Optimized blade. However, this result is not realistic as the CFD of this profile showed no power reduction at all. The main reason for this discrepancy is the irregular leading edge found at high thickness and high camber values. Moreover, for the lower meanlines the geometry yielded was not clean.
- The validation carried out on the profiles suggests that the best performing blade profile is NACA4D Optimized with an improvement of 1.84%. But the thin trailing edge and high cavitation of NACA4D profiles makes these profile impractical for the design of Marine Propellers.
- The next best performing profile is NACA66mod a=1 Optimized with 1.04% power reduction as compared to MMG Baseline. Moreover, the cavitation bucket obtained for the profile is also good and an increase of cavitation bucket width of 7.15% is observed.
- The difference between the optimization results and CFD validation is because of the two main reasons.
    1. The difference in model as the correction factors evaluated are for meanline a=0.8 but the optimizer gives the results with different meanline.
    2. High camber values at tip are prone to early flow separation and high drag which leads to high delivered power.
- The study of design space exploration of Variable Profile blades suggests that the minimum power is achieved when the profile is switched at 0.9r/R.

- The validation of Variable Profile did not lead to any performance improvement. This is because the correction factors used for variable profiles are of NACA16. The optimized design point depends on the correction factors and that is why good performance from panMARE is observed but in actual scenario that is not the case.
- The cavitation studies suggest that the Variable Profile perform well in cavitation as the optimized variants have a bigger bucket width as compared to the MMG Baseline.

7

Conclusion and Recommendations

7.1 Conclusion

The study of variable profile propellers using Panel methods is performed on three different profiles (NACA4D, NACA16 and NACA66mod). The camber distribution is varied along the radial direction to obtain a variable profile. The combination of NACA16 and NACA66mod is also studied to evaluate any enhancement in open water performance or cavitation behaviour.

The design point is evaluated using the thrust identity method and the performance of the variable profiles at the design point is studied. The optimization is performed using a panel method and the results are validated with CFD simulations. The MMG base model is set as a benchmark for the study. The cavitation study is performed with panMARE calccav, which evaluates the cavitation area, which is then post-processed to obtain the cavitation bucket width.

The sensitivity analysis of the design variables shows that the camber at 0.6r/R makes a significant contribution to the propeller performance increase. The effect of tip camber, root camber and type of meanline on open water performance is less as compared to the mid camber variation.

The best performing blade section is NACA66mod a=1 Optimized as it gives 1.04% improvement in terms of Power and 7.15% improvement in Cavitation Bucket Width. Variable Profile Propellers that are developed by the combination of two different NACA series sections showed no improvement in terms of Power. However, these profiles perform well in cavitation as their cavitation bucket width is wider than the MMG Baseline Model.

7.2 Recommendations

- In this thesis, only the effect of different NACA profiles on performance and cavitation is investigated and only the camber distribution is varied to achieve variable profile and an optimized solution. However, the maximum thickness of the profile is kept constant. The thickness distribution also affects the performance and especially cavitation performance and its effect should also be studied keeping in mind the strength constraints.
- The cavitation performance is also influenced by the pitch of the propeller. Generally, the propellers are designed to achieve a certain LRM which is achieved by varying the camber distribution and pitch distribution of the propeller. Varying the pitch distribution along the radial direction leads to a practicable solution. Therefore, the pitch distribution can be studied as a design variable for future work.
- This study is carried out using panMARE with the optimizer. This is the preliminary research to evaluate various profiles and the design variables effect on the objective. To obtain more accurate results, this study should be performed by coupling the optimization algorithm with the CFD results. This will eliminate the dependency of the design point on the correction factors and yield accurate results. However, this study is computationally expensive and not in the scope of this thesis.
- Another important aspect of the Marine propeller design is that practically the propeller operates behind a ship hull. Although a constant Taylor wake fraction is added for design point evaluation, the water inflow is not uniform on the propeller. The study with the wake field will give the true picture of propeller performance.
- Due to the wake field, the velocity experienced by the individual propeller blade is different which results in a different cavitation behaviour for each blade. Although Cavitation Bucket Width is a good measure of the cavitation behaviour of the propeller in uniform flow, the effect of wake field significantly changes the behaviour of the propeller.
- It is also observed for the cavitation area vs advance ratio plots (Appendix C.2) that the design point lies close to the suction side cavitation. This is not a good scenario since the local advance ratio at the propeller blade changes with the wake field and drops to lower advance ratio values. This effect can be studied by performing a full transient propulsion analysis of the complete propeller under wake field.
- Only sheet cavitation is evaluated in this study but the minimum width of the bucket is usually governed by the bubble cavitation. The evaluation of other cavitation phenomena such as tip vortex cavitation and bubble cavitation are also important to accurately assess the performance of the propeller.

Bibliography

John Carlton. *Marine propellers and propulsion*. Butterworth-Heinemann, 2018.

TUHH. Panel code panmare. https://www.tuhh.de/panmare/code. [Accessed 17-07-2024].

Guan Guan, Xiangyu Zhang, Panpan Wang, and Qu Yang. Multi-objective optimization design method of marine propeller based on fluid-structure interaction. *Ocean Engineering*, 252:111222, 2022.

Terry Brockett et al. Minimum pressure envelopes for modified naca-66 sections with naca a= 0.8 camber and buships type i and type ii sections. *David Taylor Model Basin report*, 1780.

Ashish C Tamhane. *Development of an Analysis and Design Optimization Framework for Marine Propellers*. Old Dominion University, 2017.

Hajime Yamaguchi, Hiroharu Kato, Masatsugu Maeda, and Makoto Toyoda. High performance foil sections with delayed cavitation inception. In *Proceedings of the 3rd ASME/JSME Joint Fluids Engineering Conference*, 1999.

Jie Dang. Improving cavitation performance with new blade sections for marine propellers. *International shipbuilding progress*, 51(4):353–376, 2004.

P Olivucci and S Gaggero. A framework for the design by optimization of hydrofoils under cavitating conditions. In *Proceedings of the 7th European Congress on Computational Methods in Applied Sciences and Engineering*, 2016.

Md Mashud Karim, K Suzuki, and H Kai. Optimal design of hydrofoil and marine propeller using micro-genetic algorithm (μga). *Journal of Naval Architecture and Marine Engineering*, 1(1):47–61, 2004.

A Arapakopoulos, R Polichshuk, Z Segizbayev, S Ospanov, AI Ginnis, and KV Kostas. Parametric models for marine propellers. *Ocean Engineering*, 192:106595, 2019.

Hao Wang, Long Zheng, and Shunhuai Chen. Marine propeller optimization based on a novel parametric model. *Mathematical Problems in Engineering*, 2022(1):5612793, 2022.

Shigenori Mishima. *Design of cavitating propeller blades in non-uniform flow by numerical optimization*. PhD thesis, Massachusetts Institute of Technology, 1996.

Jintae Lee. *A potential based panel method for the analysis of marine propellers in steady flow*. PhD thesis, Massachusetts Institute of Technology, 1987.

Chao Wang, Chunyu Guo, Xin Chang, Sheng Huang, and Pusun Cao. Analysis of cavitation performance of a 2-d hydrofoil based on mixed-iterative method. *Journal of Marine Science and Application*, 12(1):52–57, 2013.

William Bowles Coney. *A method for the design of a class of optimum marine propulsors*. PhD thesis, Massachusetts Institute of Technology, 1989.

Florian Vesting, Rickard E Bensow, Rikard Johansson, Robert Gustafsson, and Nicole Costa. Procedure for application-oriented optimisation of marine propellers. *Journal of Marine Science and Engineering*, 4(4):83, 2016.

Florian Vesting and Rickard E Bensow. On surrogate methods in propeller optimisation. *Ocean engineering*, 88:214–227, 2014.

AH Techet. Marine propellers. *2.016 Hydrodynamics*, 3:2–3, 2005.

JP Ghose. *Basic ship propulsion*. Allied publishers, 2004.

Ira H Abbott and Albert E Von Doenhoff. *Theory of wing sections: including a summary of*

airfoil data. Courier Corporation, 2012.

ITTC. 1978 ittc performance prediction method. *ITTC – Recommended Procedures and Guidelines*, 2014.

MAN Energy Solutions. Basic principles of ship propulsion optimisation of hull, propeller, and engine interactions for maximum efficiency, 2018.

WF Lindsey, DB Stevenson, and Bernard N Daley. Aerodynamics characteristics of 24 naca 16-series airfoils at mach numbers between 0.3 and 0.8. Technical report, 1948.

S. Berger, R. Gosda, M. Scharf, R. Klose, L. Greitsch, and M. Abdel-Maksoud. Efficient Numerical Investigation of Propeller Cavitation Phenomena causing Higher-Order Hull Pressure Fluctuations. In *31st Symposium on Naval Hydrodynamics*, Monterey, United States of America, 2016.

Neal E Fine. *Nonlinear analysis of cavitating propellers in nonuniform flow*. PhD thesis, Massachusetts institute of Technology, 1992.

David C Wilcox et al. *Turbulence modeling for CFD*, volume 2. DCW industries La Canada, CA, 1998.

Olof Klerebrant Klasson. A validation, comparison and automation of different computational tools for propeller open water predictions. 2011.

NWH Bulten, PW Stoltenkamp, and JJA Van Hooijdonk. Efficient propeller designs based on full-scale cfd simulations. In *Proceedings of the International Conference on High Performance Marine Vehicles, Athens, Greece*, pages 3–5, 2014.

Michael D McKay, Richard J Beckman, and William J Conover. A comparison of three methods for selecting values of input variables in the analysis of output from a computer code. *Technometrics*, 42(1):55–61, 2000.

Keith R Dalbey, Michael S Eldred, Gianluca Geraci, John D Jakeman, Kathryn A Maupin, Jason A Monschke, Daniel Thomas Seidl, Anh Tran, Friedrich Menhorn, and Xiaoshu Zeng. Dakota, a multilevel parallel object-oriented framework for design optimization, parameter estimation, uncertainty quantification, and sensitivity analysis: Version 6.16 theory manual. Technical report, Sandia National Lab.(SNL-NM), Albuquerque, NM (United States), 2021.

Brian M Adams, William J Bohnhoff, Keith R Dalbey, Mohamed S Ebeida, John P Eddy, Michael S Eldred, Russell W Hooper, Patricia D Hough, Kenneth T Hu, John D Jakeman, et al. Dakota, a multilevel parallel object-oriented framework for design optimization, parameter estimation, uncertainty quantification, and sensitivity analysis: version 6.13 user's manual. Technical report, Sandia National Lab.(SNL-NM), Albuquerque, NM (United States), 2020.

CAESES. *Dakota*. Friendship Systems, 2024.

A

Optimization Results

A.1 Optimization Convergence Plots

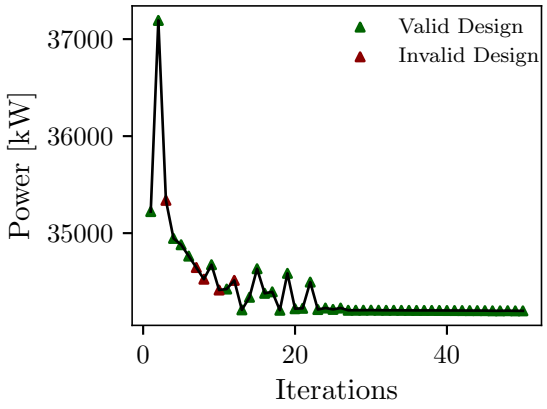

Figure A1.1: NACA16 a=0.8 meanline Optimization

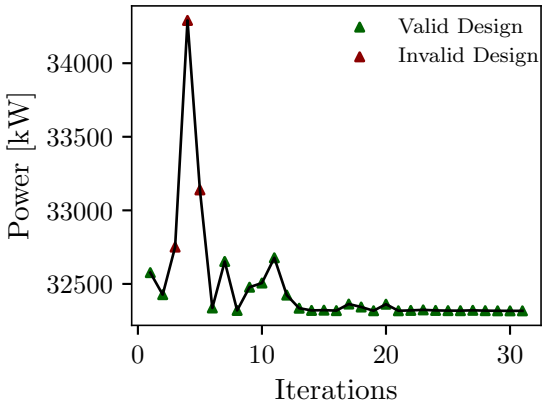

Figure A1.2: NACA16 a=0 meanline Optimization

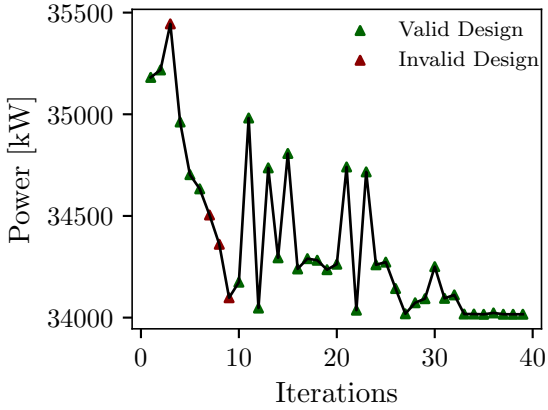

Figure A1.3: NACA66mod a=0.8 meanline Optimization

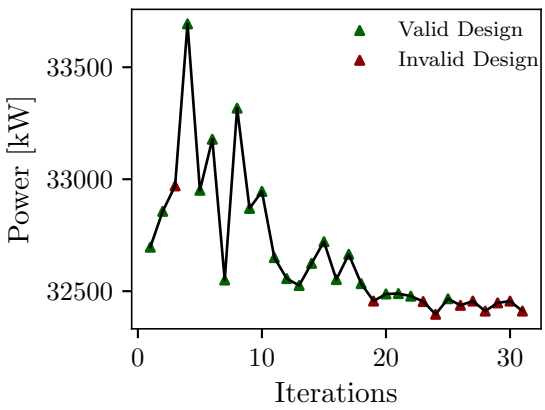

Figure A1.4: NACA66mod a=0 meanline Optimization

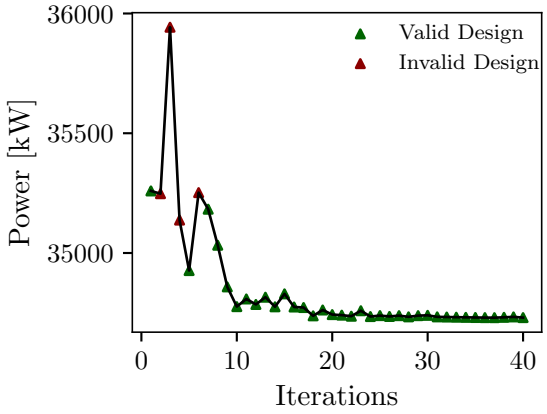

Figure A1.5: NACA16 a=1 meanline Optimization

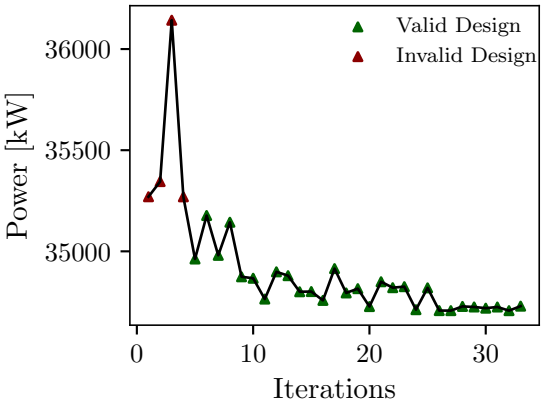

Figure A1.6: NACA66mod a=1 meanline Optimization

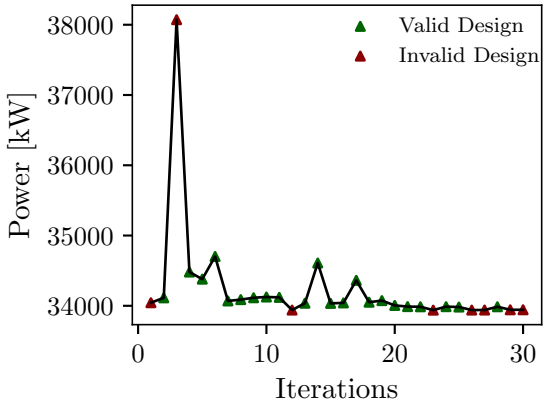

Figure A1.7: Variable Profile 23 a=0.8 meanline Optimization

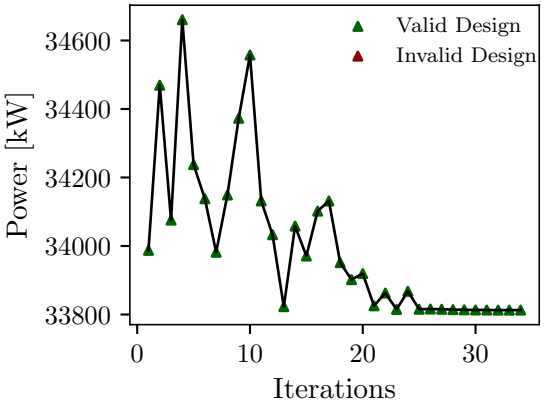

Figure A1.8: Variable Profile 32 a=0.8 meanline Optimization

A.2 panMARE Pressure Contours

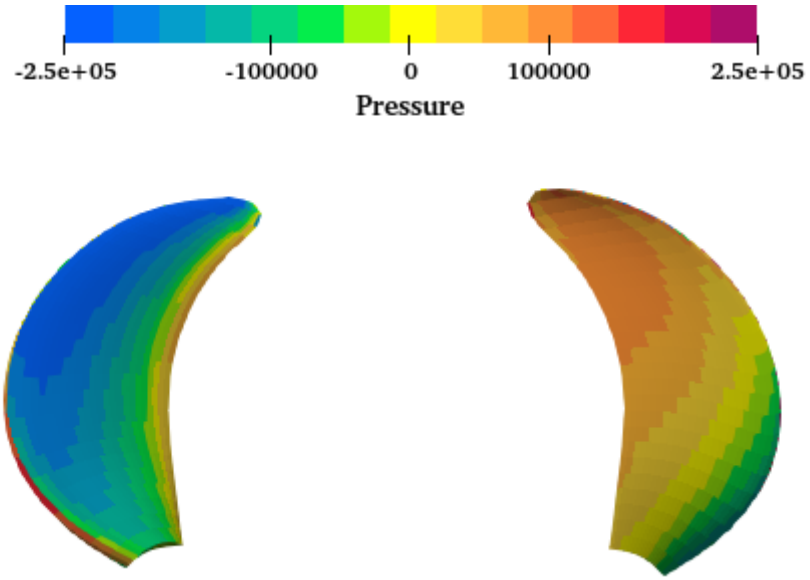

(a) Suction Side **(b)** Pressure Side

Figure A2.1: Pressure Contours of NACA4D Baseline at J=0.8

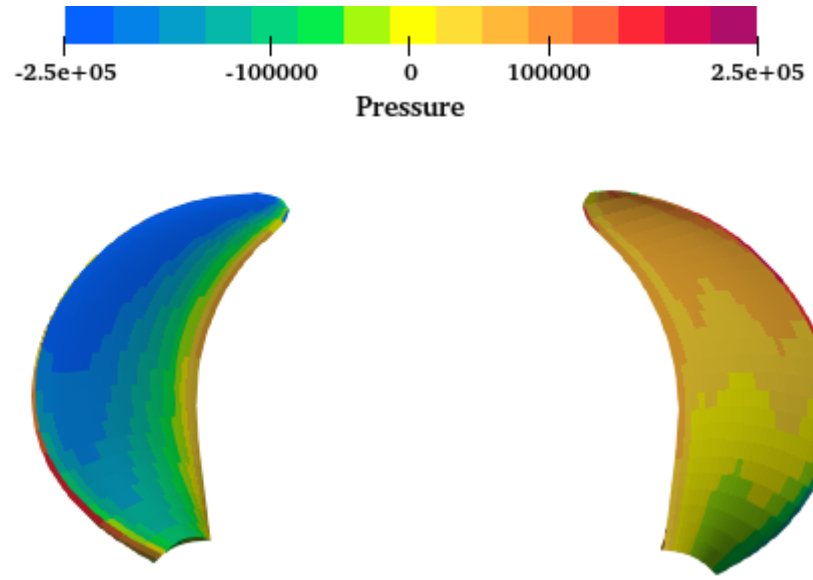

(a) Suction Side **(b)** Pressure Side

Figure A2.2: Pressure Contours of NACA4D Optimized at J=0.8

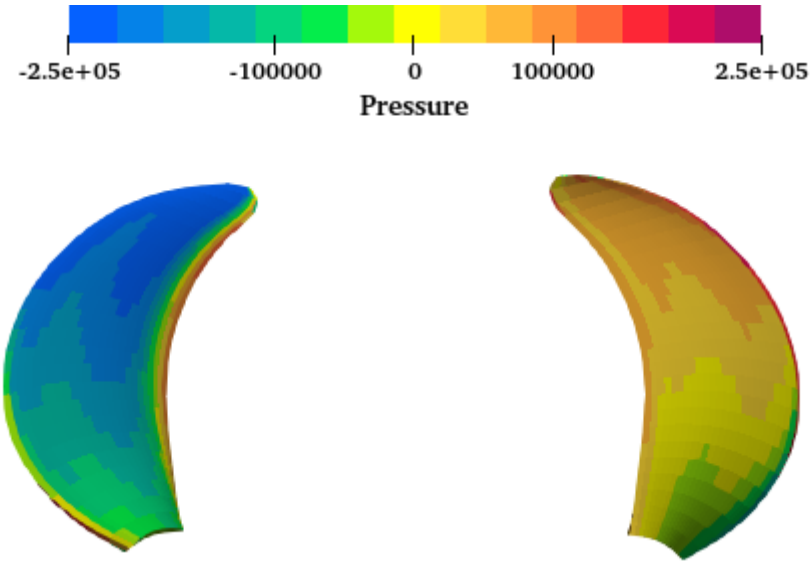

(a) Suction Side **(b)** Pressure Side

Figure A2.3: Pressure Contours of NACA16 a=0.8 Baseline at J=0.8

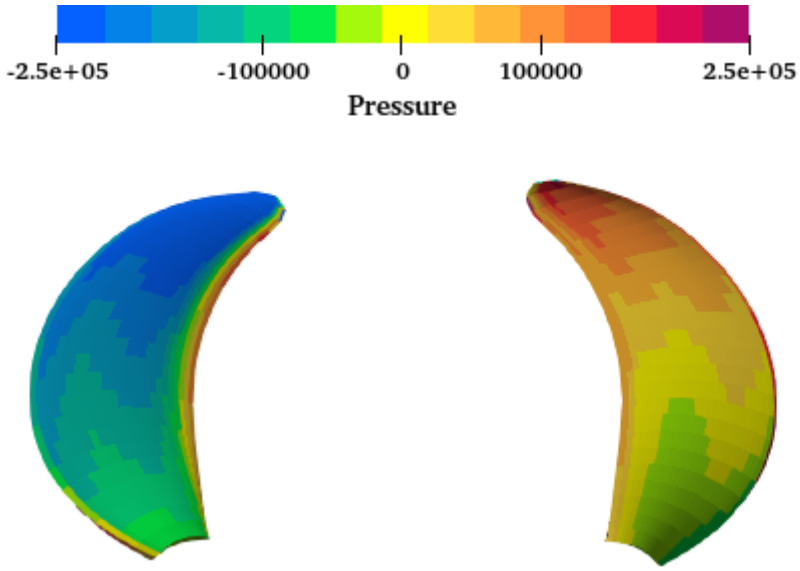

(a) Suction Side **(b)** Pressure Side

Figure A2.4: Pressure Contours of NACA16 a=0.8 Optimized at J=0.8

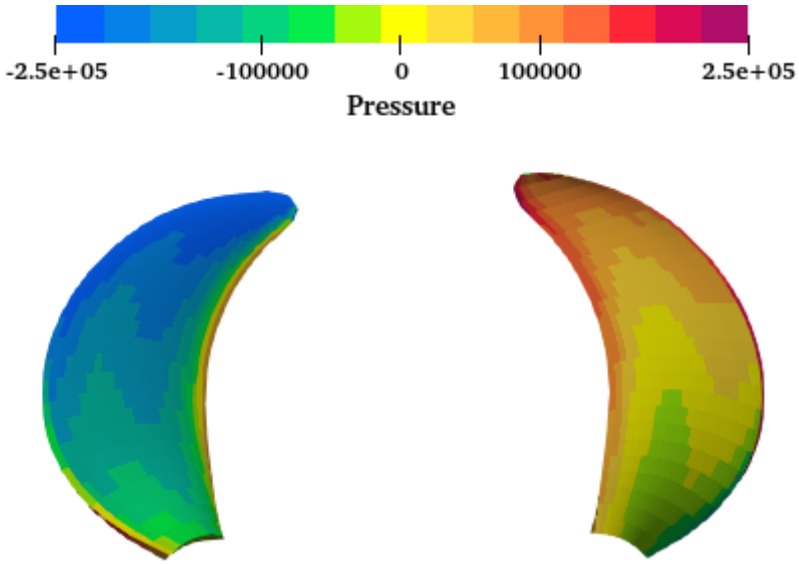

(a) Suction Side **(b)** Pressure Side

Figure A2.5: Pressure Contours of NACA16 a=1 Optimized at J=0.8

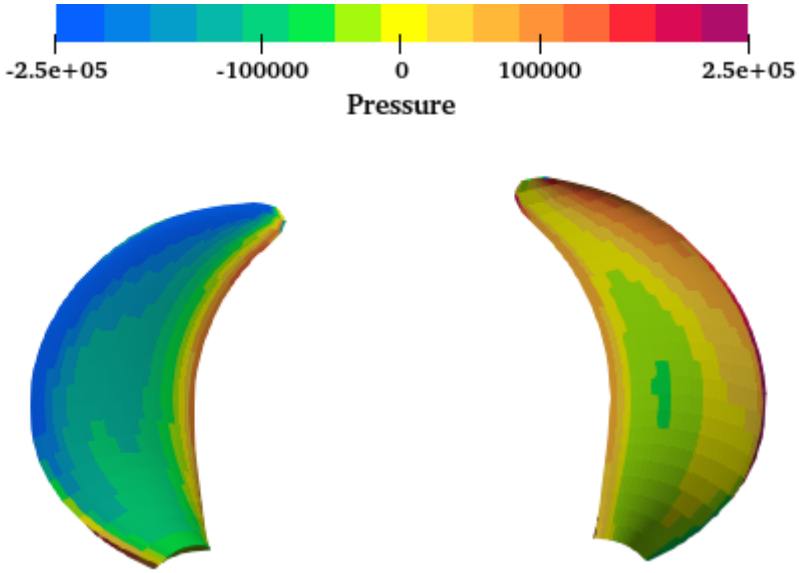

(a) Suction Side **(b)** Pressure Side

Figure A2.6: Pressure Contours of NACA16 a=0 Optimized (DSE Best) at J=0.8

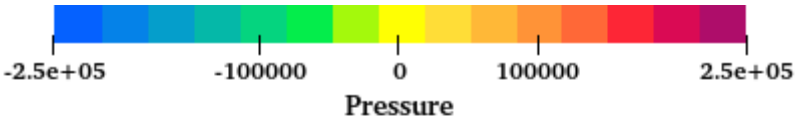

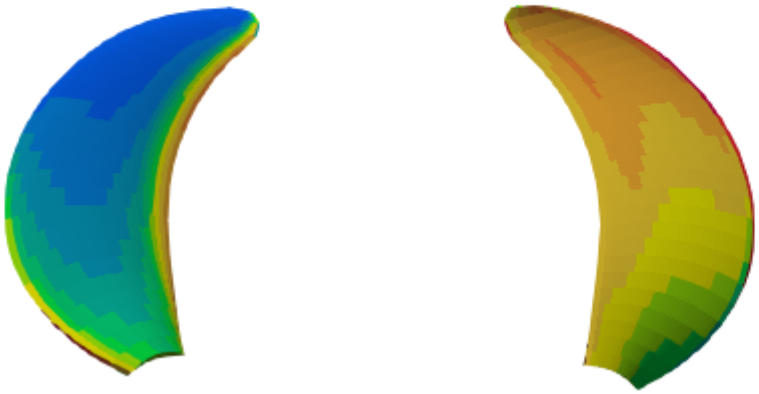

(a) Suction Side **(b)** Pressure Side

Figure A2.7: Pressure Contours of NACA66mod Baseline at J=0.8

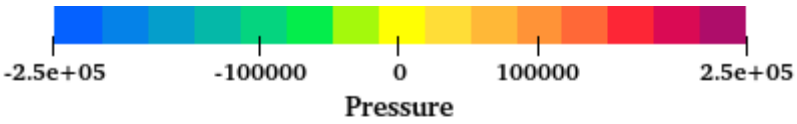

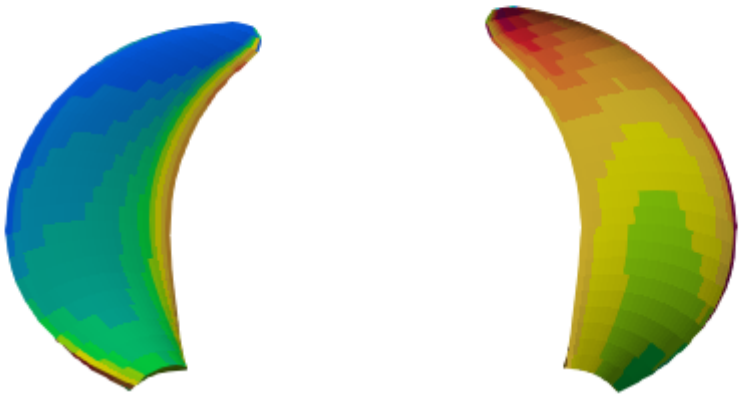

(a) Suction Side **(b)** Pressure Side

Figure A2.8: Pressure Contours of NACA66mod a=0.8 Optimized at J=0.8

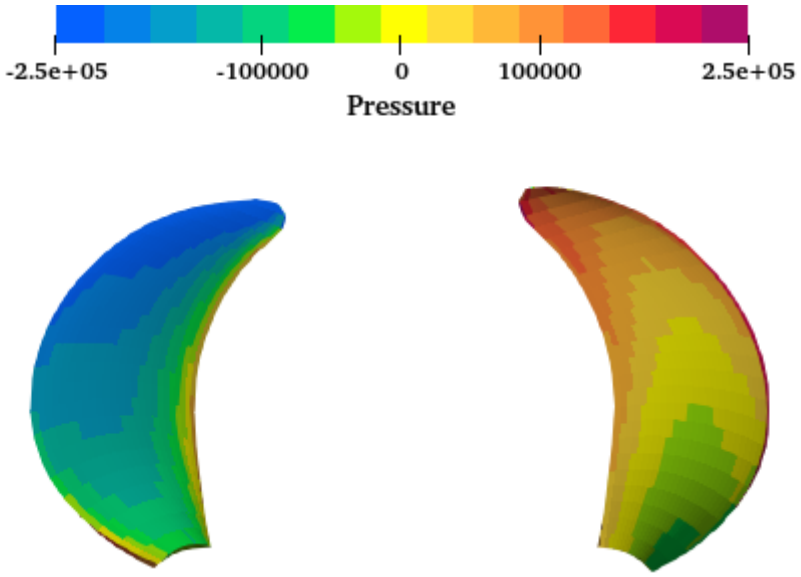

(a) Suction Side **(b)** Pressure Side

Figure A2.9: Pressure Contours of NACA66mod a=1 Optimized at J=0.8

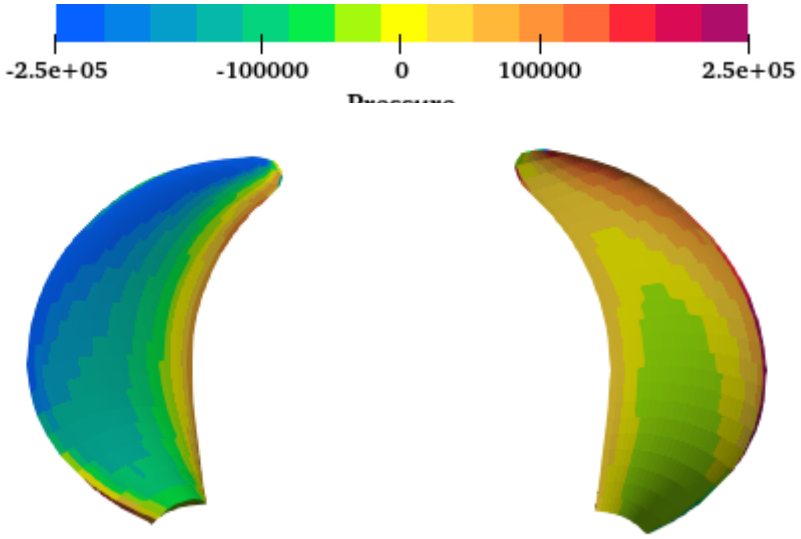

(a) Suction Side **(b)** Pressure Side

Figure A2.10: Pressure Contours of NACA66mod a=0 Optimized (DSE Best) at J=0.8

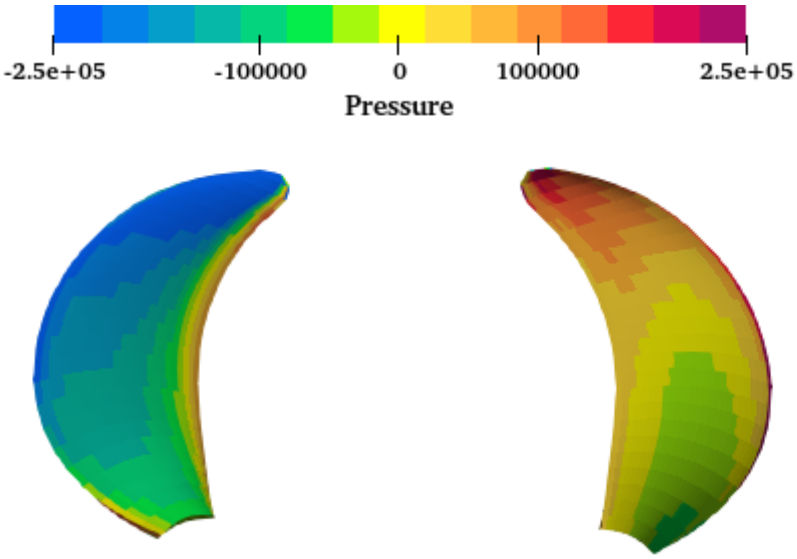

(a) Suction Side **(b)** Pressure Side

Figure A2.11: Pressure Contours of Variable Profile 32 a=0.8 Optimized at J=0.8

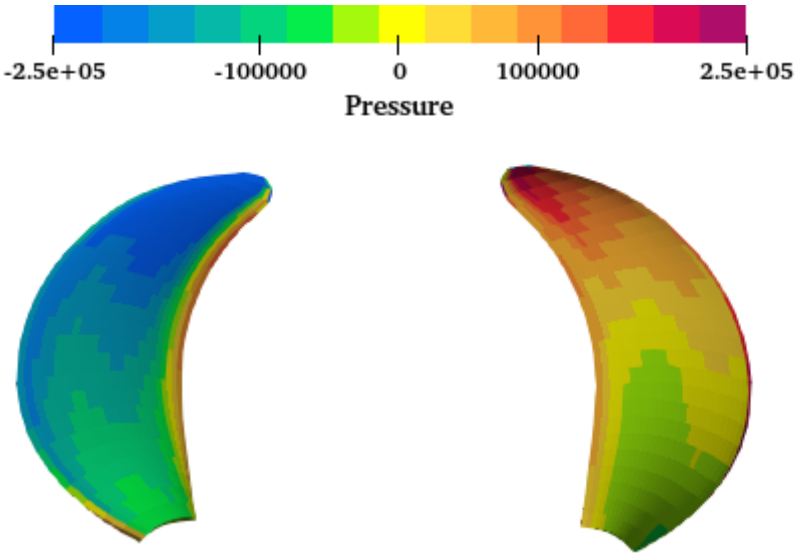

(a) Suction Side **(b)** Pressure Side

Figure A2.12: Pressure Contours of Variable Profile 23 a=0.8 Optimized at J=0.8

B

Validation Results

B.1 CFD Pressure Contours

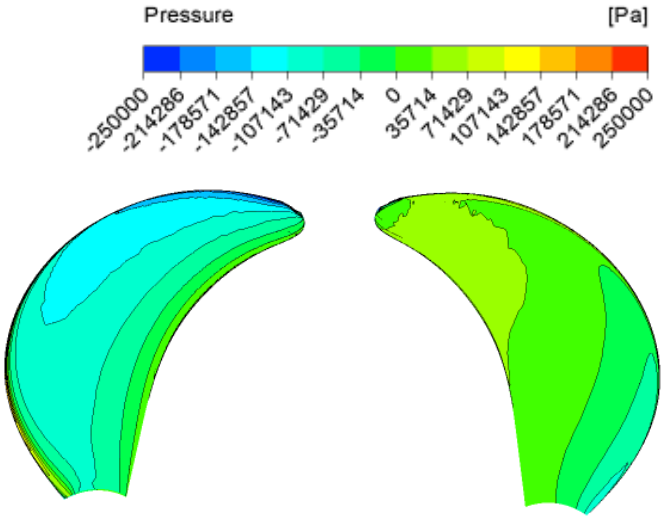

(a) Suction Side **(b)** Pressure Side

Figure B1.1: Pressure Contours of NACA4D a=0.8 Baseline at J=0.8

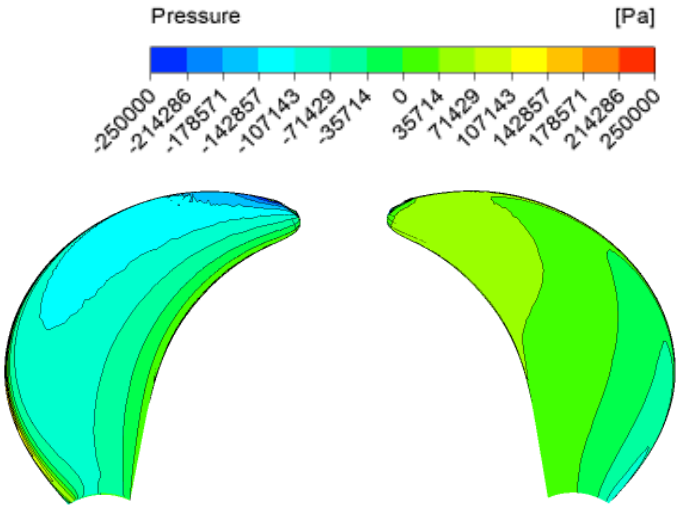

(a) Suction Side **(b)** Pressure Side

Figure B1.2: Pressure Contours of NACA4D Optimized at J=0.8

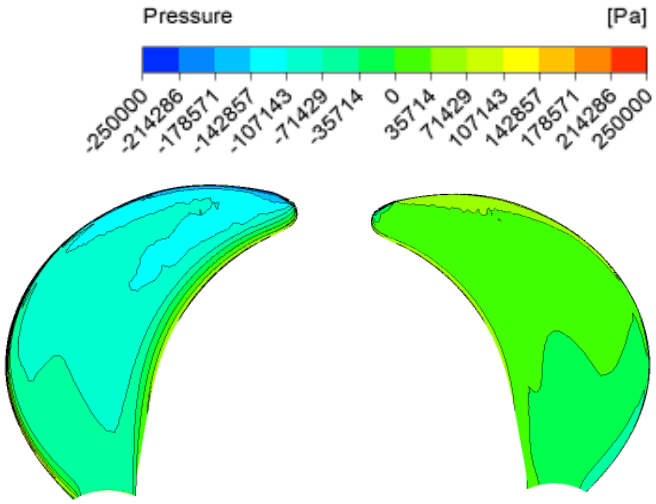

(a) Suction Side **(b)** Pressure Side

Figure B1.3: Pressure Contours of NACA16 a=0.8 Baseline at J=0.8

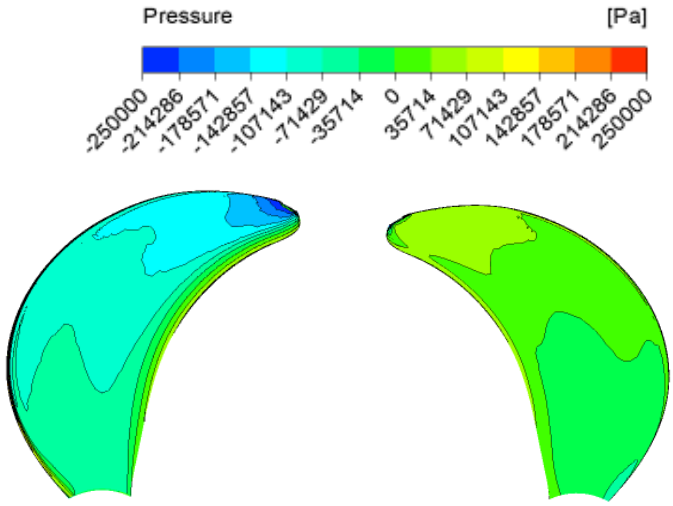

(a) Suction Side **(b)** Pressure Side

Figure B1.4: Pressure Contours of NACA16 a=0.8 Optimized at J=0.8

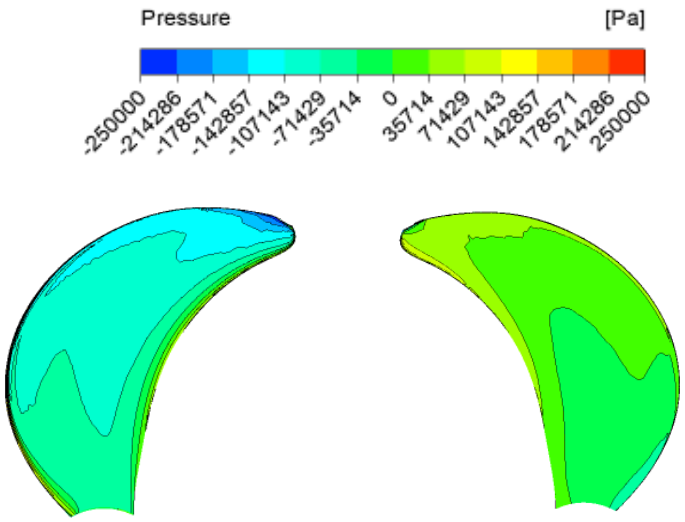

(a) Suction Side **(b)** Pressure Side

Figure B1.5: Pressure Contours of NACA16 a=1 Optimized at J=0.8

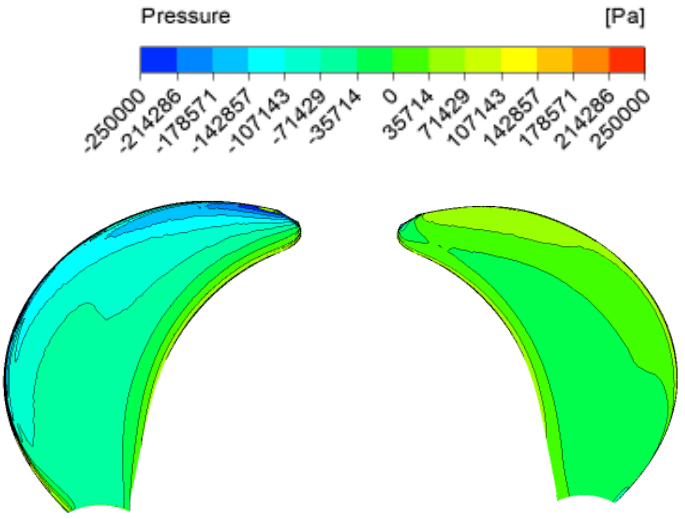

(a) Suction Side **(b)** Pressure Side

Figure B1.6: Pressure Contours of NACA16 a=0 Optimized (DSE Best) at J=0.8

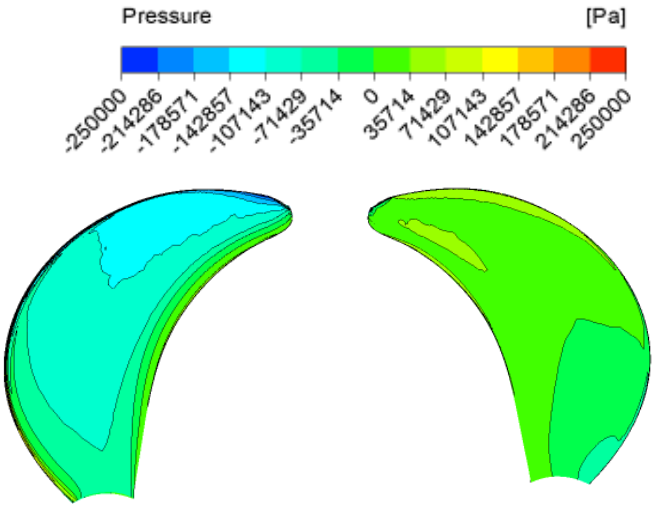

(a) Suction Side **(b)** Pressure Side

Figure B1.7: Pressure Contours of NACA66mod a=0.8 Baseline at J=0.8

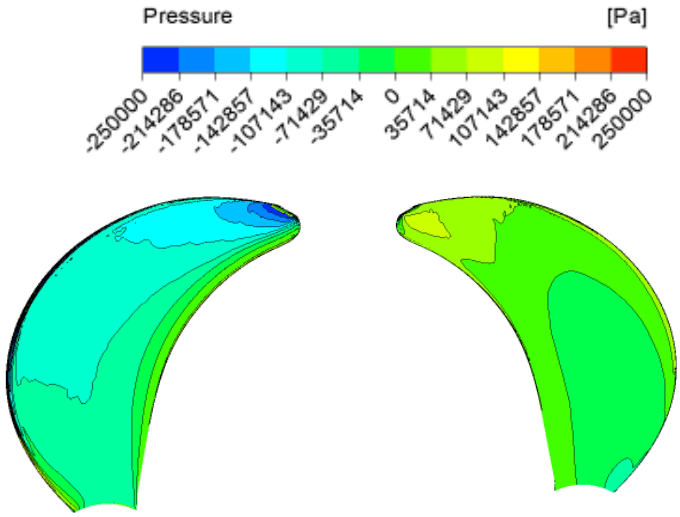

(a) Suction Side **(b)** Pressure Side

Figure B1.8: Pressure Contours of NACA66mod a=0.8 Optimized at J=0.8

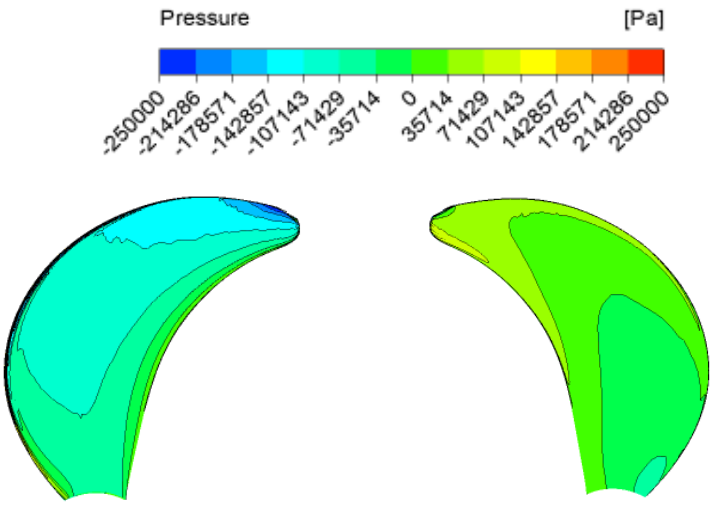

(a) Suction Side **(b)** Pressure Side

Figure B1.9: Pressure Contours of NACA66mod a=1 Optimized at J=0.8

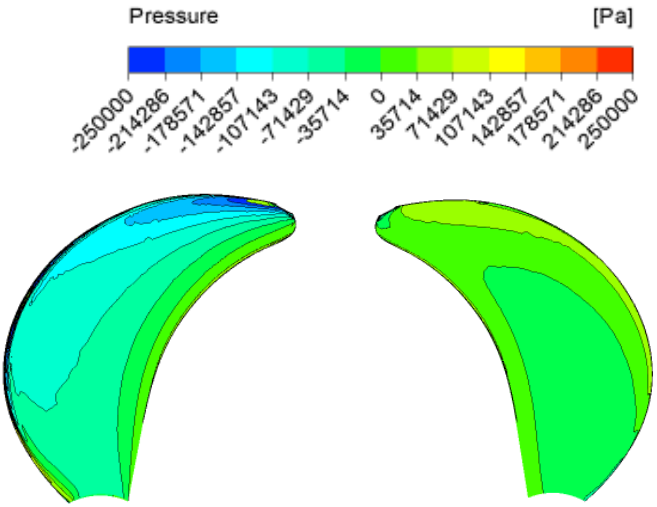

(a) Suction Side **(b)** Pressure Side

Figure B1.10: Pressure Contours of NACA66mod a=0 Optimized (DSE Best) at J=0.8

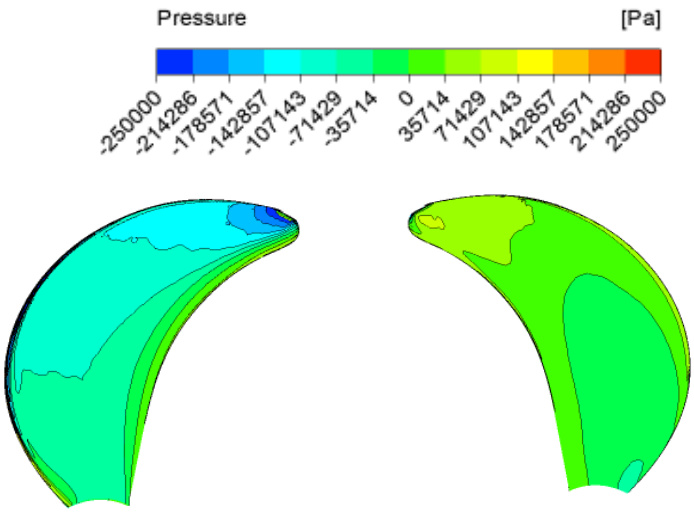

(a) Suction Side **(b)** Pressure Side

Figure B1.11: Pressure Contours of Variable Profile 32 a=0.8 Optimized at J=0.8

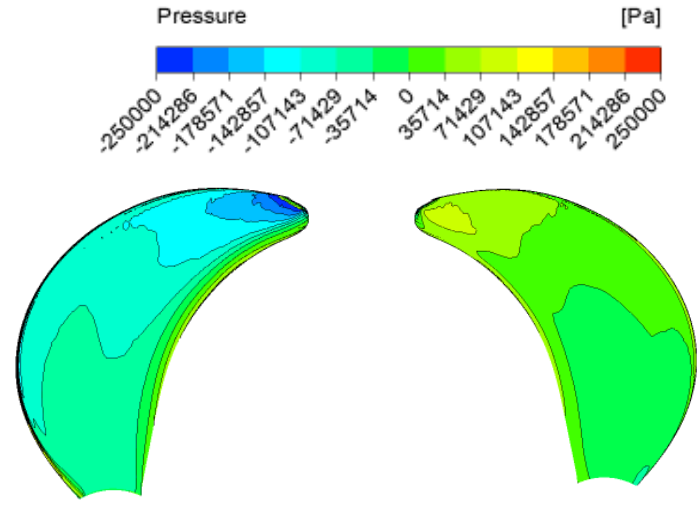

(a) Suction Side **(b)** Pressure Side

Figure B1.12: Pressure Contours of Variable Profile 23 a=0.8 Optimized at J=0.8

B.2 Comparison of Open Water Curves

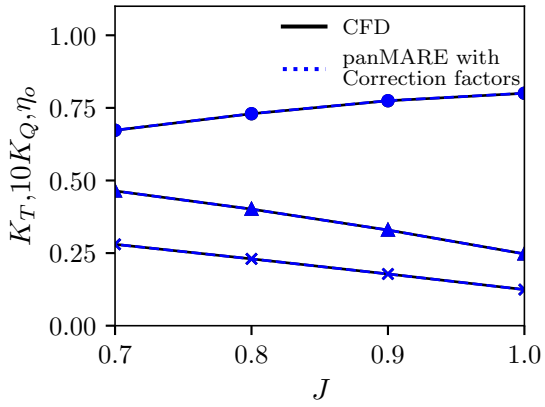

Figure B2.1: NACA4D Baseline Performance Curves

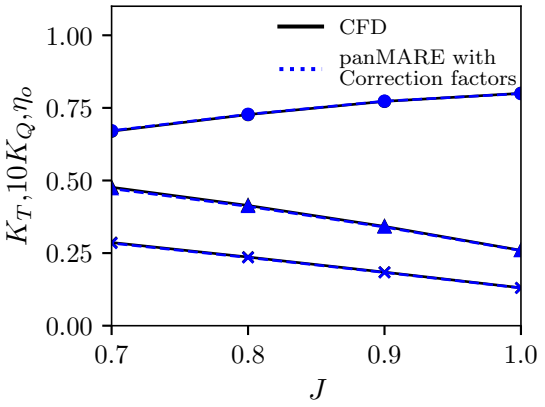

Figure B2.2: NACA4D Optimized Performance Curves

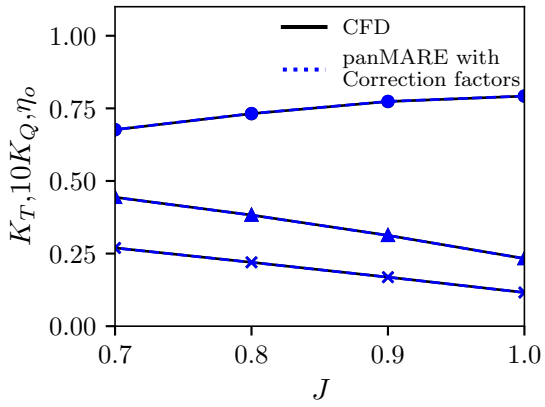

Figure B2.3: NACA16 a=0.8 Baseline Performance Curves

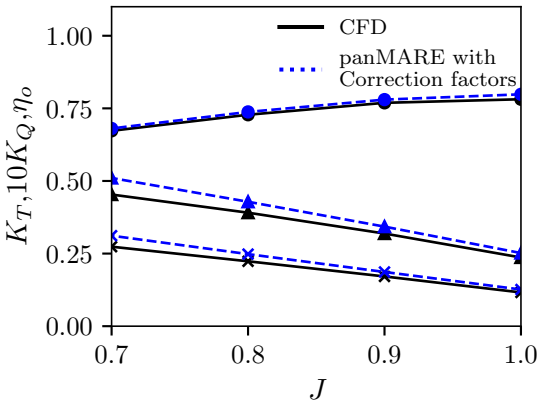

Figure B2.4: NACA16a=0.8 Optimized Performance Curves

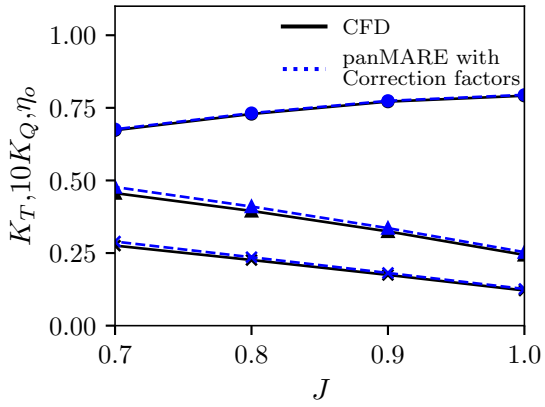

Figure B2.5: NACA16 a=1 Optimized Performance Curves

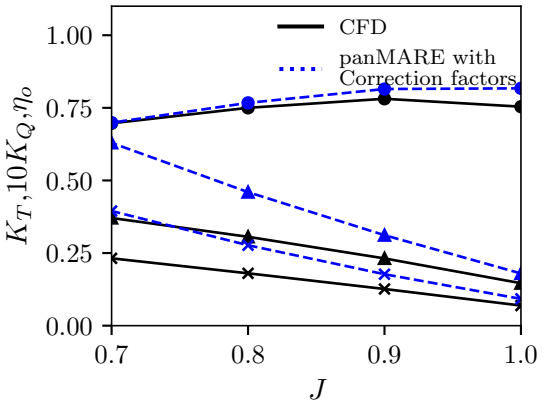

Figure B2.6: NACA16 a=0 Optimized Performance Curves

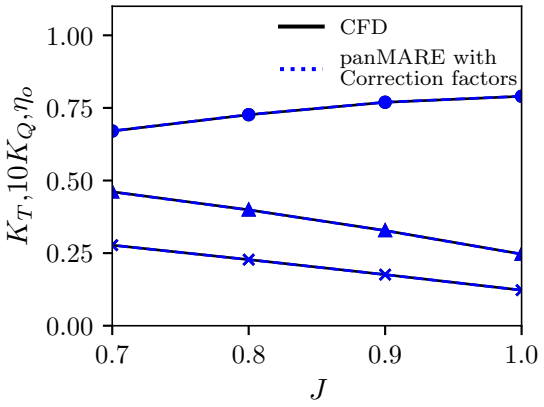

Figure B2.7: NACA66mod a=0.8 Baseline Performance Curves

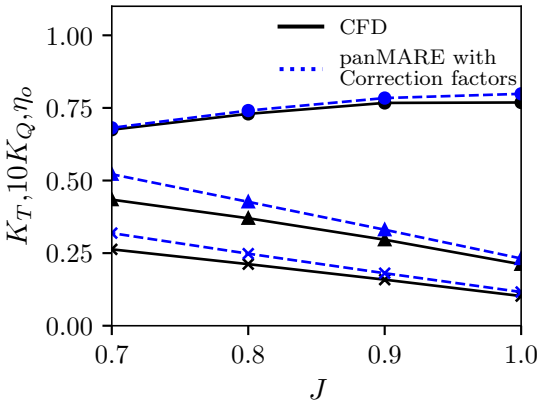

Figure B2.8: NACA66mod a=0.8 Optimized Performance Curves

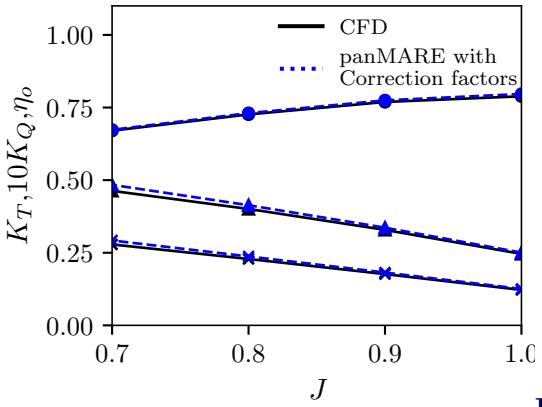

Figure B2.9: NACA66mod a=1 Optimized Performance Curves

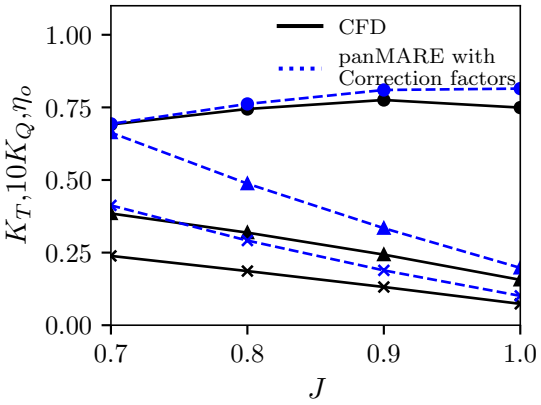

Figure B2.10: NACA66mod a=0 Optimized Performance Curves

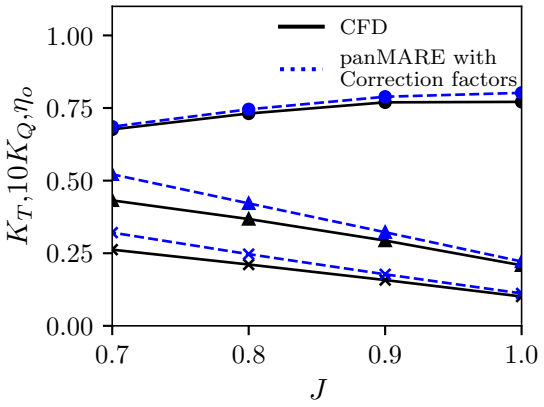

Figure B2.11: Variable Profile 32 a=0.8 Optimized Performance Curves

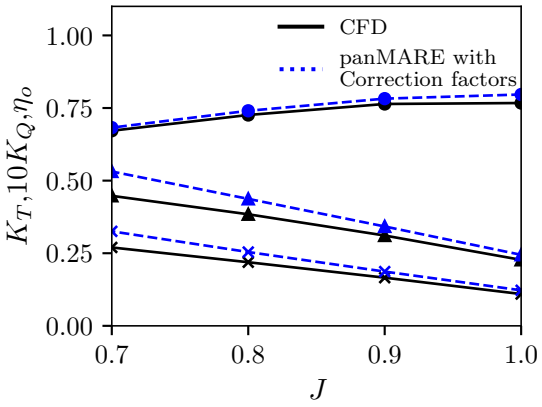

Figure B2.12: Variable Profile 23 a=0.8 Optimized Performance Curves

C

Cavitation Results

C.1 Cavitation Bucket Diagrams

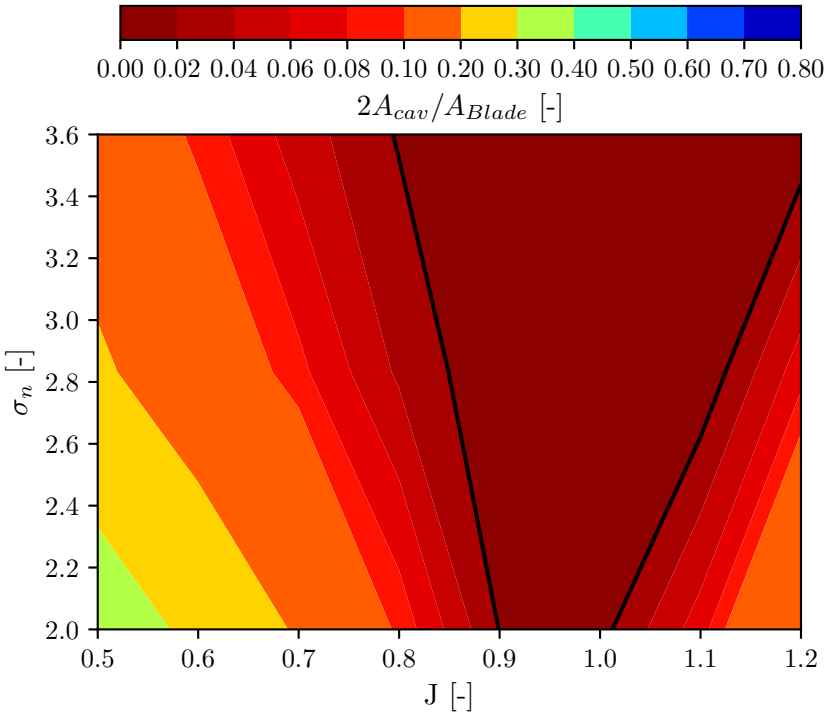

Figure C1.1: NACA4D Baseline Cavitation Bucket Diagram

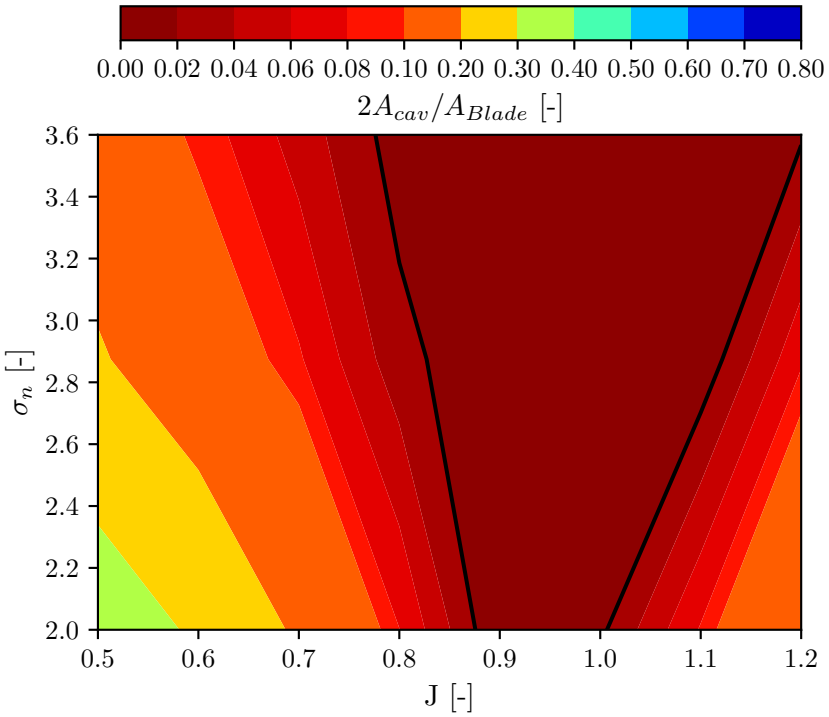

Figure C1.2: NACA4D Optimized Cavitation Bucket Diagram

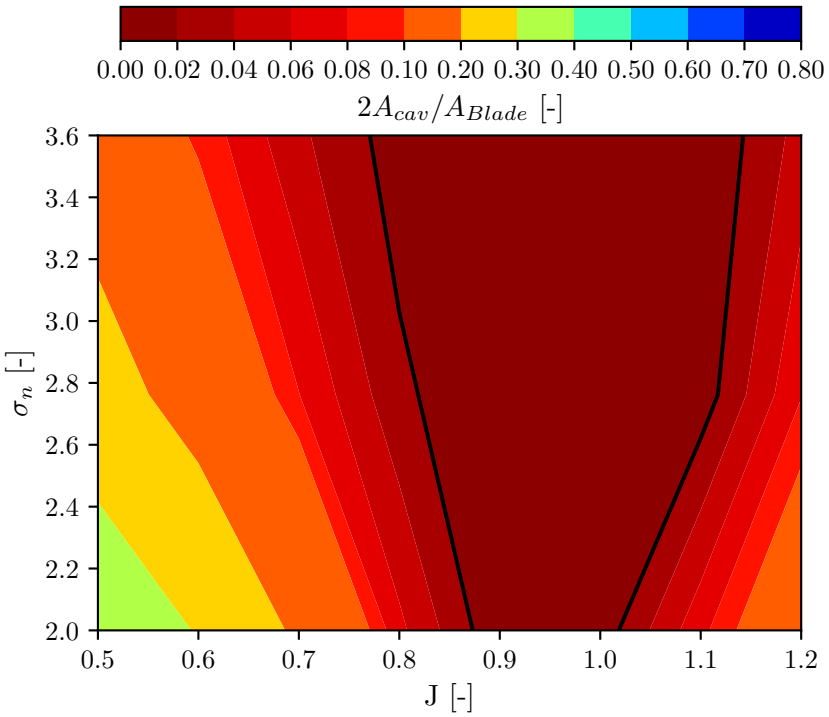

Figure C1.3: NACA16 a=0.8 Baseline Cavitation Bucket Diagram

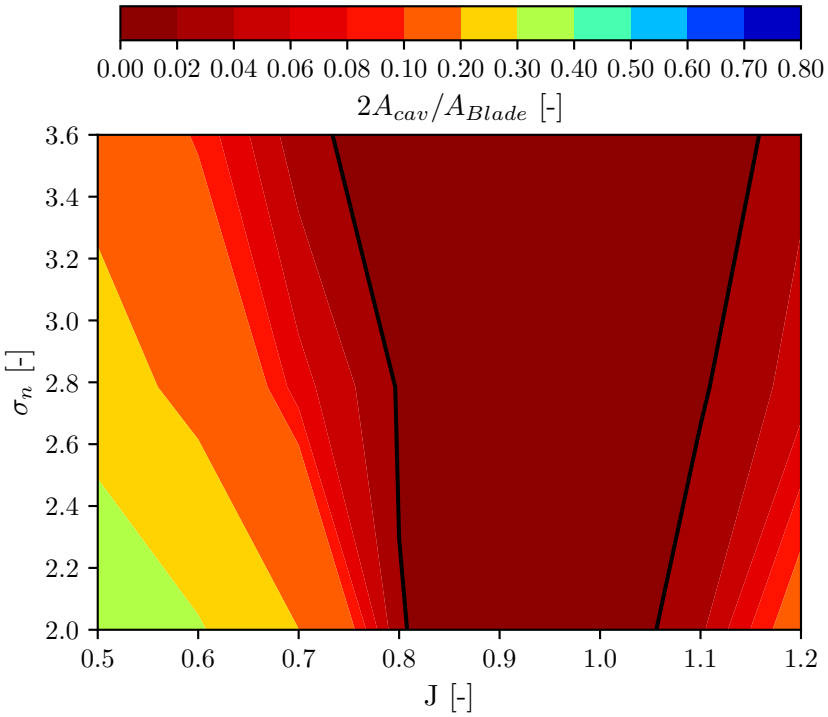

Figure C1.4: NACA16 a=0.8 Optimized Cavitation Bucket Diagram

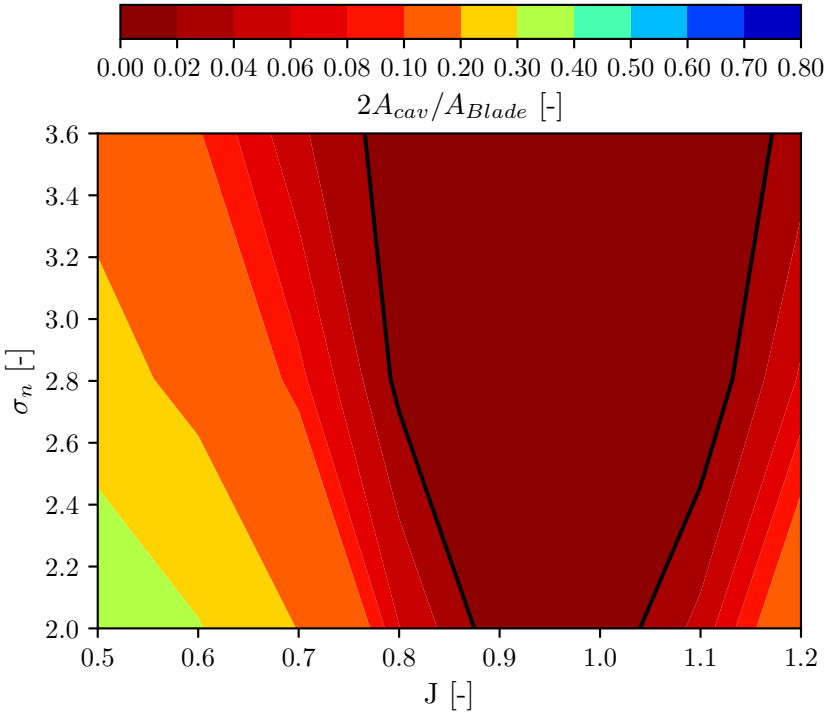

Figure C1.5: NACA16 a=1 Optimized Cavitation Bucket Diagram

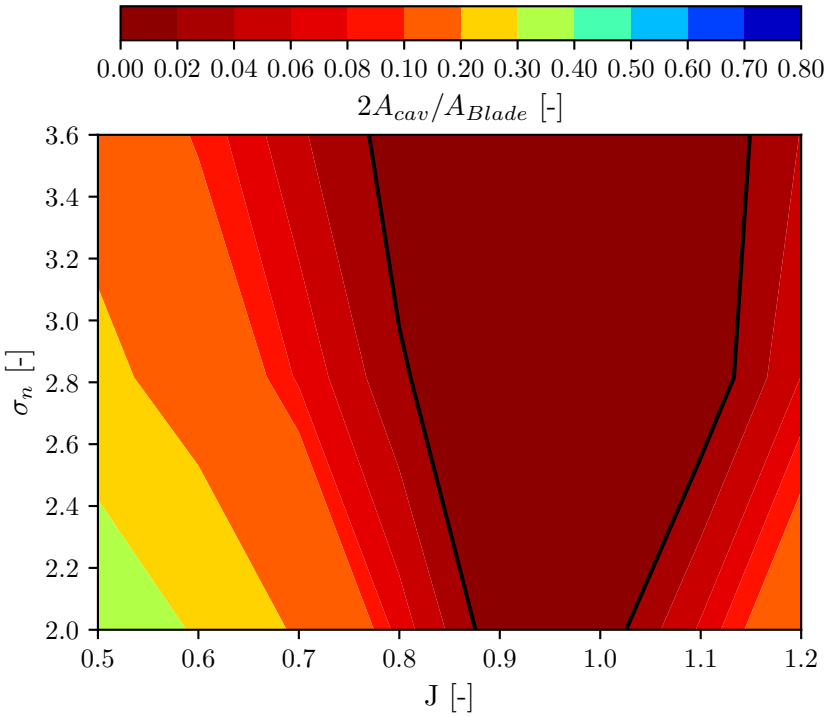

Figure C1.6: NACA66mod a=0.8 Optimized Cavitation Bucket Diagram

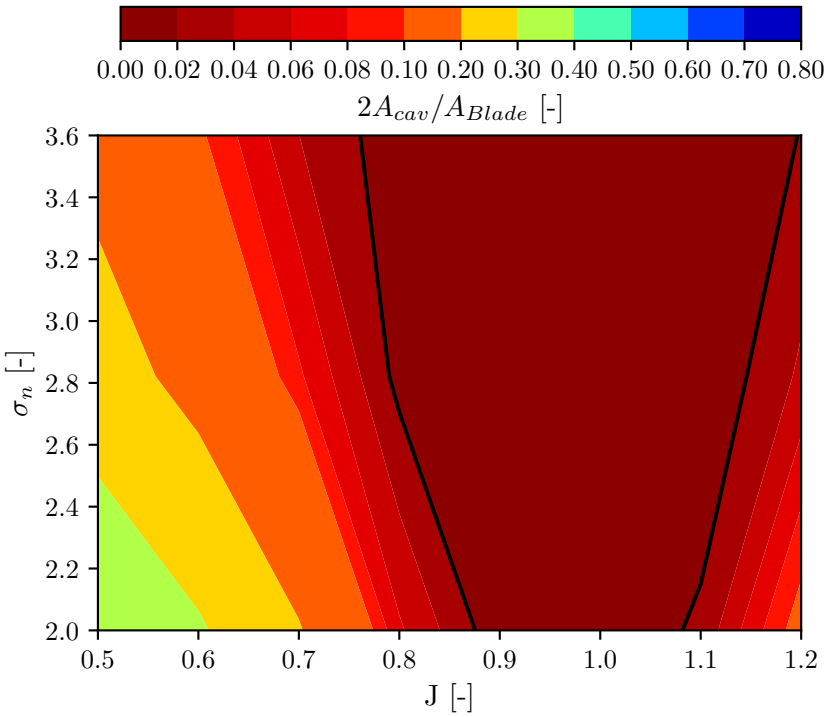

Figure C1.7: NACA66mod a=1 Optimized Cavitation Bucket Diagram

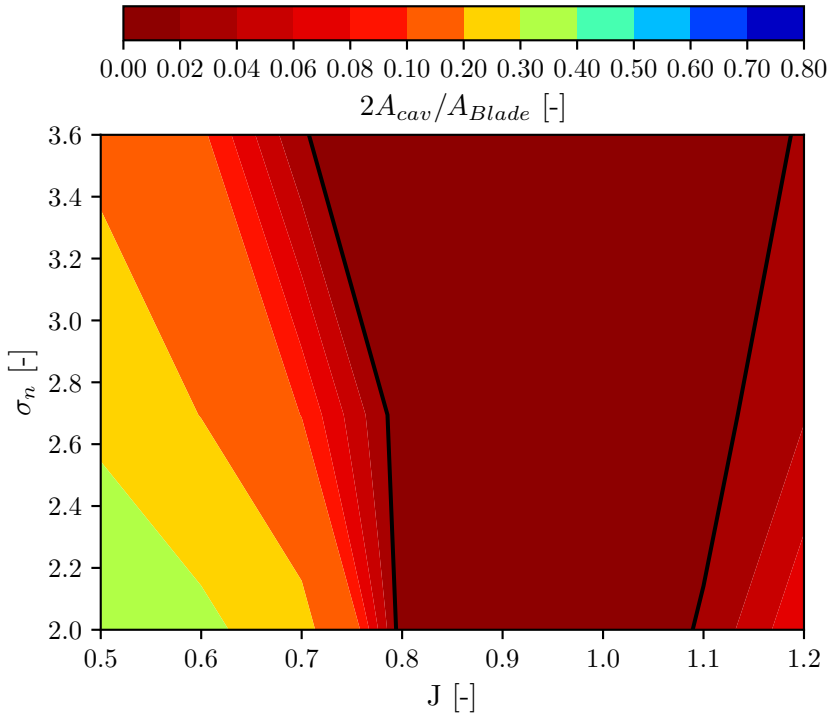

Figure C1.8: Variable Profile 32 a=0.8 Optimized Cavitation Bucket Diagram

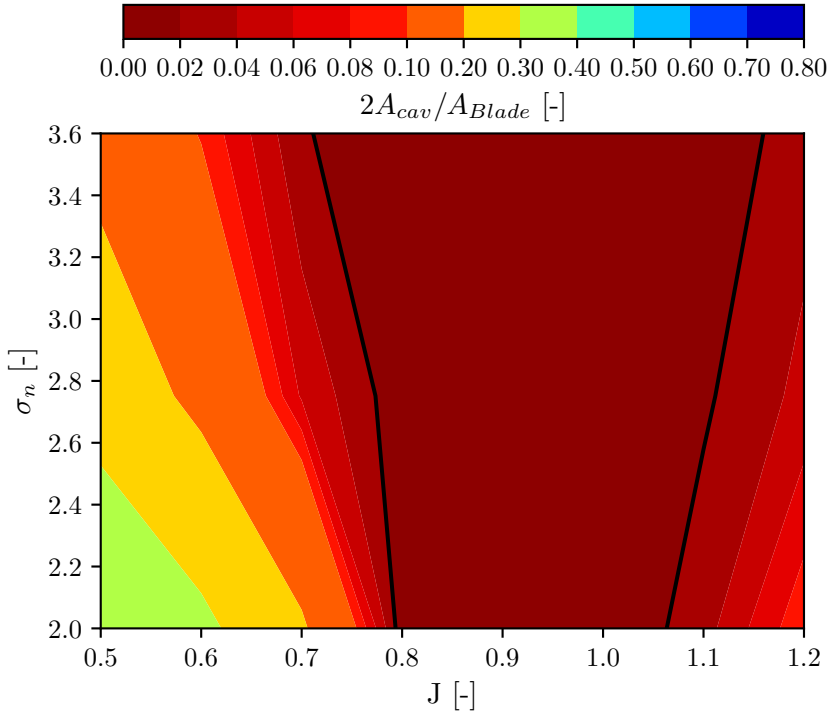

Figure C1.9: Variable Profile 23 a=0.8 Optimized Cavitation Bucket Diagram

C.2 Cavitation Area vs Advance Ratio

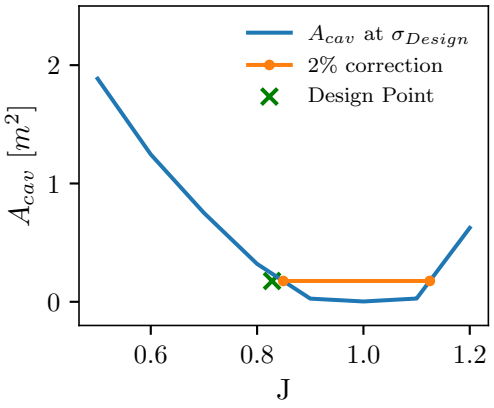

Figure C2.1: NACA4D Baseline Cavitation Area vs Advance Ratio

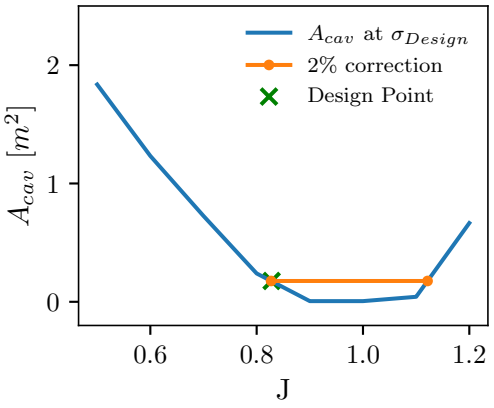

Figure C2.2: NACA4D Optimized Cavitation Area vs Advance Ratio

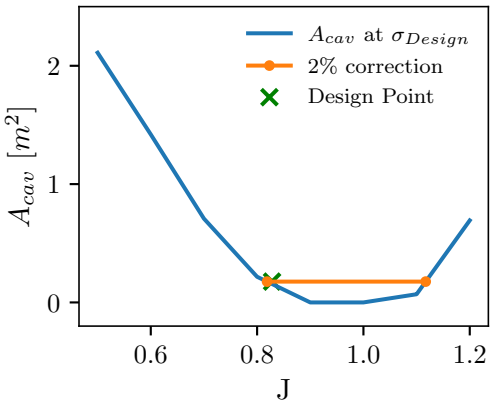

Figure C2.3: NACA16 a=0.8 Baseline Cavitation Area vs Advance Ratio

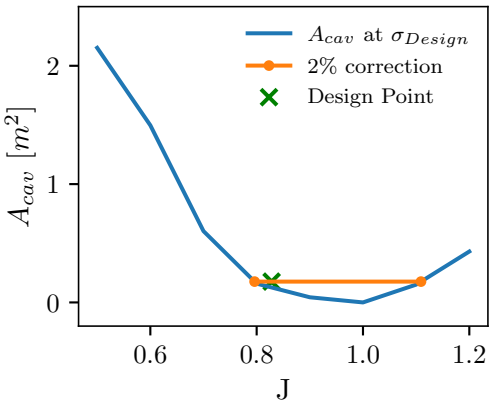

Figure C2.4: NACA16 a=0.8 Optimized Cavitation Area vs Advance Ratio

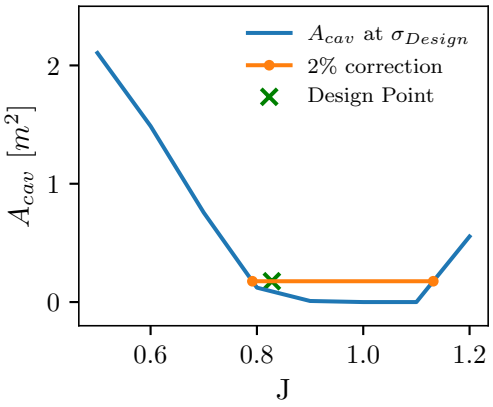

Figure C2.5: NACA16 a=1 Optimized Cavitation Area vs Advance Ratio

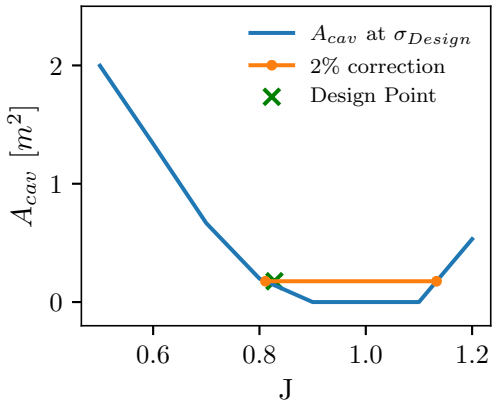

Figure C2.6: NACA66mod a=0.8 Baseline Cavitation Area vs Advance Ratio

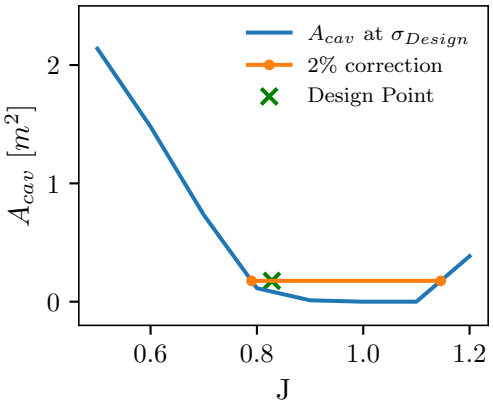

Figure C2.7: NACA66mod a=1 Optimized Cavitation Area vs Advance Ratio

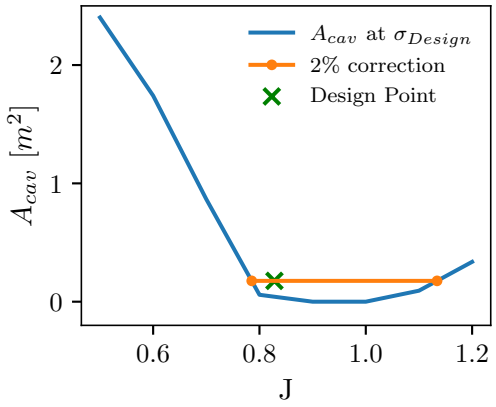

Figure C2.8: Variable Profile 32 a=0.8 Optimized Cavitation Area vs Advance Ratio

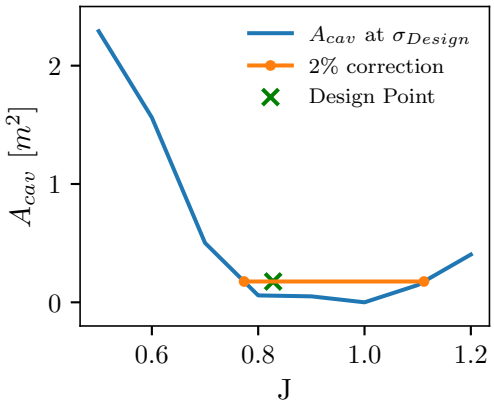

Figure C2.9: Variable Profile 23 a=0.8 Optimized Cavitation Area vs Advance Ratio

This page intentionally left blank.

D
Scripts

D.1 Design Point Calculation Script

Listing D.1: Design Point Calculation Script

```
#---------------------------
# Includes
#---------------------------
import numpy as np
#---------------------------
# Define Constants
#---------------------------
KT = 0.21395
D = 9.6
WFT = 0.166
Vs = 22.8
JT = 0.83958
ETAR = 1.003
#---------------------------
# Load Results Data
#---------------------------
data_RANS = np.loadtxt("14_V23st5opt_RANS_OWT.dat", delimiter=',',
    skiprows=3, dtype=float)
data_Nominal_Curve = np.loadtxt("Nominal_Curve.dat", delimiter=','
    , dtype=float)
#---------------------------
# Evaluations
#---------------------------
KT_inter=np.interp((KT/JT**2),(data_RANS[:,1]/data_RANS[:,0]**2),
    data_RANS[:,1])
J=np.interp(KT_inter,data_RANS[:,1],data_RANS[:,0])
KQ=np.interp(KT_inter,data_RANS[:,1],data_RANS[:,2])
ETAO=np.interp(KT_inter,data_RANS[:,1],data_RANS[:,3])
N_Inter=(Vs*.5144*(1-WFT))/(J*D)
P_Inter=(KQ*1026.026*((N_Inter)**2)*(D**5))*(N_Inter)*2*3.14/1000
N_Nom_Inter=np.interp(P_Inter,data_Nominal_Curve[:,1],
    data_Nominal_Curve[:,0])/60
LRM =(N_Inter)*100/N_Nom_Inter
#---------------------------
# Writing the Output File
#---------------------------
```

```
33      data_Interp = open("Result_interp.dat", "w")
34      data_Interp.write("J;    KT;     KQ;     ETAO;    N_nom_inter;
           N_inter;     Power;       LRM \n")
35      data_Interp.write(str(J) + ";")
36      data_Interp.write(str(KT_inter) + ";")
37      data_Interp.write(str(KQ) + ";")
38      data_Interp.write(str((J / (2 * 3.14)) * (KT_inter / KQ)) + ";")
39      data_Interp.write(str(N_Nom_Inter) + ";")
40      data_Interp.write(str(N_Inter) + ";")
41      data_Interp.write(str(P_Inter) + ";")
42      data_Interp.write(str((N_Inter)*100/N_Nom_Inter))
43      data_Interp.close()
```

D.2 Bucket Width Evaluation Script

Listing D.2: Bucket Width Evaluation Script

```
#---------------------------
# Includes
#---------------------------
import numpy as np
#---------------------------
# Variables and Declerations
#---------------------------
bladearea=17.6
cavadjust=0.02*bladearea/2  # 2% area Correction
js=[1.2,1.1,1.0,0.9,0.8,0.7,0.6,0.5]
designJ=0.8281518
#---------------------------
# Load and Manipulate Result Data
#---------------------------
data_Original=np.loadtxt("10_variableprofile23st5a08_opt_summary_cav.
    dat",delimiter=' ',skiprows=0,dtype=float)
data_Original[0]=js
data_Original=np.delete(data_Original,-1,axis=0)
data_Original=data_Original.T
for i in range(len(data_Original)):
    if data_Original[i,1] ==np.min(data_Original[:,1]):
        suctionsidecav=data_Original[0:i+1,:]
        pressuresidecav = data_Original[i:len(data_Original), :]
#---------------------------
# Evaluations
#---------------------------
cav_bucketloc1=np.interp(cavadjust,np.flip(suctionsidecav[:,1]),np.
    flip(suctionsidecav[:,0]))
cav_bucketloc2=np.interp(cavadjust,pressuresidecav[:,1],
    pressuresidecav[:,0])
Bucket_Width= cav_bucketloc1-cav_bucketloc2
print("Bucket_Width=",Bucket_Width)
cav_area_DP=np.interp(designJ,np.flip(data_Original[:,0]),np.flip(
    data_Original[:,1]))
print("cav_area_DP=",cav_area_DP)
#---------------------------
# Writing the Output File
#---------------------------
data_Interp=open(current+"/Result_interp_cav.dat","w")
data_Interp.write(str(cav_area_DP)+",")
data_Interp.write(str(Bucket_Width) + ",")
data_Interp.write(str(DPtosuctioncavdist)+",")
data_Interp.write(str(DPtopressurecavdist)+",")
data_Interp.write(str(bucketshift)+",")
data_Interp.close()
```